NOVEL CONCEPTS FOR MICROPOROUS HYBRID SILICA MEMBRANES

FUNCTIONALIZATION & PORE SIZE TUNING

À mes parents

Promotion committee

Prof. Dr. Ir. A. Nijmeijer (promotor)	University of Twente
Dr. R. Kreiter (Assistant-promotor)	Energy Research Center of the Netherlands (ECN)
Dr. A.J.A. Winnubst (referent)	University of Twente
Prof. Dr. Ir. J.E. Ten Elshof	University of Twente
Prof. Dr. Ir. L. Lefferts	University of Twente
Prof. Dr. Ir. F. Kapteijn	Technical University of Delft
Dr. A. Julbe	Institut Européen des Membranes (IEM), Montpellier (France)

Novel concepts for microporous hybrid silica membranes Functionalization and pore size tuning
ISBN: 978-90-365-3366-9
DOI: 10.3990./1.9789036533669
Printed by Gildeprint Drukkerij, Enschede, The Netherlands

NOVEL CONCEPTS FOR MICROPOROUS HYBRID SILICA MEMBRANES

FUNCTIONALIZATION & PORE SIZE TUNING

DISSERTATION

To obtain
the degree of doctor at the university of Twente
on the authority of the rector magnificus
prof.dr. H. Brinksma
on account of the decision of the graduation committee,
to be publicly defended on
Friday the 11th of May, 2012, at 12.45hrs
by
Goulven Gildas Paradis
Born on April 22nd, 1983
In Quimper, France

This dissertation has been approved by:

Prof. Dr. Ir. A. Nijmeijer (promotor)

Dr. R. Kreiter (assistant-promotor)

Table of content

Chapter 1

Introduction

1.1. General introduction

A membrane can be described as a semi permeable active or passive barrier that allows the permeation of one or more components of a liquid or a gaseous mixture and retains other components. While numerous examples of biological membranes were known since the 18th century, synthetic membranes only appeared in the middle of the 20th century [1]. This implies that creating such a selective barrier is not straightforward.

In practical membrane applications, the surface of the membrane is placed in contact with the liquid or gaseous mixture to be separated, called the feed (Figure 1.1). By applying a driving force in the form of a difference in pressure or chemical potential between the feed and permeate side of the membrane the separation proceeds [2]. The part of the feed mixture that passes through the membrane is called the permeate. The remaining part of the feed is called the retentate. The performance of a membrane is determined by both its flux and the composition of its permeate, governed by the membrane selectivity. The flux is directly related to the amount of membrane surface area needed to treat a certain feed volume, while the selectivity has implications for the number of separation steps needed to arrive at the desired purity.

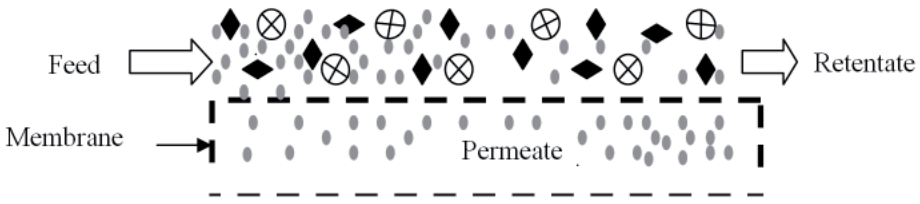

Figure 1.1. Schematic sieving (separating) mechanism of a membrane

Porous membranes are classified by the IUPAC on the basis of their pore size in the classes macroporous (pore diameter > 50 nm), mesoporous (2 - 50 nm), and microporous (< 2 nm) membranes [3]. Membrane processes can be classified according the type of driving force and/or to the size and nature of the permeating molecules. This kind of classification

leads to the classes microfiltration, ultrafiltration, nanofiltration, reverse osmosis, dialysis, pervaporation, and gas separation [4]. This thesis focuses on microporous membranes for pervaporation and/or nanofiltration.

Apart from economic aspects such as membrane or module price, the applicability of a microporous membrane is governed by the following three main parameters:

- The specific pore size of the separating layer. All membranes with pores < 2 nm are classified as microporous. However, gas separation requires pores of 0.3-0.5 nm, whereas nanofiltration requires pores of 1-2 nm.
- The hydrophilicity or hydrophobicity of the membrane or the particular affinity of the membrane for a specific molecule in the feed mixture.
- The stability of the separating layer and of the support in the feed mixture which determines the life time of the membrane.

Microporous membranes can be either organic (polymeric) or inorganic membranes. The large range of polymeric materials developed in the last decades resulted in numerous membranes with various pore sizes and affinities [5]. Hydrophobic and hydrophilic membranes, or tailor made functionalized membranes are now widely applied in different industrial processes [6-9]. Nevertheless, polymeric membranes suffer from a number of drawbacks. For most polymer membranes, their performance starts to deteriorate above 100 °C and the organic backbone starts to decompose around 250 °C. In organic solvent media, the stability window is generally limited to a small number of solvents for one polymer type. At the same time, such membranes suffer from major swelling and compaction effects induced by the organic solvent and the applied pressure in nanofiltration. These factors lead to major variations of the flux and of the effective molecular weight cut-off (MWCO) of the membranes, depending on the specific solvent-membrane combination [10-12]. Consequently, their use is limited to a low number of possible applications per membrane, and successful examples cannot be extrapolated to other conditions.

In contrast, porous inorganic membranes have generic stability in a wide range of solvents and up to very high temperatures. Among the variety of inorganic ceramic membranes, inorganic silica (SiO_2) membranes are the most widely studied [13, 14], probably because of their straightforward preparation via sol-gel techniques and tunability of their properties via the conditions of the preparation procedure. Such membranes can withstand temperatures up to 600 °C, are stable in numerous solvents and do not suffer from solvent or temperature swelling. However, the surfaces of ceramic oxide materials are intrinsically hydrophilic, because of the hydroxyl (-OH) groups present on their surface. As compared to polymeric membranes, examples of chemically functionalized microporous ceramic oxide membranes are scarce. The main examples are hydrophobized silica membranes obtained by modification with alkyltriethoxysilanes [15, 16] or fluorinated alkyltriethoxysilanes [17]. Two examples of amino-functionalized silica membranes [18, 19] were published. The major limitation of such silica-based membranes is the poor hydrothermal stability, leading to severe degradation in the presence of water. A dramatic example is the life time of only hours of inorganic silica membranes in a high temperature pervaporation process [20, 21]. Despite of numerous efforts to stabilize the silica network by introduction of transition metals [22-24], no sufficient stability could be reached by these attempts to inhibit the hydrolysis of the Si-O-Si bonds responsible of the degradation of the silica network [25].

1.2. Asymmetric supported microporous hybrid silica membranes

The acid catalyzed sol-gel process, which involves the hydrolysis and condensation of the tetraethoxysilane (Figure 1.2), is a typical route for the development of inorganic silica materials and membranes [26]. Numerous alkoxysilane precursors that contain organic fragments are commercially available. A particularly interesting class of alkoxysilanes is that of bridged α,ω-bis(triethoxysilyl)alkanes. Sah et al. used 1-2 bis(triethoxysilyl)ethane, a bis-silane precursor with an ethane bridge between the two silicon atoms, to develop the first organic-inorganic hybrid microporous silica membranes [27-30]. The observed unprecedented hydrothermal stability of these membranes can be explained by the decrease

of the number of hydrolysable bonds and the increased connectivity in the network (Figure 2). This resulted in an impressive stability of over 1000 days in the dehydration of an *n*-butanol/water mixture by pervaporation at 150 °C [31]. This exceptional stability is taken as a starting point in this thesis for further developments of hybrid silica membranes.

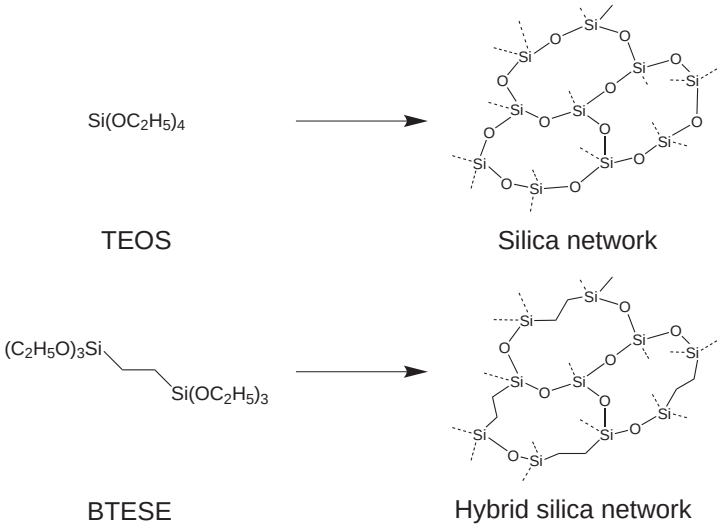

Figure 1.2. Schematic representation of a silica and a hybrid silica network

The hybrid silica membranes presented in this thesis are 30 cm long asymmetric tubular membranes coated at the outer surface (Figure 1.3). Such thin hybrid silica separating layers need to be supported by a multilayered support structure consisting of a number of layers with decreasing porosities and roughness [32]. The layers consist of an extruded α-Al_2O_3 tube with a pore size of about 4 µm, α-Al_2O_3 layers with a pore size of 170-180 nm, and a γ-Al_2O_3 layer with a pore size of 3-4 nm offering a smooth surface for the coating of thin defect free hybrid silica membranes. The synthesis of the multilayer support is extensively described elsewhere [32]. The sol gel synthesis parameters, the coating, and heat treatment conditions of the top layer are detailed in the experimental parts of the different chapters.

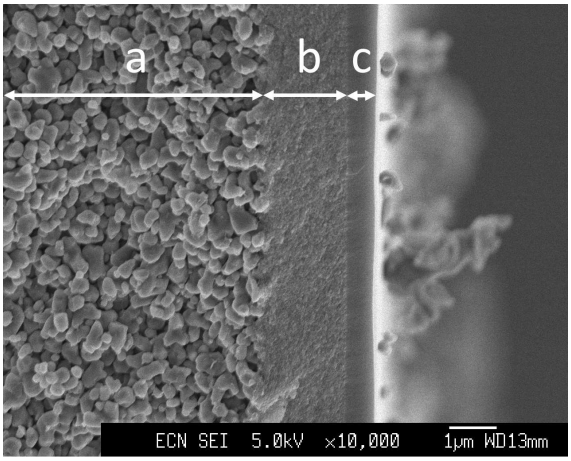

Figure 1.3. SEM cross section of the α-Al_2O_3 layer (a), the γ-Al_2O_3 layer and of the hybrid silica top layer (c)

1.3. Aim of this thesis

The introduction of an organic fragment in a silica network resulted in hybrid silica membranes with an unprecedented hydrothermal stability as compared to inorganic silica membranes. This first generation of HybSi® membranes is currently being commercialized for demanding pervaporation applications. The membrane material of HybSi® is relatively hydrophilic. Separation studies have shown that it behaves similar to other silica-based microporous membranes and its separation is governed by a size-based separation mechanism [33].

We recently showed that a range of hybrid silica membranes can be synthesized with various bridged precursors. It appeared that the nature of the bridge clearly influences the properties of the resulting membranes [34]. A wide range of functionalized alkoxysilanes are commercially available. The use of such functionalized precursors allows for the incorporation of specific functional groups in the inorganic silica matrix, similar to polymeric membranes, whilst retaining the stable hybrid network.

In addition, the current generation of HybSi® membranes has a pore size of about 0.5 nm. An additional type of HybSi® membranes with pore sizes in the range of 1-2 nm would be of

great interest to widen the applicability of this membrane family. The combination of larger pore sizes and the option of functional groups in the backbone of the membrane material would make this membrane concept widely applicable in a range of applications.

Following these considerations, the aims of this thesis are:

- Exploring the use of reactive functional groups in the preparation of hybrid silica membranes, by use of amino-functionalized precursors.
- Hydrophobizing hybrid silica materials and membranes by the introduction of a range of organic functionalities as intrinsic part of the hybrid material. This also involves a study of applicability in organophilic pervaporation and solvent nanofiltration.
- The investigation of an alternative pore size templating method of hybrid silica membranes to develop super-microporous membranes.

1.4. Outline of this thesis

Chapter 2 describes the development of hydrophilic amino-functionalized membranes by incorporation of amino-functionalized terminating groups in a hybrid silica network. The molar ratio of the amino-functionalized precursors in the matrix of 1,2-bis(triethoxysilyl) ethane (BTESE) was varied in the range of 25-100 mol%. XPS measurements were performed to determine the resulting amounts of amino precursor in the membranes. The membranes were characterized in single gas permeance measurements and in dehydration of n-BuOH/water (95/5 wt%) and EtOH/water (95/5 wt%) feed mixtures.

Chapter 3 describes the synthesis and characterization of a wide range of hydrophobic hybrid xerogels based on mixtures of 1,2-bis(triethoxysilyl)ethane (BTESE) and R-triethoxysilanes (RTES, R = C_1-C_{18} alkyl). The influence of the starting concentrations of acid and water in the sol and order of precursor addition were also investigated. The microstructure of the xerogels was characterized using SAXS measurements and CO_2, N_2 adsorption. The hydrophobicity of the materials was determined using contact angle measurements.

Chapter 4 covers hydrophobic hybrid silica membranes based on the sols of Chapter 3. The membrane properties were investigated in single gas permeance experiments and in pervaporation of 95/5 wt% and 5/95 wt% n-butanol/water mixtures. For the most hydrophobic membranes a study of different process parameters was made.

Chapter 5 is devoted to the testing of several hybrid silica membranes in nanofiltration. Pure acetone and toluene fluxes were measured and retention measurements with Sudan Blue (350 g/mol) and Bengal Rose (1017 g/mol) are described.

Chapter 6 describes an alternative templating method for hybrid silica membranes using thermo-labile groups. This templating method is based on the use of the Diels Alder and retro-Diels Alder reactions.

Finally, chapter 7 is dedicated to the evaluation of the work presented in this thesis and to the recommendations for future work on hybrid silica membranes.

References

[1] Overview Membrane Technology, in: C.J.M.van Rijn (Ed.), *Journal of membrane technology: Nano and Micro Engineered Membrane Technology*, Vol. 10. Elsevier, 2004

[2] M.H.V. Mulder, Basic principles of membrane technology, Kluwer Academic Publishers, 2000

[3] W.J. Koros, Y.H. Ma, and T. Shimidzu, Terminology for membranes and membrane process, 1995

[4] A.J. Burggraaf and L. Cot, Fundamentals of inorganic membranes science and technology, Amsterdam, 1996

[5] M. Ulbricht, Advanced functional polymer membranes, *Polymer*, 47, 7, 2217-2262, 2006

[6] S.P. Nũnes and K.V. Peinemann, Membrane technology in the chemical industry, Wiley-VCH, Weinheim, 2001

[7] P. Vandezande, L.E.M. Gevers, and I.F.J.Vankelecom, Solvent resistant nanofiltration: separating on a molecular level, *Chemical Society Reviews*, 37, 365-405, 2008

[8] R.W. Baker, Membrane Technology and Applications, 2007

[9] K.V. Peinemann, S.P. Nũnes, and L. Giorno, Membranes for food applications, Wiley-VCH Verlag GmbH & Co.KGaA, 2010

[10] D.R. Machado, D. Hasson, and R. Semiat, Effect of solvent properties on permeate flow through nanofiltration membranes. Part I: Investigation of parameters affecting solvent flux, *Journal of Membrane Science*, 163, 93-102, 1999

[11] D.F. Stamatialis, N. Stafie, K. Buadu, M. Hempenuis, and M. Wessling, Observations on the permeation performance of solvent resistant nanofiltration membranes, *Journal of Membrane Science*, 279, 424-433, 2006

[12] E.S. Tarleton, J.P. Robinson, S.J. Smith, and J.J.W. Na, New experimental measurements of solvent induced swelling in nanofiltration membranes, *Journal of Membrane Science*, 261, 129-135, 2005

[13] R.M. de Vos and H. Verweij, High-selectivity, high-flux silica membranes for gas separation, *Science*, 279, 1710-1711, 1998

[14] M. Kanezashi and M. Asaeda, Hydrogen Permeation characteristics and stability of Ni-doped silica membranes in steam at high temperatures, *Journal of Membrane Science*, 271, 1-2, 86-93, 2006

[15] R.M. de Vos, W.F. Maier, and H. Verweij, Hydrophobic silica membranes for gas separation, *Journal of Membrane Science*, 158, 1-2, 277-288, 1999

[16] J. Campaniello, C.W.R. Engelen, W.G. Haije, P.P.A.C. Pex, and J.F. Vente, Long-term pervaporation performance of microporous methylated silica membranes, *Chemical Communications*, 834-835, 2004

[17] Q. Wei, F.Wang, Z.R. Nie, C.L. Song, Y.L Wang, and Q.Y. Li, Highly hydrothermally stable microporous silica membranes for hydrogen separation, *Journal of Physical Chemistry B*, 112, 31, 9354-9359, 2008

[18] B.A. McCool and W.J. DeSisto, Amino-functionalized silica membranes for enhanced carbon dioxide permeation, *Advanced Functional Materials*, 15, 1635-1640, 2008

[19] G. Xomeritakis, C.Y. Tsai, and C.J. Brinker, Microporous sol-gel derived aminosilicate membrane for enhanced carbon dioxide separation, *Separation and Purification Technology*, 42, 3, 249-257, 2005

[20] S. Giessler, L. Jordan, J.C.D. da Costa, and G.Q. Lu, Performance of hydrophobic and hydrophilic silica membrane reactors for the water gas shift reaction, *Separation and Purification Technology*, 32, 1-3, 255-264, 2003

[21] R.S.A. de Lange, K. Keizer, and A.J. Burggraaf, Aging and stability of microporous sol-gel-modified ceramic membranes, *Industrial & Engineering Chemistry Research*, 34, 3838-3847, 1995

[22] V. Boffa, D.H.A. Blank, and J.E. ten Elshof, Hydrothermal Stability of microporous silica and Niobia-Silica membranes, *Journal of Membrane Science*, 319, 256-263, 2008

[23] M. Asaeda, M. Kanezashi, T. Yoshioka, and T. Tsuru, Gas permeation characteristics and stability of composite silica-metal oxide membranes, *Materials Research Society Symposium Proceedings*, 752, AA10.3, 213-218, 2003

[24] M. Kanezashi and M. Asaeda, Hydrogen permeation characteristics and stability of Ni-doped silica membranes in steam at high temperature, J*ournal of Membrane Science*, 271, 86-93, 2006

[25] H. Imai, H. Morimoto, A. Tominaga, and H. Hirashima, Structural changes in Sol-Gel derived SiO_2 and TiO_2 films by exposure to water vapor, *Journal of Sol-Gel Science and Technology*, 10, 45-54, 1997

[26] C.J. Brinker and G.W. Scherer, Sol-Gel Science-The Physics and Chemistry of Sol-Gel Processing, Academic Press, New York, 1990

[27] H.L. Castricum, A. Sah, J. Geenevasen, R. Kreiter, D.H.A. Blank, J.F. Vente, and J.E. ten Elshof, Structure of hybrid organic-inorganic sols for the preparation of hydrothermally stable membranes, *Journal of Sol-Gel Science and Technology*, 48, 11-17, 2008

[28] H.L. Castricum, A. Sah, R. Kreiter, D.H.A. Blank, J.F. Vente, and J.E. ten Elshof, Hydrothermally stable molecular separation membranes from organically linked silica, *Journal of Materials Chemistry*, 18, 2150-2158, 2008

[29] H.L. Castricum, A. Sah, R. Kreiter, D.H.A. Blank, J.F. Vente, and J.E. ten Elshof, Hybrid ceramic nanosieves: stabilizing nanopores with organic links, *Chemical Communications*, 1103-1105, 2008

[30] A. Sah, H.L. Castricum, J.F. Vente, D.H.A. David, and J.E. ten Elshof, Microporous molecular separation membrane with high hydrothermal stability, 2006-100388 A, WO 2007081212, 2007

[31] H.M. van Veen, M.D. Rietkerk, D.P. Shanahan, M.M.A. van Tuel, R. Kreiter, H.L. Castricum, J.E. ten Elshof, and J.F. Vente, Pushing membrane stability boundaries with HybSi® pervaporation membranes, J*ournal of Membrane Science*, 380, 124-131, 2011

[32] B.C. Bonekamp, Preparation of Asymmetric Ceramic Membrane Supports by Dip-Coating, in: A.J. Burggraaf and L. Cot (Eds.), Fundamentals of Inorganic Membrane Science and Technology, Elsevier, Amsterdam, 1996

[33] R. Kreiter, M.D.A. Rietkerk, H.L. Castricum, H.M. van Veen, J.E. ten Elshof, and J.F. Vente, Stable hybrid silica nanosieve membranes for the dehydration of lower alcohols, *ChemSusChem*, 2, 2, 158-160, 2009

[34] H.L. Castricum, G.G. Paradis, M.C. Mittelmeijer-Hazeleger, R. Kreiter, J.F. Vente, and ten J.E. Elshof, Tailoring the Separation Behavior of Hybrid Organosilica Membranes by Adjusting the Structure of the Organic Bridging Group, *Advanced Functional Materials*, 21, 9, 2319-2329, 2011

Chapter 2

Amino-functionalized microporous hybrid silica membranes

This chapter has been published in Journal of Materials Chemistry:

Goulven G. Paradis, Robert Kreiter, Marc M.A. van Tuel, Arian Nijmeijer, and Jaap F. Vente, J. Mater. Chem., 22 (15), 7258 - 7264, 2012

Abstract

The present study describes the effect of the incorporation of amino-functionalized terminating groups on the behaviour and performance of an organic-inorganic hybrid silica membrane. A primary amine, a mixed primary and secondary amine, and an imidazole functionality were selected. The molar ratio of the amino-functionalized precursors in the matrix forming 1,2-bis(triethoxysilyl)ethane (BTESE) precursor was varied in the range of 25-100 mol%. Strong water adsorption, which remains at temperatures up to 523 K, was found for all membranes. The observed low gas permeances, and contrasting high water fluxes in pervaporation were explained in relation with the strong water adsorption. XPS measurements indicate a relation between the concentration of amino functional groups in the hybrid layers and the starting amine concentration of the sols. XPS measurements also revealed the existence of a maximum loading of the amino-functionalized precursor. Depending on the precursor, a maximum N/Si element ratio between 0.07 to 0.45 was found. At amine concentrations higher than a precursor dependent threshold value, membrane selectivity is constant over the range of amine concentrations. For alcohol/water (95/5 wt%) feed mixtures, the observed water concentrations in the permeate were over 90 wt% for EtOH and 95 wt% for n-BuOH dehydration.

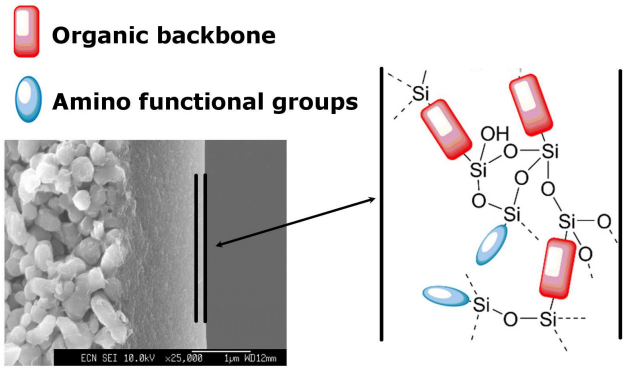

2.1. Introduction

Molecular separations using inorganic microporous membranes (pores ≤ 2 nm) are governed by a combination of molecular sieving effects and membrane affinity. Key methods to direct the dominant separation mechanism are tuning of the pore size and tailoring of the affinity by the introduction of functional groups [1]. Up to recently, microporous inorganic silica membranes were subject of most of the research efforts in this field, and many of these studies focused on microstructure control [2]. Successful examples of highly selective gas separation and pervaporation membranes were reported [2, 3]. Despite their relative ease of synthesis and a high thermal resistance, silica membranes have not become a commercial success. This is most likely related to their low hydrothermal stability [4]. This is especially apparent in separations in which water is present at high temperatures, such as water gas shift conditions, or high temperature dewatering of organic solvents [5, 6]. Recently, we developed hybrid organic-inorganic HybSi® membranes to overcome the stability boundaries of inorganic silica [7]. The introduction of an organic fragment in a silica network by using bridged bis-silane precursors leads to membranes having a life time of at least 1000 days in alcohol dehydration at high temperature without selectivity decrease [8]. The governing separation mechanism of this hybrid silica network is based on molecular sieving, as the dehydration performance depends on the alkyl bridge length [9]. The incorporation of well-defined functional groups has been studied in relation with ion transport [10]. For molecular separation applications, a limited number of attempts have been made to functionalize microporous silica membranes [11], whereas this has not been reported for organic-inorganic hybrid silica membranes. The influence of the shape, length, and flexibility of the organic bridges in the hybrid silica network on the membrane pore size, structure, and affinity was recently described by Castricum et al. [12]. Strong differences in gas permeance properties and pervaporation performances were observed.

Here, we present the first results on the incorporation of functional terminating groups in microporous hybrid silica (HybSi®) membranes. The aim of the present study was to explore the further hydrophilization of organic-inorganic hybrid materials whilst keeping

the organic fragments the backbone intact. Three different triethoxysilanes with an amine group were selected for this purpose and introduced in a matrix of 1,2-bis(triethoxysilyl) ethane (BTESE), assuming these would increase the affinity for CO_2 and for water. As a first candidate the primary amine 3-aminopropyltriethoxysilane (PA) was chosen. Further, an imidazole, N-(3-triethoxysilylpropyl)-4,5-dihydroimidazole (IM), and a long alkyl chain with a primary and a secondary amine group, 3-(2-aminoethylamino)propyltrimethoxysilane (LDA), were selected (Figure 2.1).

The use of 3-aminopropyltriethoxysilane (PA) was reported by Brinker et al. in periodic mesoporous silica thin films by co-condensation with tetraethoxysilane (TEOS) in a so-called EISA procedure [13]. Later it was used for surface functionalization of siliceous materials [14-18] or biocompatible materials [19, 20]. Xomeritakis et al. [21] presented the first microporous PA-functionalized silica membranes for CO_2 separation, followed by a comparison with nickel doped silica membranes [22]. The two other precursors are novel precursors in membrane technology. The membrane properties were determined using gas permeation tests and alcohol dehydration measurements.

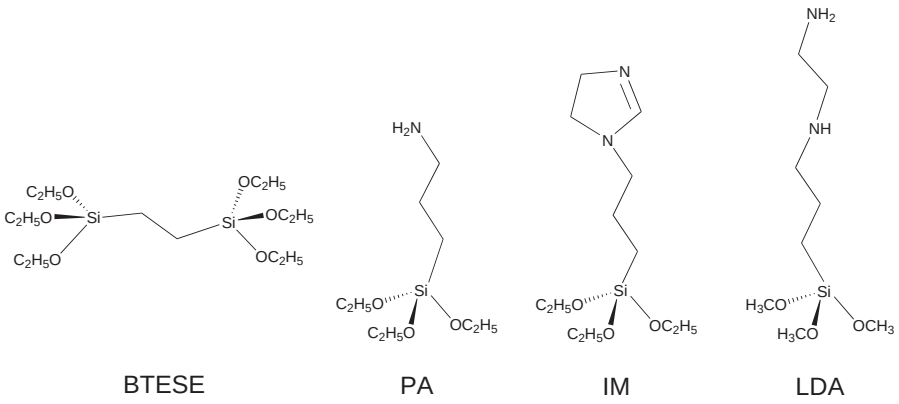

Figure 2.1. Overview of the precursors used in this chapter

2.2. Experimental

1,2-Bis(triethoxysilyl)ethane (BTESE, ABCR, 97%), 3-aminopropyltriethoxysilane (PA, ABCR, 98%), N-(3-triethoxysilylpropyl)-4,5-dihydroimidazole (IM, ABCR, 97%), 3-(2-aminoethylamino)propyltrimethoxysilane (LDA, ABCR, 96%), nitric acid (69 wt%, Aldrich), and EtOH (p.a. Aldrich) were used as received. Water was deionized at 18 MΩ/cm using a Millipore purification system. The abbreviations used for the precursors refer to their structure. PA, IM, and LDA stand for Primary Amine, Imidazole, and Linear DiAmine.

Pure triethoxysilane sols were synthesized using a single-step synthesis. The desired amounts of nitric acid, distilled water and EtOH were premixed. Amino-functionalized precursors were subsequently added in one shot to the nitric acid, distilled water and EtOH mixture and the sols were refluxed for three hours under stirring at 333 K. The sols based on two precursors were prepared in a two-step procedure. Nitric acid, distilled water and EtOH were premixed in this order and BTESE was subsequently added. This mixture was heated at 333K for 3 hours under stirring. The amino-functionalized precursor was diluted in EtOH and added to the BTESE sol. This final mixture was stirred at RT for 30 min before coating. Precursor amounts were adjusted to obtain final molar concentrations of 25, 50, and 75 mol% of the amino-functionalized precursor.

The membrane layers were coated on 30 cm long tubular mesoporous γ-Al_2O_3 supports [23] in a class 1000 clean room. Sols were filtered over 0.8 μm cellulose acetate (CA) Whatman® filters before coating. The coating procedure and setup are described by Bonekamp [23]. The withdrawal speed of the dip coating procedure was set at 5 mm/s. After overnight drying in the clean room, the membranes were heat treated at 523 K under N_2 for two hours with heating and cooling rates of 0.5 °C/min. Four cycles of vacuum/N_2 purge of one hour each were performed before the heat treatment. All membranes were sealed using stainless steel caps and graphite as packing material [24]. One single membrane for each composition was used for both gas permeation and all pervaporation measurements. Reproducibility was checked on selected membranes such as PA25.

Colloid sizes of the sols were determined by dynamic light scattering (DLS) using a Malvern Zetasizer nano ZS. All sols were measured at the same silica concentration of 0.5 mol/L.

Layer thickness determinations and surface characterizations were carried out on a high resolution JEOL JSM-6330F Field Emission scanning Electron Microscope (SEM). Circular samples were cut from the middle of the 30 cm heat-treated membrane, fractured, cleaned with compressed air and sputtered before measurement using a Pd/Pt alloy. These layers thicknesses were used to calculate the permeability of the membranes.

X-ray Electron Spectroscopy (XPS) measurements were performed on heat treated membrane samples using a Quantera SXM (Scanning XPS Microprobe) from Physical Electronics. Spectra were acquired using an Al Kα radiation monochromatic at 1486.6 eV. Quoted binding energies are referred to the C1s emission at 283.65 eV from Si-C*-C carbon atom as the network backbone consists of Si-C-C-Si. The expected atomic N/Si ratios were calculated on the basis of a fully condensed network. Measurements were performed on the same sample as used for SEM measurements. Depth profile thicknesses were calculated from the sputtering time, assuming that the sputter-speed on the hybrid silica membrane surface is equivalent to the speed on a SiO_2 network.

Permporometry of supported hybrid membranes was carried out with water vapour as the condensable gas and He as the permeating gas [25]. A drying temperature of 473 K and a measurement temperature of 314 K were used. Pore size distributions were determined using the Kelvin equation.

Single gas permeance measurements were performed at 523, 423 and 323 K with feed pressures from 9 to 3 bara. Pressure differences of 2 bara were applied except for the point at 3 bara feed pressure for which a pressure difference of 1.5 bara was used. A retentate flow of 50 mL/min was applied for all measurements. Measurements were performed using He, H_2, N_2, CH_4, and CO_2 in a 5.0 purity. Before measurement, each membrane was dried for two hours at 523 K under N_2. H_2 permeance measurements were performed as first and last measurement.

Pervaporation measurements were carried out with feed mixtures of alcohol/water (95/5 wt%) at 368 K and 343 K for n-BuOH and EtOH respectively. Permeate pressure was kept constant at 10 mbar and measurements were performed at regular intervals. More details on the experimental set up can be found elsewhere [8]. Throughout this paper, the membranes and sols are named according to the precursor used and the molar concentration of this precursor in the sol. For example, the PA/BTESE sols and membranes with 25, 50, and 75 mol% of PA are named PA25, PA50, and PA75 respectively. A sample based on PA only is named PA100.

2.3. Results

The development of a sol suitable for the formation of a microporous top layer involves the use of an acid-catalyst rather than a basic one [26]. The incorporation of amine groups may thus lead to complications due to their basic nature and possible catalytically activity. Indeed, in the case of PA-based sols, instantaneous precipitation was observed when the acid/water mixture was added to the BTESE/PA-based mixture. To counter this, amine-protection by protonation with HCl was attempted [13, 21]. The obtained BTESE/PA sols were clear and homogeneous, but during drying phase separation into an opaque top fraction and a clear bottom fraction was observed. The use of a two-step synthesis by addition of non-hydrolyzed PA precursor to a pre-hydrolyzed BTESE sol was tried as the second possible alternative [18, 21]. A BTESE sol was synthesized with compositional ratios of $Si/EtOH/H^+/H_2O$ = 1/11.4/0.12/6. Subsequently, a PA solution in ethanol of the same silicon concentration of 1.5 M was added to the BTESE sol. After heating this mixture to 333 K gelation occurred within a few minutes. After reducing the silicon concentrations to 0.5 M for both the BTESE sol and the PA solution and setting the reaction temperature for the second step at RT, amino-functionalized sols were obtained. These sols are stable in time at RT and have suitable particle sizes (5-10 nm) for coating of thin microporous layers. Based on these observations, the two step synthesis was selected for further study. The sol development was performed on PA/BTESE sols, after which the same procedure was adopted for IM/BTESE and LDA/BTESE sols.

Sols based on the sole amino-functionalized precursor were synthesized following a one-step synthesis procedure with ratios of $Si/EtOH/H^+/H_2O = 1/11.4/0.06/3$ at a silica concentration of 1.5 $mol.L^{-1}$. Particles sizes of 2 to 3 nm were obtained for the pure PA sols. A possible explanation for these smaller particle sizes is the formation of small PA clusters through hydrogen bonding between primary amine groups [27], inhibiting chain growth. After coating at a silica concentration of 0.3 $mol.L^{-1}$ on the γ-Al_2O_3 support and the subsequent heat treatment, SEM measurements showed thin and defect free amino-functionalized hybrid silica layers (Figure 2.2). The thicknesses of PA-based membranes ranged from 80 to 180 nm and no infiltration into the support layer was observed. Membranes containing the precursors IM or LDA were also defect free with thicknesses between 100 and 300 nm.

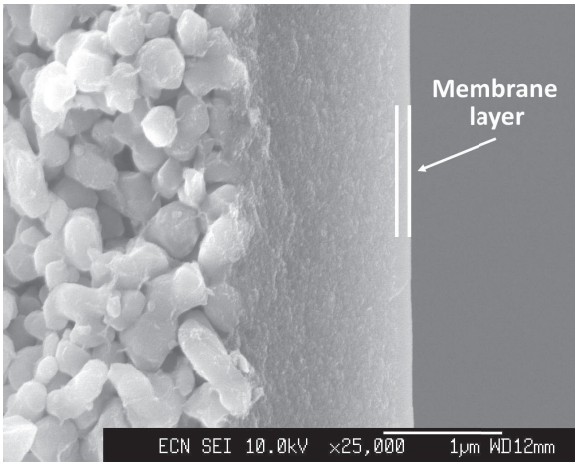

Figure 2.2. SEM image of a cross section of an PA50 membrane

Atomic N/Si ratios of membrane samples were determined using XPS measurements on a sputtered surface. The expected trend of an increase of the N/Si ratios as the concentration of amino-functionalized precursor increases was in all cases observed (Table 2.1). Compared to the expected N/Si ratios, the measured values were significantly lower. The smallest differences were observed for the LDA-based membranes. In addition, measurements were performed on green and heat treated powders for PA75. Measured N/Si ratios were 0.62 for the green and 0.52 for the heat treated powder. In contrast to the membrane samples, these values are in good accordance with the expected values.

Table 2.1. Measured (M) and expected (E) N/Si ratios of heat treated amino-functionalized membranes

	PA		IM		LDA	
mol % of amino-precursor	M	E	M	E	M	E
25%	0.04	0.14	0.016	0.28	0.14	0.28
50%	0.06	0.33	0.06	0.66	0.32	0.66
75%	0.07	0.63	0.15	1.25	0.45	1.25
100%	0.3	1	0.62	2	0.52	2

Figure 2.3 shows the XPS depth profile analysis on the PA75 heat-treated membrane. Four sections could be distinguished: a first layer of about 15 nm rich in adventitious carbon (A), the effective hybrid layer of about 65 nm (B), about 60 nm of infiltrated sol in the γ-Al_2O_3 support (C), and the clean γ-Al_2O_3 support (D). The residual C, Si, and N measured at depths of over 140 nm are resulting from element pushing by the sputtering beam. The actual membrane layer (B) had a N/Si ratio of about 0.08 in agreement with the value measured on the sputtered surface of the same sample.

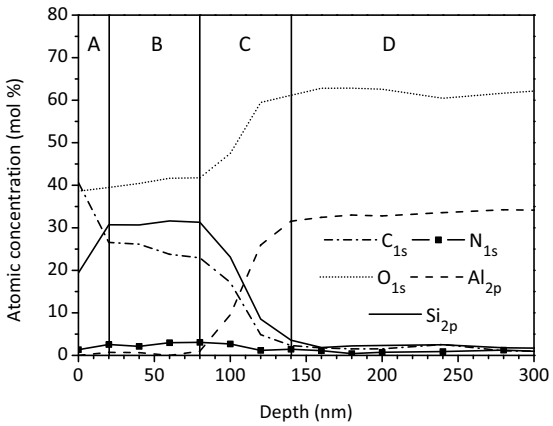

Figure 2.3. Depth profile of the PA75 supported layer. A: Surface rich in C due to adventitious carbon deposition; B: Effective hybrid layer; C: Layer infiltrated in the γ-Al_2O_3 support; D: γ-Al_2O_3 support

The PA membranes do not show any dependence on the average pressure in gas permeance measurements. Such a pressure dependency of the permeance would be an indication for viscous flow through defects. In accordance with permporometry (Figure 2.4), the absence of viscous flow is therefore taken as an indication of the membrane quality and the absence of large defects [28]. In all cases minor (<10%) differences between the first and the second H_2 permeance measurement were observed, so no major structural changes occurred over the measurement series.

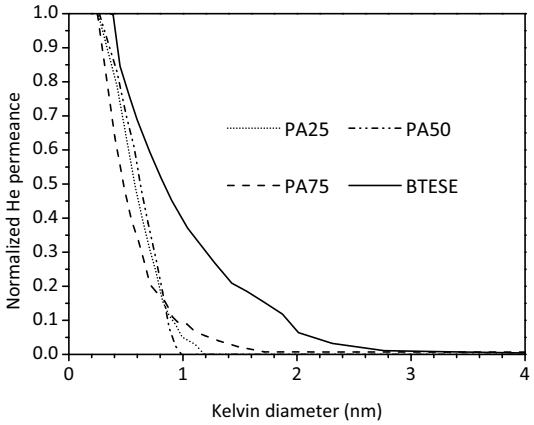

Figure 2.4. Normalized pore size distributions of the BTESE/PA membranes and a BTESE membrane

More importantly, the amount of PA in the BTESE matrix has a strong influence on the H_2 permeability. A nearly linear decrease of an order of magnitude was observed for the H_2 permeability with increasing PA molar concentration at constant temperature (Figure 2.5, as for all figures the lines connecting the data points are here to only guide the reader and are not a fitting) with very low values of about 1.10^{-5} mol.nm/m^2.Pa.s for PA75 and PA100. This trend was observed over a 200 K temperature range.

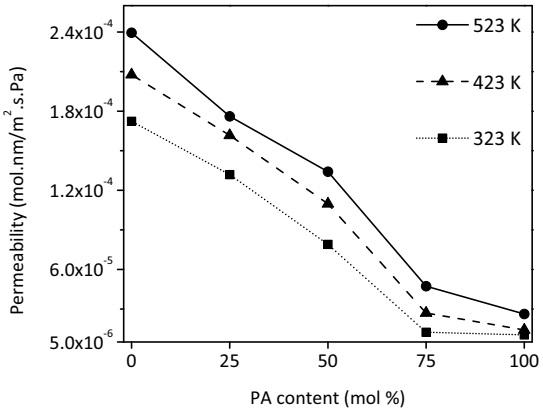

Figure 2.5. H_2 permeability as a function concentration of PA in the BTESE matrix at 323, 423, and 523K

The permeabilities are plotted against the kinetic diameter for all measured gases at different temperatures in Figure 2.6. For PA25 only minor H_2 and He permeability changes with temperature were observed, whereas for PA100 a major permeability increase was observed for these gases. In contrast, for PA25 the CO_2 permeability is significantly higher at the lowest measurement temperature of 323 K, whereas no temperature dependency of the CO_2 permeability was observed for PA100. The N_2 and CH_4 permeabilities were constant at all temperatures for both membranes. All membranes exhibited H_2/N_2 permeability ratios higher than the Knudsen value of 3.74 [29] (Table 2.2). This ratio is relatively constant at the measured temperatures for BTESE. However, the measurement temperature clearly affects the H_2/N_2 permeability ratio for the PA membrane series. At the lowest measurement temperature of 323 K, the BTESE membrane exhibited the highest ratio of 15.2 and the lowest ratios were found for PA25 and PA100. However at 523 K, all membranes showed ratios higher than 10 and even higher than 20 for PA75. Surprisingly, PA100 showed an equivalent ratio to BTESE at 523 K, despite its low performance at 323K. In contrast, all PA membranes show higher H_2/N_2 permeability ratio at higher temperatures. This effect seems to be stronger for higher concentrations of PA in the membrane. For PA100 the strongest relative increase of the H_2/N_2 permeability ratio was observed, ranging from 4.3 at 323 K to almost 13.9 at 523 K. This represents an increase of 220 %. This increase in ratio results from a higher H_2 permeability combined to a constant N_2 permeability.

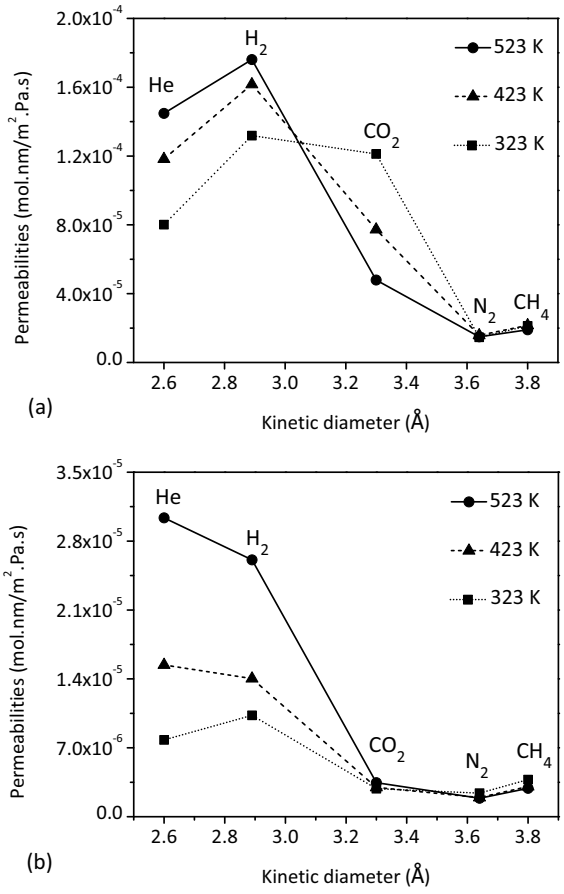

Figure 2.6. Permeability of PA25 (a) and PA100 (b) against the kinetic diameter of the gas at different measurement temperatures

The CO_2/N_2 permeability ratio was also affected by the temperature and the PA content. BTESE, PA25 and PA50 exhibited similar values at 323 K, while for PA75 and PA100 lower ratios were found at the same temperature. At the two higher measurement temperatures the CO_2/N_2 ratio drops for all membranes except the PA100. For this membrane type the CO_2/N_2 ratio increased slightly with temperature.

Table 2.2. H_2/N_2 and CO_2/N_2 permeability ratios of BTESE and BTESE/PA membranes at various temperatures

	H_2/N_2			CO_2/N_2		
Membrane	323K	423K	523K	323K	423K	523K
BTESE	15.2	14.5	13.6	10.0	4.9	3.2
PA25	9.0	10.3	11.8	8.3	4.9	3.2
PA50	13.7	15.1	16.9	9.1	5.8	3.6
PA75	12.1	18.8	20.7	4.0	4.9	2.9
PA100	4.3	7.2	13.9	1.2	1.5	1.8

Membrane performance in single gas permeance experiments clearly depends on the PA concentration in the BTESE matrix. In addition, the permporometry measurements indicate that water adsorbs strongly in the PA containing membranes. Therefore, we were interested if these effects would also translate to the water selectivity and transport through these membranes. To this end, all membranes were tested for dehydration of alcohol/water (95/5 wt%) mixtures by pervaporation. The PA membranes were first tested in the dehydration of EtOH/H_2O mixtures for several days. Subsequently, after drying at RT for two weeks, the membranes were used for dehydration of a *n*-BuOH/H_2O mixture, and finally again put in an EtOH/H_2O mixture without drying in between. The values presented are averaged over several days of testing.

In the first series of EtOH dehydration measurements all PA containing membranes exhibited water concentrations of 43-67 wt% in the permeate, compared to 90 wt% for a BTESE membrane (Figure 2.7). The lowest water concentration was observed for PA25 at 43 wt%, whereas the highest were for PA50 and PA75 with respectively 65 and 67 wt% of water in the permeate. In the separation of a *n*-BuOH/H_2O mixture all membranes exhibited water purities in the permeate of at least 93 wt%. Over the range of PA concentrations, a similar trend was observed as for the EtOH dehydration.

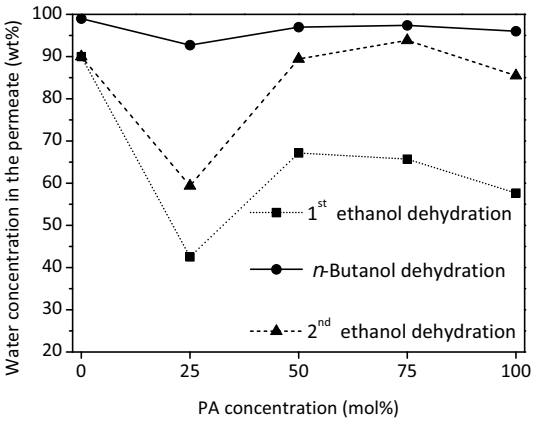

Figure 2.7. Water concentration in the permeate in the dehydration of EtOH and n-BuOH using BTESE/PA membranes

All membranes had a high selectivity in this separation and PA50 and PA75 were equivalent to the reference BTESE membrane. In the subsequent second dehydration test in the EtOH/H_2O mixture, all PA membranes exhibited a higher water concentration in the permeate than in the first measurement series. Interestingly, the differences between membranes over the range of PA concentrations are still the same in this second set of measurements. Apparently, the influence of the measurement sequence on the membranes was the same for all PA/BTESE ratios.

The amount of amino-functionalized precursor in the membrane has a pronounced influence on the selectivity for water. Therefore, we aimed to also explore the influence of the nature of the amino substituent on the membrane behaviour. To this end the IM/BTESE and LDA/BTESE mixed membranes were tested first in a *n*-BuOH/H_2O mixture and subsequently in a EtOH/H_2O mixture without intermediate drying.

For IM/BTESE membranes in *n*-BuOH dehydration, the same trend was observed as for PA/BTESE (Figure 2.8). All membranes, except the IM25, were highly selective for water. The selectivities of IM75 and IM100 are high and 95 and 92 wt% of water in the permeate were obtained respectively. In EtOH dehydration, a much lower selectivity was observed for IM25 giving only 40 wt% of water in the permeate. In this mixture, IM75 is slightly less selective than its 50 or 100 wt% counterpart.

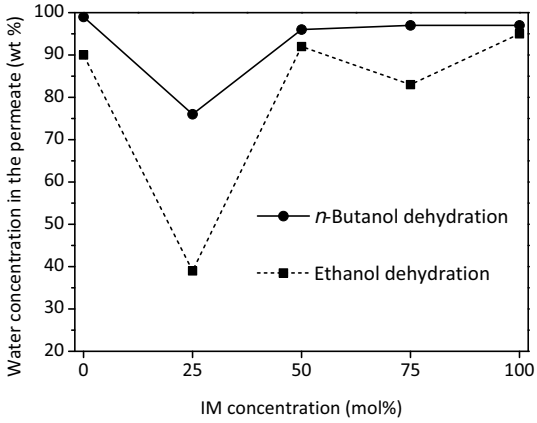

Figure 2.8. Water concentration in the permeate in the dehydration of EtOH and n-BuOH for IM/BTESE membranes

For all LDA/BTESE membranes in *n*-BuOH dehydration the water purities in the permeate were comparable to a BTESE reference membrane and in the range of 96 to 98 wt% (Figure 2.9). In EtOH dehydration the water concentration in the permeate ranged from 86 to 93 wt%. In this case no clear difference in selectivity was observed for any of the membranes compositions, in contrast to the other two precursors. Interestingly, the LDA75 and LDA100 membranes were highly selective for the separation of water from EtOH, having respectively 91 and 93 wt% of water in the permeate.

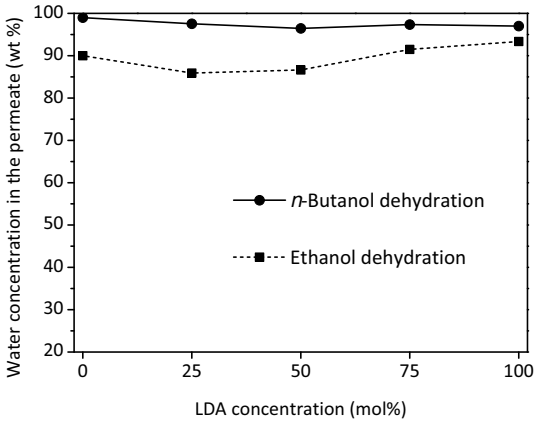

Figure 2.9 Water concentration in the permeate in the dehydration of ETOH and n-BuoH for LDA/BTESE membranes

The water fluxes ranged from 1.6 to 6.2 $kg.m^{-2}.h^{-1}$ in n-BuOH dehydration and from 0.2 to 3.4 $kg.m^{-2}.h^{-1}$ in EtOH dehydration (Table 2.3). For all membranes the fluxes in EtOH dehydration were a factor two to four lower than in n-BuOH dehydration. Only the IM50 membrane exhibited both a relatively high flux and high selectivity in EtOH dehydration, with 92 wt% of water in the permeate and a water flux of 2.4 $kg.m^{-2}.h^{-1}$. As a comparison, a previously published BTESE membrane exhibited 90 wt% of water in the permeate at a water flux of 1.5 $kg.m^{-2}.h^{-1}$ [9].

Table 2.3. Water fluxes ($kg/m^2.h$) of the three types of membranes for the dehydration of alcohol/water (95/5 wt %) mixtures

	PA	IM	LDA
Alcohol	J_{H2O}	J_{H2O}	J_{H2O}
n-BuOH	1.6-3.9	3.9-6.2	2.2-4.1
EtOH	0.2-2.1	1-3.4	0.35-1.1

2.4. Discussion

In this study three different amino functional precursors were successfully incorporated into an hybrid silica network over a wide range of molar ratios. The amino-functionalized precursors have a pronounced influence on the membrane properties, as is apparent from the gas permeance data and the performance in alcohol dehydration.

The thin hybrid layers proved to be free of macro defects, as no indications of viscous flow were found during single gas permeation. In addition, XPS confirmed the amine functionalization of the BTESE network. However the measured N/Si ratios on heat-treated membranes were significantly lower than those expected. Still and as expected, the N/Si ratio does increase with increasing amount of PA in the sol. Hence, the membranes properties can be attributed to the presence of these amino-functionalized precursors as well as to their concentration in the BTESE network.

All measurements suggest that the polar nature of the amine in PA enhanced the water adsorption capacity of the membranes. Combined to a microporous structure, this resulted in unprecedented gas tight membranes that are at the same time water permeable.

The low permeability of the PA membranes and the decrease of the H_2 permeability with increasing PA concentration can be ascribed to progressive pore blocking by adsorbed water. The AP25 slightly deviate from the trend. Nevertheless, this progressive increase of the water affinity of these membranes resulted in a significant decrease of the CO_2 affinity, as indicated by the large decrease of the CO_2/N_2 ratios from BTESE to PA100 and the constant CO_2 permeance of PA100 over the temperature range. This is probably due to inhibition of the N_2 transport and to the shielding of the possible CO_2 adsorption sites (NH_2 and/or OH) by adsorbed water. For CO_2, this prevents adsorption diffusion transport phenomena characterized by higher CO_2 permeances at lower temperatures observed for the BTESE membrane. The well-known formation of carbonates and/or carbamates on amine groups [30] could not be confirmed for our systems using XPS, as no shift of the N1s binding energy from 400 to 402 eV was detected. This means that the majority of the amine

groups is present as in a non-protonated form. The increasing temperature dependence of the H_2/N_2 permeability ratio at higher PA concentrations could be typical for activated transport in microporous membranes [31]. However, similar pores sizes were measured by permporometry for all compositions. As a result, a decrease of the pore size cannot explain this observation. We propose that the increase of the content of PA in the network leads to a more flexible membrane structure. This flexibility then enhances the mobility of the network at higher temperatures and in turn leads to a faster H_2 permeation. The permeances of N_2 and CH_4 are less affected, as the pores are too small for these gases.

Turning to the pervaporation experiments, all membranes show reasonable to high fluxes in alcohol dehydration, despite their low gas permeances. Interestingly, the PA membranes have a higher selectivity in EtOH/water after testing in *n*-BuOH/H_2O. Possibly, this is related to the formation of multilayered adsorption of water, blocking larger pores for transport of the organic component (EtOH). Alternatively, butanol is irreversibly attached to the membrane. This would be consistent with the frequently found flux decrease over time in long term dehydration experiments [8]. An aging phenomenon by further polymerization of the silica structure [26] is unlikely to explain this behavior, as the water flux is not affected and only the solvent flux decreases strongly.

In gas permeation experiments, the permeabilities are linearly dependent on the concentration of the amino precursor. On the other hand, a minimum amine loading seems to be required in pervaporation to reach the optimal membrane performances. The permeate stream for all pervaporation experiments showed a high water concentration in the permeate for both *n*-BuOH and EtOH dehydration. The only exceptions were PA25 and IM25. The N/Si ratios of these membranes were 0.04 and 0.016 respectively, which correspond to an amino-functionalized precursors loading of respectively 6.4 and 1.6 mol%. In contrast, PA50 and IM50 membranes showed Si/N ratios corresponding to amino-functionalized precursor loading of 11.5 and 5.5 mol% respectively. A bimodal pore size distribution has already been observed for membranes based on mixtures of BTESE and triethoxysilanes [9, 32]. It was ascribed to a limited interpenetration of the polymeric particles in the sol during drying.

This could be a possible explanation for the poor performances of the PA25 and IM25. A minimum loading of the BTESE network between 6.4 and 11.5 mol% of PA precursor and between l.6 to 5.5 mol% of IM is required to counter the performance decrease from the assumed bimodal distribution of the PA25 and IM25. The LDA is apparently more easily accommodated in the BTESE network membranes and showed a minimum loading of 12.5 mol% and therefore exhibited a constant high water purity in the permeate over the composition range.

This minimum loading also indicates that there is no need to strive for a higher amine concentration in these microporous hybrid membranes. A low concentration of terminally functionalized precursors enhances the network connectivity and this likely has a positive effect on the hydrothermal stability. XPS measurements show that a maximum loading of amino-functional groups in the BTESE matrix is reached, similarly to Periodic Mesoporous Organosilicas (PMOs) [33, 34]. The observed low N/Si ratios cannot arise from thermal degradation during heat treatment or PA evaporation, as the values for both the dried and heat treated powders were equal to those expected. A more likely explanation is that the relatively short reaction time of the PA molecules promoted the formation of small clusters by hydrogen bonding [27] and that only a limited fraction of the PA molecules reacts with the BTESE oligomers present in the sol. The largest particles in the sol are deposited on the surface of the γ-alumina layer support layer, whereas the smaller sized fraction infiltrates into the γ-alumina layer. The depth profile obtained by XPS confirms this infiltration of an PA rich sol. Using the current procedures a maximum of 13.5 % of PA and IM and 30-35% of LDA can be introduced in a BTESE network. Consequently, only small amounts of amino precursors are required to benefit from the hydrophilic properties of the amino-functionalized precursors.

2.5. Conclusions

We developed and characterized the first amino functionalized microporous hybrid silica membranes based on three precursors with different amine type, shape, and structure (PA,

IM and LDA). After optimization of the sol synthesis, defect free membranes were obtained. Although the degree of incorporation was lower than expected, the highly polar nature of amine groups resulted in an increasing adsorption of water molecules in the pores with increasing concentration of amine functional group. As a consequence, the H_2 permeability decreased by an order of magnitude in the range from pure BTESE to pure PA membranes. Lower affinity for CO_2 due to shielding of adsorption sites by the adsorbed water molecules was also observed. Pervaporation measurements clearly showed that a minimum loading of amino-functionalized precursor is required to obtain water selective membranes. This minimum loading depends on the precursor and is between 6.4 to 11.5 mol% for PA and between 1.6 and 5.5 mol% for IM. After a first n-BuOH dehydration and independent of the precursor, all membranes with an effective amino loading higher than this threshold value proved to be highly efficient in dehydration of both EtOH and *n*-BuOH with respective permeate water purities of at least 90 and 95 wt%. All of these results clearly showed the ability to modify the affinity of BTESE-based membranes by introducing a suitable precursor. The result of this is a membrane type that is gas tight and at the same time highly water permeable. Further flux/selectivity optimization may be possible in the range of 10-20 mol% of amino-functionalized precursor. The unique properties of these amino-functionalized precursors allow for selectivity improvement which is not solely dependent on pore size or defect control, but also on affinity, and therefore open up a highly promising option.

References

[1] C. Sanchez, B. Julian, P. Belleville, and P. Popall, Application of organic-inorganic nanocomposites, *Journal of Materials Chemistry*, 15, 3559-3592, 2005

[2] R.M. de Vos and H. Verweij, High-selectivity, high-flux silica membranes for gas separation, *Science*, 279, 1710-1711, 1998

[3] R.S.A. de Lange, J.H.A. Hekkink, K. Keizer, and A.J. Burggraaf, Formation and characterization of supported microporous ceramic membranes prepared by sol-gel modification techniques, J*ournal of Membrane Science*, 99, 1, 57-75, 1995

[4] H. Imai, H. Morimoto, A. Tominaga, and H. Hirashima, Structural changes in Sol-Gel derived SiO_2 and TiO_2 films by exposure to water vapor, *Journal of Sol-Gel Science and Technology*, 10, 45-54, 1997

[5] J. Campaniello, C.W.R. Engelen, W.G. Haije, P.P.A.C. Pex, and J.F. Vente, Long-term pervaporation performance of microporous methylated silica membranes, *Chemical Communications*, 834-835, 2004

[6] H.M. van Veen, Y.C. van Delft, C.W.R. Engelen, and P.P.A.C. Pex, Dewatering of Organics by Pervaporation with Silica Membranes, *Separation and Purification Technology*, 22-23, 361-366, 2001

[7] H.L. Castricum, A. Sah, R. Kreiter, D.H.A. Blank, J.F Vente, and J.E. ten Elshof, Hydrothermally stable molecular separation membranes from organically linked silica, *Journal of Materials Chemistry*, 18, 2150-2158, 2008

[8] H.M. van Veen, M.D. Rietkerk, D.P. Shanahan, M.M.A. van Tuel, R. Kreiter, H.L. Castricum, J.E. ten Elshof, and J.F. Vente, Pushing membrane stability boundaries with HybSi® pervaporation membranes, *Journal of Membrane Science*, 380, 124-131, 2011

[9] R. Kreiter, M.D.A. Rietkerk, H.L. Castricum, H.M. van Veen, J.E. ten Elshof, and J.F. Vente, Stable hybrid silica nanosieve membranes for the dehydration of lower alcohols, *ChemSusChem*, 2, 2, 158-160, 2009

[10] M. Michau and M. Barboiu, Self-organized proton conductive layers in hybrid proton exchange membranes, exhibiting high ionic conductivity, *Journal of Materials Chemistry*, 19, 6124-6131, 2009

[11] B.A. McCool and W.J. DeSisto, Amino-functionalized silica membranes for enhanced carbon dioxide permeation, *Advanced Functional Materials*, 15, 1635-1640, 2008

[12] H.L. Castricum, G.G. Paradis, M.C. Mittelmeijer-Hazeleger, R. Kreiter, J.F. Vente, and J.E. ten Elshof, Tailoring the Separation Behavior of Hybrid Organosilica Membranes by Adjusting the Structure of the Organic Bridging Group, *Advanced Functional .Materials*, 21, 9, 2319-2329, 2011

[13] N. Liu, R.A. Assink, B. Smarsly, and C.J. Brinker, Synthesis and characterization of highly ordered functional mesoporous silica thin films with positively chargeable -NH_2 groups, *Chemical Communications*, 1146-1147, 2003

[14] G.S. Caravajal, D.E. Leyden, G.R. Quinting, and G.E. Maciel, Structural characterization of (3-aminopropyl)triethoxysilane-modified Silicas by Silicon-29 and Carbon-13 Nuclear magnetic Resonance, *Analytical Chemistry*, 60, 1776-1786, 1988

[15] N. Gartmann, C. Schütze, H. Ritter, and D. Drühwiler, The effect of water on the functionalization of Mesoporous Silica with 3-Aminopropyltriethoxysilane, *J.Phys.Chem. Lett.*, 1, 1, 379-382, 2010

[16] J.C. Hicks, R. Dabestani, A.C. Buchanan, and C.W. Jones, Assesing site-isolation of amine groups on aminopropyl-functionalized SBA-15 silica materials via spectroscopic and reactivity probes, *Inorganica Chimica Acta*, 361, 3024-3032, 2008

[17] I.A. Rahman, M. Jafarzadeh, and C.S. Sipaut, Synthesis of organo-functionalized nanosilica via a co-condensation modification using γ-aminopropyltriethoxysilane (APTES), *Ceramics International*, 35, 1883-1888, 2009

[18] J.M. Rosenholm and M. Lindén, Wet-chemical Analysis of Surface Concentration of Accessible Groups on different Amino-functionalized Mesoporous SBA-15 silicas, *Chemistry of Materials*, 19, 5023-5034, 2007

[19] M. Durrieu, S. Pallu, F. Guillemot, R. Bareille, J. Amédée, and C.H. Baquey, Grafting RDG containing peptides onto hydroxyapatite to promote osteoblastic cells adhesion, J*ournal of materials Science: Materials in Medicine*, 15, 779-786, 2004

[20] E. Verné, C. Vitale-Brovarone, E. Bui, C. L. Binachi, and A. R. Boccaccini, Surface functionalization of bioactive glasses, *Journal of Biomedical Materials Research Part A*, 981-992, 2009

[21] G. Xomeritakis, C. Y. Tsai, and C. J. Brinker, Microporous sol-gel derived aminosilicate membrane for enhanced carbon dioxide separation, *Separation and Purification Technology*, 42, 3, 249-257, 2005

[22] G. Xomeritakis, C. Y. Tsai, Y. B. Jiang, and C. J. Brinker, Tubular ceramic-supported sol-gel silica-based membranes for flue gas carbon dioxide capture and sequestration, *Journal of Membrane Science*, 341, 1-2, 30-36, 2009

[23] B.C. Bonekamp, Preparation of Asymmetric Ceramic Membrane Supports by Dip-Coating, in: A.J. Burggraaf and L. Cot (Eds.), *Fundamentals of Inorganic Membrane Science and Technology,* Elsevier, Amsterdam, 1996

[24] F.T. Rusting, G. de Jong, P.P.A.C. Pex, and J.A.J. Peters, Sealing socket and method for arranging a sealing socket to a tube., WO 01/63162 A1or EP 1257758 B1, 2001

[25] T. Tsuru, T. Hino, T. Yoshioka, and M. Asaeda, Permporometry characterisation of microporous ceramic membranes, *Journal of Membrane Science*, 186, 2,257-265, 2001

[26] C.J. Brinker and G.W. Scherer, Sol-Gel Science-The Physics and Chemistry of Sol-Gel Processing, Academic Press, New York, 1990

[27] J.C. Hicks, R. Dabestani, A.C. Buchanan, and C.W. Jones, Spacing and site isolation of amine groups in 3-Aminopropyl-Grafted Silica Materials: The Role of Protecting Groups, *Chemistry of Materials*, 18, 5022-5032, 2006

[28] R. S. A. de Lange, Microporous sol-gel derived ceramic membranes for gas separation, Thesis Dissertation, University of Twente, 1993

[29] R.W. Baker, Membrane Technology and Applications, 2007

[30] V. Zelenak, M. Badanicova, D. Halamova, J. Cejka, A. Zukal, N. Murafa, and G. Goerigk, Amine modified ordered mesoporous silica: Effect of pore size on carbon dioxyde capture, *Chemical Engineering Journal*, 144, 336-342, 2008

[31] R.S.A. de Lange, K. Keizer, and A.J. Burggraaf, Analysis and theory of gas transport in microporous sol-gel derivated ceramic membranes, *Journal of membrane Science*, 104, 81-100, 1995

[32] C.J. Brinker, R. Sehgal, S.L. Hietala, R. Deshpande, D.M. Smith, D.A. Loy, and C.S. Ashley, Sol-gel strategies for controlled porosity inorganic materials, J*ournal of Membrane Science*, 94, 85-102, 1994

[33] M.C. Burleigh, M.A. Markowitz, M.S. Spector, and B.P. Gaber, Amine-functionalized Periodic Mesoporous Organosilicas, *Chemistry of Materials*, 13, 4760-4766, 2001

[34] M.C. Burleigh, M.A. Markowitz, M.S. Spector, and B.P. Gaber, Direct synthesis of Periodic Mesoporous Organosilicas: Functional Incorporation by Co-condensation with Organosilanes, *J.Phys Chem.B*, 105, 9935-9942, 2001

Chapter 3

Structural organization in hydrophobic hybrid silica xerogels

This chapter is submitted for publication. The published version might differ from this chapter. The paper will be published with the co-authors:
Goulven G. Paradis, Hessel L. Castricum, Robert Kreiter, and Jaap F. Vente

Abstract

In this chapter we report the synthesis and characterization of a novel class of hybrid microporous materials, with tunable hydrophobicity and degree of organization. The reaction conditions, the molar ratio and the nature of the precursor mixtures of 1,2-bis(triethoxysilyl) ethane (BTESE) and R-triethoxysilanes (RTES, R = C_1-C_{18} alkyl) had a profound influence on the prepared xerogels. The visual appearance of the xerogels varied from transparent, opaque, and opaque domains of about a few mm in a transparent matrix. Small Angle X-rays Scattering (SAXS) measurements showed the presence of nano-domains, arising from self-organization of the amphiphilic RTES precursors. These domains become more apparent for longer R-groups, higher RTES content, and increased [H^+]/[Si] and [H_2O]/[Si] ratios. The prehydrolysis of RTES lead to an increased degree of organization. The characteristic size of these domains ranges from 1.3 to 4.5 nm for R = C_3 and C_{18} respectively. In adsorption experiments, the higher carbon contents associated with the R-groups resulted in a lower CO_2 adsorption capacity. The CO_2 adsorption was less affected by the RTES/BTESE molar ratio. No N_2 adsorption was observed for the RTES/BTESE materials. Importantly, the introduction of the alkyl groups resulted in a hydrophobic character, related to the length and concentration of the R-group in the materials. The largest water contact angles measured was 111°.

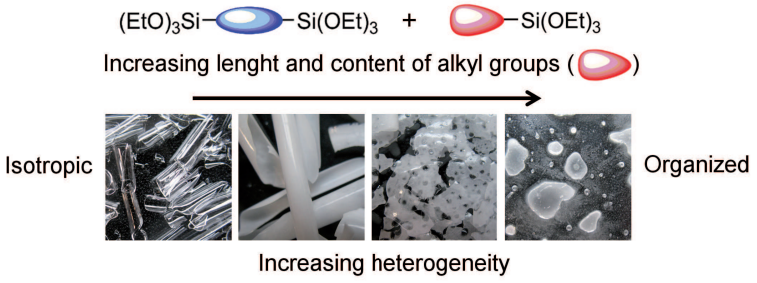

3.1. Introduction

Historically, the fabrication of inorganic (ceramic) materials has been based on the use of harsh synthesis conditions, while developments were mostly following trial and error [1]. A contrasting concept of chimie douce (mild chemistry) coined by Livage [2] in 1960s was inspired by the ability of diatoms to synthesize glass shells from dissolved silicates and opened up a new école de pensée (school of thought). It involved a bottom-up approach allowing the development of novel materials via understanding of materials chemistry and using mild synthesis conditions [1]. The sol-gel process, which involves the polycondensation of e.g. metal- or silica-alkoxyde precursors, is a typical route for this approach [3]. Temperatures and pressures close to ambient conditions are applied and the reactions (hydrolysis and condensation) are kinetically controlled. As a consequence, adjustment of the experimental synthesis conditions allows the control of the materials properties [4]. One of the major challenges in this field has been the control over the organization at nanometer scale of materials. A first synthetic route involves the use of Structure Directing Agents (SDAs) as pore templates. This was discovered in the early 1990s by Mobil researchers who used the self-organization properties of long-chain quaternary ammonium salts to develop the first siliceous materials with ordered mesopores: the well-known MCM series [5]. Remarkable is that the materials between the mesoporous is in a non-ordered glassy state. Their wide applicability as adsorbents or catalysts led to the development of numerous highly organized (hybrid) silica materials with different pore channel geometries as well as with diverse functionalities [1, 6-8]. Another route is based on the self-organization of the precursor itself through van der Waals, π-π or lipophilic interactions. Nanoscale materials with long-range order have been synthesized by hydrolysis and polycondensation of hybrid bridged polysilsesquioxanes with rigid phenyl or ethene bridges [9, 10], from pure alkyltrichlorosilanes or alkyltriethoxysilanes, or from mixtures of such precursors with tetramethoxysilane (TMOS) or tetraethoxysilane (TEOS) [11].

Materials synthesized from bridged silsesquioxanes currently receive much attention because of their excellent applicability as functional porous materials, for example as

molecular separation membranes [12-15]. Their excellent hydrothermal stability allows long-term operation (> 1000 days) at high temperature and under both solvent and water-rich conditions [15]. An additional field of interest is that of low-k materials in which the mechanical properties of the hybrid structure are beneficially used [16]. We have recently shown that the structure of the organic bridge can be adjusted to tailor the membrane towards specific applications [17]. Here, we report another strategy to modify the structure and adsorption properties of bridged organosilica, i.e. by the introduction of pendant alkyl groups. To this end, we performed co-condensation of 1,2-bis(triethoxysilyl)ethane (BTESE) together with alkyltriethoxysilanes (RTES) with various lengths for the alkyl group (Figure 3.1). We anticipated that this approach would result in a more hydrophobic material for the application in processes with non-polar solvents. Considering that two precursors are involved in the synthesis, we investigated the influence of the preparation procedure on the organization of the alkyl groups in the material. Membranes based on methyltriethoxysilane mixed with tetraethoxysilane (TEOS) [18] and BTESE [12] have already been reported. However to the best of our knowledge, no example of microporous materials based on BTESE mixed with R-triethoxysilanes (RTES, R = C_nH_{2n+1}, n > 1) has been reported. The influence of the length of the R-group (n = 1-18), the molar ration of RTES/BTESE, and the synthesis procedure, on the properties of the resulting xerogels were systematically investigated. The focus was on the contribution of these variables to the structural organization, the adsorption capacity, and hydrophobicity of these materials.

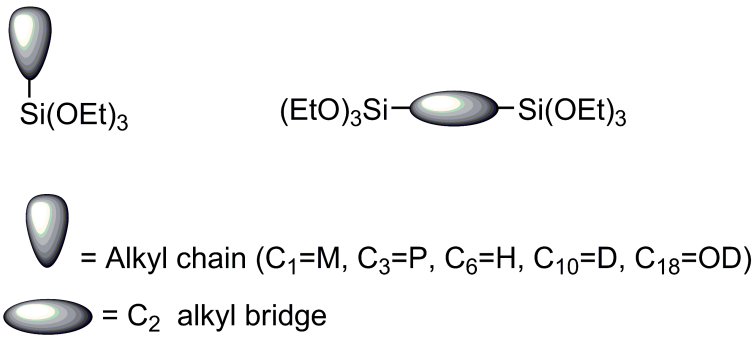

Figure 3.1. Precursor overview

3.2. Experimental

1,2-Bis(triethoxysilyl)ethane (BTESE, ABCR, 97%), methyltriethoxysilane (MTES, ABCR, 98%), *n*-propyltriethoxysilane (PTES, ABCR, 97%), *n*-hexyltriethoxysilane (HTES, ABCR, 95%), *n*-decyltriethoxysilane (DTES, ABCR, 97%), *n*-octadecyltriethoxysilane (ODTES, ABCR, 95%, 5-10% branched C_{18}-isomers), nitric acid (69 wt%, Aldrich), and ethanol (p.a. Aldrich) were used as received. Water was deionized at 18 MΩ/cm using a Millipore purification system.

The RTES/BTESE mixed sols were synthesized according to a two-step synthesis procedure. In all cases the required amounts of nitric acid and water were mixed beforehand. For sols in which the BTESE and RTES precursors were co-reacting from the start, both precursors were pre-mixed with ethanol. The sol preparation was started by adding the first half of the acid/water mixture in a drop wise manner under stirring to the precursor/EtOH mixture. After 90 minutes of continuous stirring, the second half of the acid/water mixture was added drop wise. Subsequently, the mixture was stirred another 1.5 hours, During the whole procedure the temperature was kept constant at 333 K. The amounts of precursor were varied to obtain molar concentrations of 25, 50, 75, and 90 mol% of RTES. For the equimolar HTES/BTESE composition and in addition to the above mentioned procedure, two other synthesis routes were explored. In these cases, one of the precursors was pre-reacted for 1.5 hours before the other precursor was added to the mixture together with the second part of the water/nitric acid mixture. The $[H_2O]:[H^+]:[Si]$ ratio was kept constant during the whole synthesis procedure. The sols containing only BTESE or only RTES were synthesized using a similar two-step synthesis procedure. Xerogels were prepared by drying 10 ml of the sols in Petri dishes under a fume hood. After complete drying, the material was ground and further characterization.

To determine the contact angles, glass microscope slides were coated by pouring sols onto leaning slides, which were subsequently dried vertically under atmospheric conditions. Ground xerogels and coated glass slides were heat treated at 523 K under N_2 for two hours with heating and cooling ramps of 0.5 °C/min. To remove all traces of oxygen, four vacuum/N_2 flushing cycles of one hour each were performed prior to the heat treatment.

The sols, xerogels and coated glass slides are named according to the used alkyltriethoxysilane and its molar concentration, the molar ratio of the sols and the two step synthesis used for the sol synthesis (Table 3.1).

Fourier-Transform IR Spectroscopy measurements were performed at 298 K on heat-treated powders, using a Diffuse Reflectance IR Fourier Transform cell in a Midac M4000 equipped with a Mercury-Cadmium-Telluride (MCT) detector. In specific cases, an ATR cell was used. All samples were stored for identical periods and under identical conditions (298 K and ambient air) prior to the FTIR measurements. TGA measurements were performed with a MT TGA/SDTA851 in pure oxygen. A heating ramp of 1°C/min was used.

SAXS measurements were carried out at the DUBBLE beamline BM-26B of the European Synchrotron Radiation Facility in Grenoble, France [19]. Scattering data were obtained with 16 keV X-rays. The samples were placed at a distance of 1.5 m from the detector and the intensity was measured in the range $0.4 < q < 8$ nm^{-1}. The raw data were corrected for the pixel-dependent detector sensitivity and integrated for channels with the same q values. In-situ drying experiments were carried out by using a specially designed set-up consisting of a vertically rotating cylinder covered with Kapton foil [20]. Scattering patterns were acquired at time intervals between 1 and 5 min. The system was heated using an IR lamp to promote quick drying. Measurements on xerogel samples were obtained by applying them onto a Kapton foil. The scattering intensity of Kapton foil under the same conditions was subtracted as background correction.

Nitrogen sorption measurements were performed on dried ($p < 10^{-4}$ mbar at 423 K) thermally treated xerogel powders on a Autosorb II at 77 K. Carbon dioxide isotherms were obtained on a Micromeritics Gemini VII at 273 K after drying overnight at 473 K in dry N_2. From the CO_2 adsorption isotherms, surface areas were calculated according to the Dubinin method, modified by Radushkevich [21]. From the micropore adsorption capacity ($cm^3.g^{-1}$) the micropore surfaces were determined assuming a molecular cross-sectional area of 0.179 nm^2 [22].

Contact angles were measured on the coated and heat-treated glass slides with a Krüss goniometer using water as the liquid phase. Static contact angle values were obtained using a sessile drop configuration and the Drop Shape Analysis 3 (DSA3) software from Krüss. Contact angles were measured at three different positions on each slide. For each position, the contact angle was measured five times within one second after deposition of the water drop.

Table 3.1. Overview of the recipes, codes, molar ratios of the sols and of the two steps synthesis used along the article

RTES used	RTES content (mol%)	Name	Molar ratios $Si/EtOH/H^+/H_2O$	Two-step synthesis procedure used for the sol synthesis
MTES	25	M25	1/6.36/0.08/3	Both precursors were pre-mixed with ethanol and co-reacted from the start
	50	M50		
	75	M75		
	90	M90		
PTES	25	P25		
	50	P50		
	75	P75		
	90	P90		
HTES	25	H25		
	50	H50		
	75	H75		
	90	H90		
DTES	25	D25		
	50	D50		
	75	D75		
	90	D90		
ODTES	50	OD50		
HTES	50	$H_2O/2$	1/6.36/0.08/**1.5**	
	50	H_2O*2	1/6.36/0.08/**6**	
	50	$H^+/10$	1/6.36/**0.008**/3	
	50	H^+*10	1/6.36/**0.8**/3	
	50	H/E	1/6.36/0.08/3	HTES was pre-reacted for 1.5 hours before BTESE was added together with the second part of the water/nitric acid mixture
	50	E/H	1/6.36/0.08/3	BTESE was pre-reacted for 1.5 hours before HTES was added together with the second part of the water/nitric acid mixture

3.3. Results and discussion

3.3.1 Sol and xerogel appearance

A series of sols with the BTESE and RTES precursors was synthesized using the molar ratios Si/EtOH/H^+/H_2O = 1/6.36/0.08/3. The R-triethoxysilanes (RTES, R=C_1-C_{10} alkyl) were mixed in ratios of 25, 50, 75, and 90 mol% with BTESE. For the longest RTES species ODTES (C_{18} alkyl) only the equimolar ratio with BTESE was chosen (Table 3.2). Most of the sols remained clear after three hours at 333 K. The D90 sol was turbid at 333 K under stirring and phase separated when stored at RT. The OD50 separated into two solid opaque phases immediately after addition of the acid/water mixture. The BTESE/HTES sols were clear at 333 K, but were turbid when cooled to 298 K for H50 and at higher molar ratios. Interestingly, all DTES/BTESE sols up to D75 remained clear after cooling to RT.

Table 3.2. Appearance of RTES/BTESE sols and xerogels over the range of compositions

Name	Sols		Xerogels		
	Clear	Turbid	Transparent	Opaque	Resin
M25	X		X		
M50	X		X		
M75	X			X	
M90	X			X	
P25	X		X		
P50	X			X	
P75	X			X	
P90	X				X
H25	X		X		
H50	333K	RT		X	
H75	333K	RT			X
H90	333K	RT			X
D25	X			X	
D50	X			X	
D75	X				X
D90		X			X
OD50		X		X	

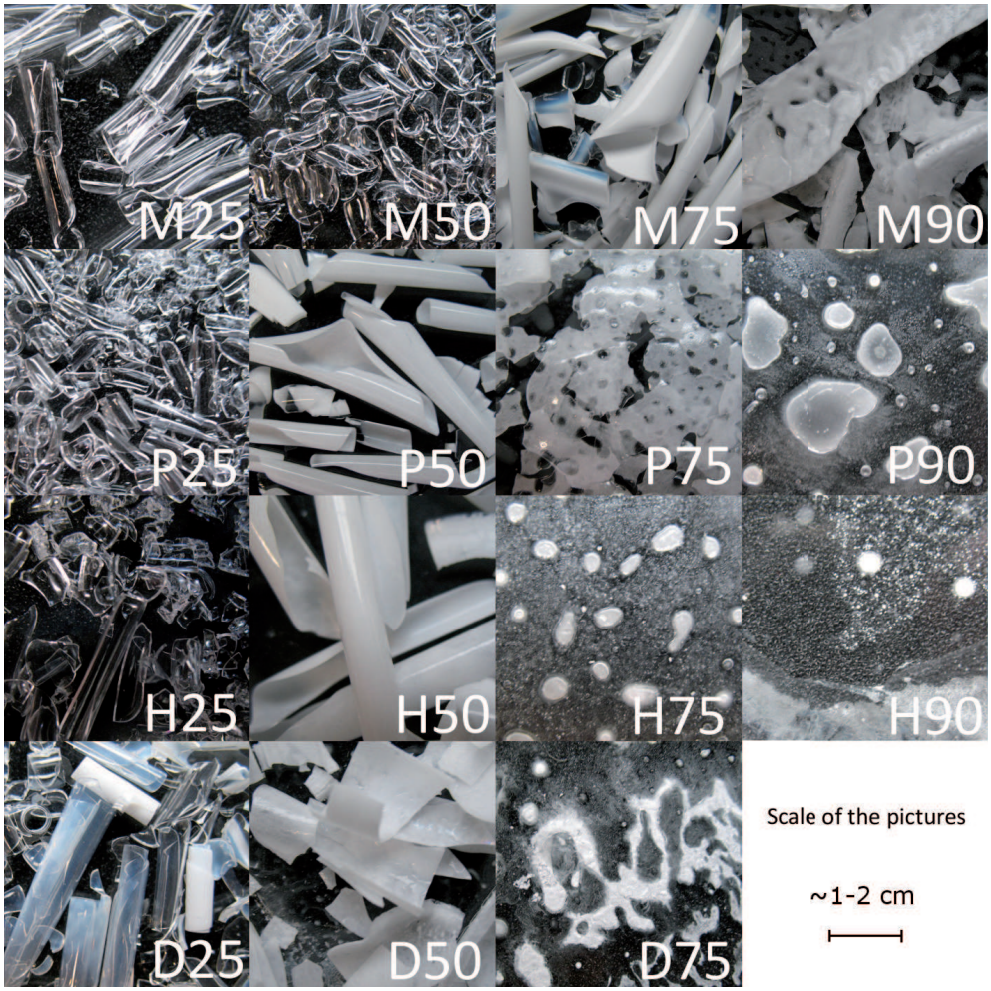

Figure 3.2. A selection of pictures of the xerogels after overnight drying

The length of the R-groups and the content of RTES drastically influenced the appearance of the xerogels (Figure 3.2). At a low content of RTES and a moderate length of the R-group (M25, M50, P25 and H25), transparent xerogels were obtained. At higher RTES content and for longer alkyl groups, the xerogels were either opaque (M75, P50, H50, D25 and D50) or opaque with transparent domains (M90 and P75). The combination of a high RTES content with long R-groups resulted in resinous materials, exhibiting either solid opaque domains surrounded by a transparent resin (P90, H75, H90, and D75) or a fully transparent resin (D90). These macroscopic indications for increased heterogeneity of the

xerogels for higher RTES contents and for longer R-groups were confirmed in microscope images at micrometer scale (Figure 3.3). The synthesis of sols from pure alkyltriethoxysilane precursors resulted in a clear sol for PTES, a turbid sol for HTES, and two liquid phases with different densities for DTES, which after drying all resulted in clear resins.

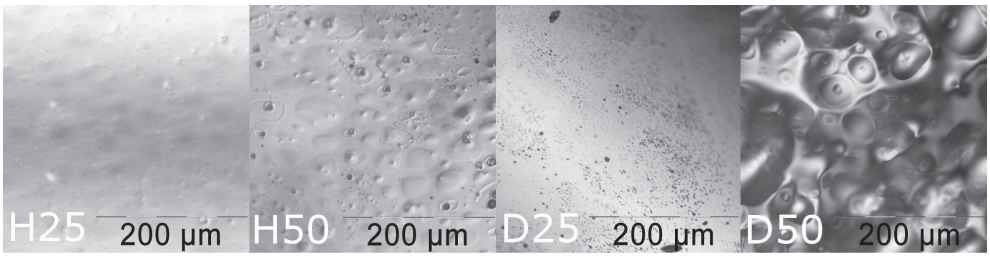

Figure 3.3. Optical microscope pictures of the surface of some dried xerogels

The equimolar HTES/BTESE mixture was selected to investigate the influence of different ratios of the reactant for the same base recipe on the final properties of the sols and xerogels. $[H_2O]/[Si]$ ratios of 1.5 and 6, and $[H^+]/[Si]$ ratios of 0.008 and 0.8 were used, while all other parameters were constant. The two-step synthesis procedure, the reflux time (3 hours), temperature (333 K) and the Si/EtOH ratio (6.36) were similar to the H50 sol (Table 3.1). Pre-reaction of each of the precursors (HTES or BTESE) before addition of the other was also investigated. Clear differences in the resulting sols and xerogels were observed (Table 3.3, Figure 3.4). The $[H_2O]/2$ and $[H^+]/10$ sols were clear, also at room temperature. After drying, opaque xerogels similar to H50 were obtained. The $[H_2O]*2$ and $[H^+]*10$ were initially turbid and subsequently phase separated after the second addition of the acid/water mixture. The resulting xerogels were opaque and contained bubbles.

The H/E and E/H sols were clear at 333 K and became turbid at RT, similar to the H50 sol. The E/H xerogel had the same appearance as H50, whereas the H/E xerogel contained transparent solid material and resin. Both the resin and solid material were compared to the dried HTES material and the pure BTESE xerogel using FTIR and TGA (Figure 3.4). The H/E resin and solid material showed similar weight losses as the pure HTES resin and pure BTESE flakes, respectively. Also the resin fraction of H/E and the pure HTES material exhibited identical FTIR spectra in the 2750-3050 wave number region, confirming that the resin fraction of the H/E xerogel contains mostly HTES oligomers.

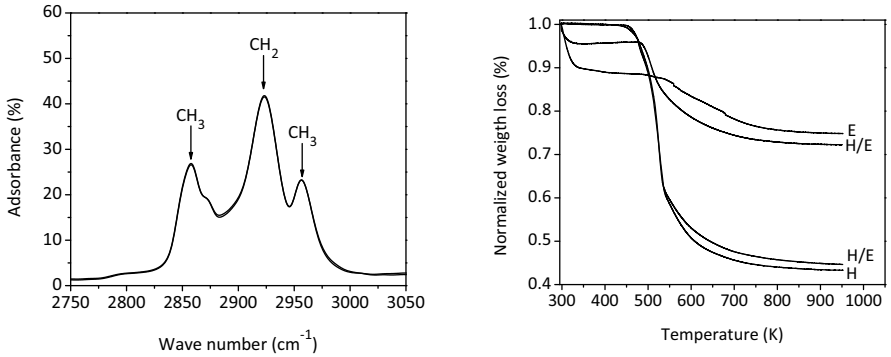

Figure 3.4. FTIR spectra of the oily phase of the H/E dried xerogel and of the pure HTES resin (left). TGA measurements of pure BTESE powder (E), pure HTES resin (H) and flacks and resin the H/E dried xerogels (H/E) (right)

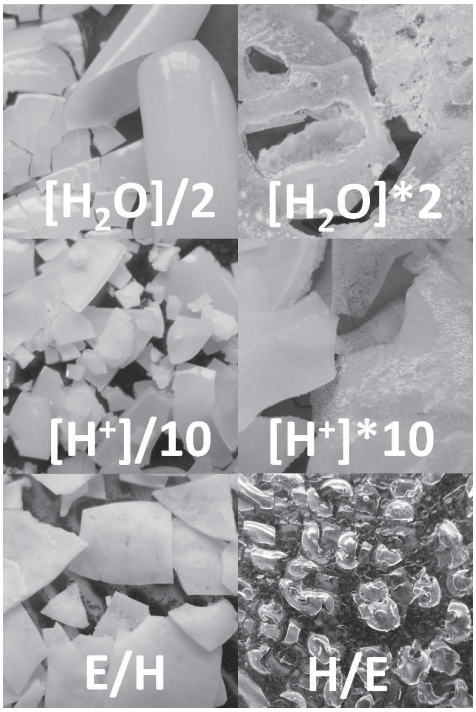

Figure 3.5. Pictures of HTES/BTESE xerogels obtained after different synthesis procedures

Table 3.3. Appearance of H50 sols and xerogels over the range of recipes

Name	Sols		Xerogels		
	Clear	Turbid	Transparent	Opaque	Resin
$[H_2O]/2$	X			X	
$[H_2O]*2$		X		X	
$[H^+]/[Si]/10$	X			X	
$[H^+]/[Si]*10$		X		X	
E/H	X	RT		X	
H/E	X	RT			X

Most of the sols were clear. Only in a few cases, especially for long alkyl chains and/or a large amount of alkyl groups, turbid or phase separated sols were observed. These effects presumably arise from the amphiphilic nature of the hydrolyzed RTES molecules. When the R-group of the molecules is sufficiently long and present above a critical concentration in the sol, the hydrophobic alkyl chains can interact and self-organize, while the hydrophilic heads condense to form micellar structures. This critical concentration is most likely dependent on the length of the R-group and on concentration of the RTES, and would result in more pronounced opaqueness or phase separation for longer R-groups and higher RTES concentrations. If these structures are small enough clear or weakly turbid sols are obtained. Large structures can lead to phase separation or even precipitation. Loy reports a similar phase separation for pure RTES-based sols in the presence of a substantial amount of water [23].

Similar arguments can be used to explain that only four xerogels (M25, M50, P25, H25) were transparent (Table 3.2). In the drying process, the RTES concentration increases and can reach the critical value. Probably not all the RTES can be incorporated in the BTESE backbone when the RTES concentration is high and the R-groups are long. We propose that this mixed RTES/BTESE fraction forms the opaque domains, while the remainder of the RTES-based species forms a resin for samples P90, H75, H90, and D75. In the extreme case of the D90 the accommodation in a BTESE matrix only occurs at a very low level and the formation of oligomers resulted in resinous materials after drying, similar to the pure RTES samples. The same phenomenon is likely to occur for the H/E recipe. The oligomeric structures, that are formed in the sol phase, separate in the dried material to a HTES based resin. In this specific sol mixture, the BTESE forms a separate network that

can be recognized from the transparent dried material. For E/H, the BTESE clusters that grow during the first 1h30 min likely exhibit open structures allowing accommodation of the HTES molecules. For HTES, high $[H_2O]/[Si]$ and $[H^+]/[Si]$ ratios possibly increased the polarity of the sol compared to the standard ratios. This would enhance the formation of micellar structures and decrease the solubility of these structures, leading to enhanced phase separation in the xerogels.

3.3.2 Presence of organic groups after thermal treatment

To ensure that the organic groups are present in the xerogels after heat treatment, drift FTIR measurements were performed on heat-treated powders of equimolar mixtures of RTES and BTESE (Figure 3.6). The characteristic symmetric and asymmetric stretching of the C-H bonds of the organic groups were observed between 2750 and 3050 cm^{-1}, similar to what was found in a previous study of MTES/BTESE materials [12]. The peak at about 2960 cm^{-1} is the CH_3 asymmetric in-plane C-H stretching, at 2925 cm^{-1} the CH_2 asymmetric stretching, the peak at 2855 cm^{-1} the CH_3 symmetric stretching and the one at 2800 cm^{-1} can be attributed to CH_2 symmetric stretching [24]. Clearly, the major part of the organic groups was intact after heat treatment and no indications were found that decomposition of the organosilica groups occurred. As expected, the intensity ratio of the peaks corresponding to CH_3 and CH_2 decreased for longer R-groups.

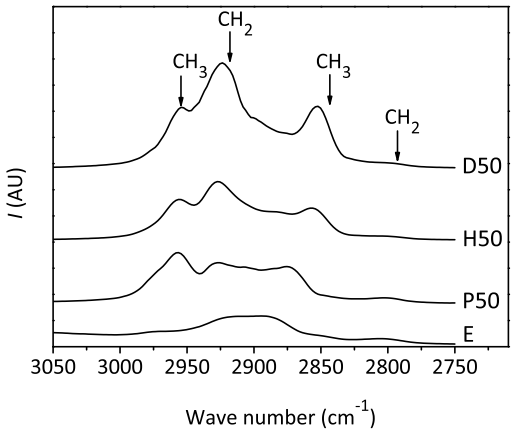

Figure 3.6. FTIR spectra of thermally treated unsupported RTES/BTESE-based xerogels as compared to a BTESE-based xerogel (E)

3.3.3 Microstructural organization-SAXS

Influence of the length of the R-group

SAXS scattering patterns were acquired on heat-treated RTES/BTESE powders to obtain structural information at the nm scale. For HTES/BTESE sols with alternative mixing procedures, in-situ drying experiments were also performed. SAXS patterns of the equimolar heat-treated xerogels showed different intensity profiles depending on the length of the R-group (Figure 3.7). A very broad peak superimposed onto a background signal is observed for all samples. While the background is nearly flat for the P50 xerogel, it becomes more pronounced for materials with increasing alkyl length and has a clear power-law dependency for OD50.

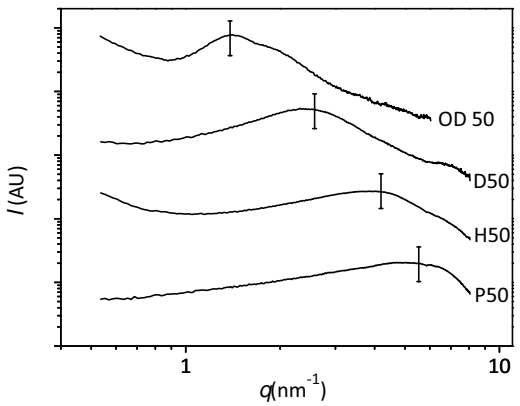

Figure 3.7. SAXS patterns of RTES/BTESE heat treated xerogels. For all graphs scattering curves have a fixed offset realtive to each other for sake of clarity. No absolute intensities have been measured.

For longer R-groups sharper and the more pronounced maxima were found at decreasing q-value. The peaks are too broad to be assigned to a regular long-range ordering similar to a crystalline network, but rather express the presence of organized domains at the nanoscale. This suggests that almost no organization is present in P50, whereas the increasingly defined peaks for the H50, D50, and OD50 xerogels indicate more pronounced organization. To better quantify the width of the maxima of intensity, background subtraction procedure using power law relations as a background was applied.

The relative widths of the asymmetric peaks (W) were calculated according to:

$$W = \frac{\left(\frac{q_m}{q_{hl}} + \frac{q_{hh}}{q_m}\right)}{2} \qquad (3.1)$$

With q_m the scattering vector of the maxima of intensity, and q_{hl} and q_{hh} the scattering vectors at the half of the intensity maximum at the low q side and at the high q side, respectively. Clearly, the relative width of the peak (W) decreased with the increase of the length of the R-group (Table 3.4), confirming the trend observed in figure 3.7.

Table 3.4. Relative width of the scattering maxima for P50, H50, D50, and OD50 xerogels

	P50	H50	D50	OD50
W	1.65	1.50	1.43	1.38

In addition, the positions of the maximum were found at lower q for longer R-groups. Considering that the scattering vector q is related to a correlation distance d in real-space as:

$$q \sim \frac{2\pi}{d} \qquad (3.2)$$

The maxima of intensity correspond to real-space correlation distances of 1.3±0.1, 1.7±0.1, 2.7±0.1 and, 4.5±0.1 nm for P50, H50, D50 and, OD50 respectively. These values indicate the dimensions of short-range organized domains at the nanometer scale.

This is the first observation of organization of RTES with BTESE precursors. Similar self-organization had been observed for mixtures of RTES with TMOS [25], which was explained by the amphiphilic properties of the RTES precursors. A relation between the measured correlation distance and the length of the alkyl group is shown in Figure 3.8. The length of a C-C bond can be estimated at 0.125 nm for an all-trans alkyl chain. This would mean that the measured basal spacings are equivalent to 10.5, 13, 22, and 36 C-C distances for P50, H50, D50, and OD50 respectively. For H50, D50 and, OD50, these values are equivalent to twice the length of the R-group in the precursor. The somewhat longer correlation distance

observed for PTES can be related to an overestimation due to the deflection of the scattering pattern at higher q, positioned at the upper edge of the measured range. Another cause of the observed larger correlation distance could be that RTES precursors with shorter alkyl chains will more readily co-react with BTESE. Incorporation of BTESE leads to somewhat larger mean structure sizes and may also explain the 'blurring' of the correlation peak at shorter alkyl lengths. For longer R-groups, the large polar-non polar contrast lowers the probability for a fully random and homogenous structure. Therefore, more defined structures with a higher degree of organization can be expected for longer R-groups, and therefore to sharper scattering maxima. While in a previous study involving organization in the presence of alkyl groups both layered and 2D-hexagonal structures have been observed [25-27], in our case the observed width of the peaks is too broad to allow a similar interpretation.

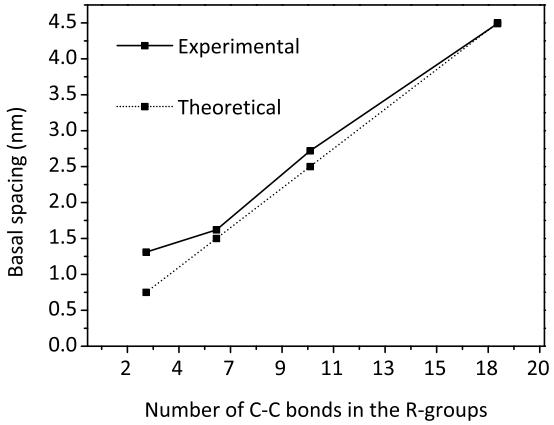

Figure 3.8. Comparison between the experimental and the theoretical basal spacing as a function of the length of the R-groups. The theoretical value is based on an all-trans bi-layered structure

Influence of the synthesis conditions

Since the degree of organization is strongly influenced by the length of the R-groups, we were interested if variations of the [BTESE]/[RTES], the [H^+]/[Si], and the [H_2O]/[Si] molar ratios, and the mixing sequence would also affect the xerogel structure. All of these studies were carried out for a HTES precursor.

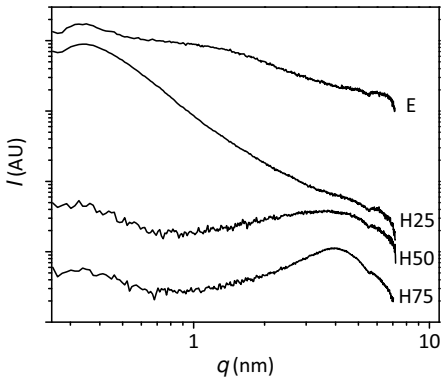

Figure 3.9. SAXS patterns of BTESE/HTES xerogels with different molar % of HTES in the BTESE matrix

The scattering patterns of xerogels with different HTES/BTESE ratios and of pure BTESE show strongly different levels of organization, similar to the series of R-groups (Figure 3.9). The BTESE sample showed no intensity maxima as a result of a purely isotropic network. The H25 exhibited a largely amorphous network with the first sign of the presence of a maximum of intensity at q between 3 and 5 nm^{-1}. Its patterns exhibited a power-law relation between q=0.5 and q=2, which could indicate a fractalic structure. The fitting the relationship $I \sim q^{-\beta}$ of the scattering pattern gives a value of the fractal dimension β of 2.44.

The H50 and H75 samples exhibited clear signs of nanoscale organization with maxima at a q of 3.9, corresponding to a basal spacing of about 1.7±0.1 nm. The relative width of the maximum observed for H75 (1.39) was somewhat smaller than that observed for H50. This suggests a slightly higher degree of organization in H75. The SAXS patterns indicate a homogenously co-condensed network at low HTES/BTESE ratio, with nearly all the HTES accomodated within the BTESE network. At higher HTES/BTESE ratios self-organized nanodomains were observed. This is in line with the visual appearance of the samples, which is transparent at 25 mol% of HTES and opaque at higher HTES molar concentrations.

The $[H^+]/[Si]$ and $[H_2O]/[Si]$ ratios affect the hydrolysis and condensation rates of the sol gel synthesis [3], whereas their effect on the xerogel structure is dependent on more factors. Clear gels were obtained for $[H^+]/10$ and $[H_2O]/2$ ratios while opaque gels with transparent bubbles were formed at high $[H^+]*10$ and $[H_2O]*2$ ratios. Surprisingly, limited changes in the xerogel structures were observed in the SAXS patterns (Figures 3.10 and 3.11). We therefore think that the acid and water ratios in the given ranges do not play a major role for the nanoscale ordering of these materials.

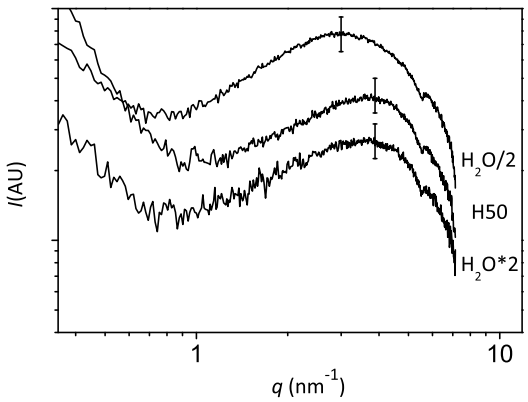

Figure 3.10. SAXS patterns of sintered the $H_2O/2$, H50 and H_2O*2 xerogels

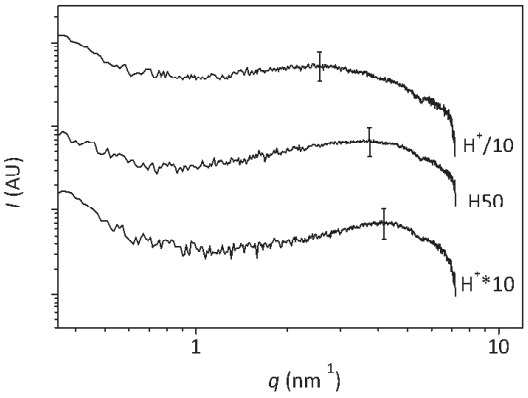

Figure 3.11. SAXS patterns of sintered the $H^+/10$, H50 and H^+*10 xerogels

Again, broad peaks were observed for all materials. The maximum of intensity is only slightly sharper for $[H_2O]/2$ but little difference can be found in shape between H50 and $[H_2O]*2$. In Table 3.5, the size of the domains corresponding to the scattering vector q of the peak maxima are reported. The trend towards a smaller basal spacing at a higher reactivity (acid or H_2O) again confirms the higher degree of short-range order for materials that also exhibit a heterogeneous visual appearance (Figure 3.5). The results suggest a higher nanoscale homogeneity for the materials with the lowest reactivity than the H50 material according to the parent conditions, despite their similar visual appearance.

Table 3.5. Domain size d corresponding to the value of q of the intensity maximum for different $[H^+]/[Si]$ and $[H_2O]/[Si]$ in BTESE/HTES xerogels

Xerogel	$[H^+]/[Si]$	$[H_2O]/[Si]$	*d* [nm]
$[H^+]/10$	0.008	3	2.7±0.1
$[H_2O]/2$	0.08	1.5	2.1±0.1
H50	0.08	3	1.7±0.1
$[H_2O]*2$	0.08	6	1.7±0.1
$[H^+]*10$	0.8	3	1.4±0.1

The effect of the addition order on the formation of the xerogel structure was also studied by in-situ acquisition of SAXS patterns during the drying process, carried out at 333 K (Figure 3.12). At the onset of drying all samples were transparent, and similar patterns were observed. While a change in slope can be observed around q = 5 nm^{-1}, the patterns look very similar to those of sols prepared from only BTESE and consisting of nm-sized colloids [17]. No indication was found in these sols for short-range ordering. During drying, enhanced signs of organization appeared in the formation of a distinct maximum of intensity for all three compositions. Clear differences were observed in the patterns of the dried xerogels. A broad peak of low intensity was present for H50. For E/H, this maximum was narrower and lower in intensity. For H/E, a narrower intensity maximum superimposed on a power-law background was observed. A power-law relation was also observed for pure BTESE-based and H25 xerogels.

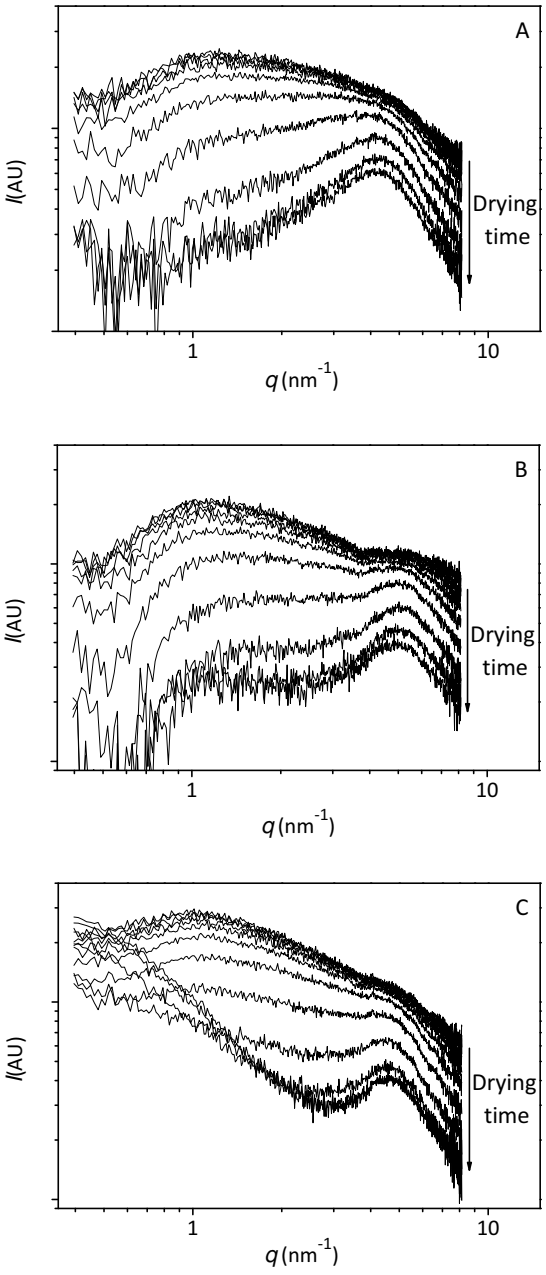

Figure 3.12. SAXS patterns of in-situ dried equimolar BTESE/HTES sols. A: H50, B: E/H and C: H/E

For precursors that self-organize via π-π interactions, Boury suggested that the self-organized nano-domains are already present during the sol synthesis and that the drying process promotes the formation of larger organized domains [28,29]. The same phenomenon possibly occurs for the amphiphilic precursor molecules described here. Importantly, agglomeration to larger organized domains is only observed after a certain time, i.e. after the evaporation of a certain amount of the solvent reaching the critical concentration of micelle formation. The different degrees of organization can be related to differences in growth mechanism depending on the order of precursor addition. The pre-reaction of BTESE results in a pre-condensed BTESE-based network which provides reactive (hydrolysed) sites onto which the RTES molecules can anchor. In addition, auto-organisation of hydrolyzed HTES molecules may still occur if sufficent HTES is present. Similarly, in the case of a co-reaction from the start of the synthesis, BTESE-BTESE, HTES-HTES and BTESE-HTES network bonds can all be formed. We have shown earlier that the condensation rates of silsesquioxane and alkyltriethoxysilane precursors are of the same order [30]. The structure is however more random as less BTESE-BTESE bonds have been formed before. This likely explains the broader correlation maximum for H50. If HTES is pre-reacted, hydrolysis of the ethoxy groups results in highly amphiphilic molecules that can readily self-organize and condense to form well-defined oligomers. The strongly apolar nature of the alkyl groups may prevent subsequent reaction with BTESE moieties. As a consequense, the BTESE molecules tend to form a separate phase next to that of the oligomeric RTES-based structures, rather than a random mixture. This leads to phase-separation upon drying and a resinous appearance of the HTES-based oligomers. The fractalic (power-law) structure observed in the SAXS pattern would thus be the result of the mostly BTESE-based network. A smaller basal spacing of 1.4 nm was again observed for the two more ordered networks, in which one precursor had pre-reacted, compared to 1.7 nm for the H50 material, in which the precursors had co-reacted. Smaller basal spacing confirms the higher degree of short-range order when one precursor pre-reacted. As the reactivity of the sols, in which the HTES pre-reacted, were similar the HTES molecules self-organized under similar structures with equivalent basal spacing.

3.3.4 Porosity and hydrophobicity of the hybrid xerogel

Molecular separation selectivity of hybrid silica membranes is based on a combination of pore size and affinity. As the presence of alkyl chains significantly influences the affinity of the material, it may also change the applicability of the materials in membrane separations [17, 31]. N_2 and CO_2 sorption measurements were performed on the heat-treated RTES/BTESE xerogels to investigate the effect of the incorporation of alkyl groups on the adsorption capacity (Table 3.6).

Table 3.6. Surface area ($m^2.g^{-1}$) of RTES/BTESE heat treated self-supported powders measured by CO_2 adsorption measurement. Some compositions could not be determined as the dried materials were resinous (n.a.)

	Mol % RTES			
Mol %	25 %	50 %	75 %	90 %
M	274	236	161	124
P	194	107	80	n.a.
H	70	56	26	n.a.
D	87	43	18	n.a.

All xerogels had zero adsorption of N_2, except M50 that had a small surface area of about 10 $m^2.g^{-1}$.This value could only be determined after two days of equilibration. The xerogels did adsorb CO_2 with much lower surface areas than that of xerogels of BTESE. For the latter material, a surface area of 379 $m^2.g^{-1}$ was measured, which is similar values reported earlier for a BTESE-based xerogel [17]. The CO_2 adsorption properties of the xerogels were inversely proportional to the length and content of the alkyl fraction: an increase of one of both resulted in a large decrease of the CO_2 surface area. Over the range of R-group lengths, for the equimolar RTES/BTESE xerogels a 5.5 times lower surface area (from 236 to 43 $m^2.g^{-1}$) was observed for R = C_{10} as compared to C_1. Over the range of compositions, the CO_2 surface area decreased by a factor of 1.7 (for MTES) to 5 (for DTES) for 75 mol% compared to 25 mol%. In the case of the largest alkyl content and the longest R-groups, the xerogels were nearly dense for CO_2.

The fact that zero adsorption was measured for N_2 and at the same time substantial adsorption of CO_2, despite their comparable kinetic diameters (0.364 and 0.33 nm respectively), is likely related to the low temperature of the N_2 sorption measurements (77 K). This result in kinetic hindrance of N_2 transport into the material and is probably associated with a high rigidity of the alkyl groups at low temperature [17]. From the absence of N_2 adsorption, we can conclude that no mesopores were present in the heat-treated xerogels.

The non-polar nature of the alkyl chains is likely responsible for the lower CO_2 surface area at higher RTES molar content or alkyl chain length. It has been shown before that inorganic silica exhibits a particular affinity for CO_2 due to the presence of silanols groups and that incorporation of methyl groups with MTES leads to weaker interactions [18]. The use of longer R groups and higher RTES concentrations is unfavorable to CO_2 adsorption as silanol groups are shielded by the hydrophobic alkyl chains. Only small differences were found between the surface areas of the HTES/BTESE-based xerogels synthesized with different $[H_2O]/[Si]$ and $[H^+]/[Si]$ ratios (Table 3.7). For the E/H xerogel, a surface area of 70 $m^2 \cdot g^{-1}$ was measured, which is slightly higher than for H50. No measurement was performed on the H/E xerogel as the xerogel was resinous. These differences are too small to relate the internal organization of the structure to the adsorption capacity of the materials.

Table 3.7. CO_2 adsorption measurement data of equimolar HTES/BTESE heat-treated xerogels with various $[H^+]/[Si]$ / $[H_2O]/[Si]$ ratios

	$[H^+]/[Si]$		$[H_2O]/[Si]$	
Ratios values	0.008	0.8	1.5	6
Surface area ($m^2.g^{-1}$)	64	76	62	53

Contact angle measurements on coatings of the xerogels on glass slides show an increase of the hydrophobicity at higher alkyl contents (Table 3.8). All RTES/BTESE materials showed contact angles higher than that of pure BTESE, for which a contact angle of 70° was measured. The length of the alkyl chain had a larger effect on the water contact angle than the actual molar RTES content. This suggests that a low fraction of the alkyl groups is sufficient to shield the silanol groups at the surface.

Table 3.8. Water contact angle of BTESE/ RTES sols coated on glass slides. Some compositions led to partially covered slides (n.a.)

	Mol % RTES			
	25	50	75	90
M	84	86	90	n.a.
P	85	89	98	n.a.
H	103	109	n.a.	n.a.
D	101	111	n.a.	n.a.

These observations were confirmed by the FTIR measurements that also indicate a more hydrophobic material for longer alkyl chains (Figure 3.13). For the BTESE-based material, the -OH stretching modes characteristic for water at 3000 to 3700 cm^{-1} and the HO-H bending mode at about 1625 cm^{-1} are clearly visible. For P50 these peaks are significantly smaller as compared to the alkyl spectroscopic region (2800-3000 cm^{-1}), and they are even absent for H50 and D50. Prior to the measurements, all materials were stored under the same atmospheric conditions at 298 K for the same period. Therefore, the clear difference in intensity of these peaks can only be explained by a significantly lower amount of adsorbed water in the pores due to the presence of the R-groups in the hybrid network.

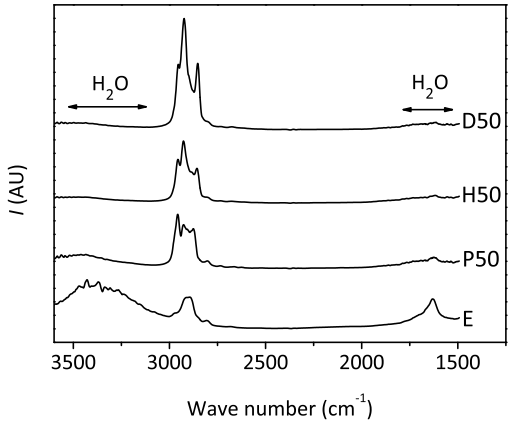

Figure 3.13. FTIR spectra of thermally-treated unsupported equimolar RTES/BTESE materials as compared to BTESE exhibiting the hydrophobic nature of the RTES/BTESE materials

3.3. Conclusions

We have developed a range of hybrid silica materials based on mixtures of BTESE and R-triethoxysilanes (RTES, R = C_1-C_{18} alkyl). The RTES/BTESE ratio was varied between 0.33 and 9. Clear differences were observed in the micro- and macro structures of the dried xerogels. At low alkyl content the xerogels are transparent, opaqueness and inhomogeneity was observed at higher alkyl content, and phase separation was found for conditions with long alkyl groups and high alkyl content. The heterogeneity of the xerogels is most likely related to the amphiphilic nature of the hydrolyzed RTES moiety, allowing the R-groups to self-organize into hydrophobic domains. In this process, the non-polar R-groups interact softly through Van-der-Waals interactions, while the polar silicon hydroxides condense to form oligomeric structures. At high $[H_2O]/[Si]$ or $[H^+]/[Si]$ ratios, which are considered more reactive conditions, more inhomogeneous materials were formed than under milder conditions. Under conditions where the RTES precursor is allowed to pre-react, low accommodation (i.e. higher self-organization) of the RTES in the BTESE matrix is observed. This can be related to a higher probability of the formation of self-organized oligomeric structures that are further unreactive. SAXS measurements confirmed the presence of organized nano-domains, especially for those compositions that form turbid or phase-separated xerogels. For such samples a higher degree of organization was observed at the nano-scale, with narrow and pronounced scattering intensity maxima, compared to the transparent samples.

The gas adsorption capacity and hydrophobicity of the series of materials are strongly influenced by the introduction type of R-group into the BTESE matrix. All RTES/BTESE xerogels are dense for N_2, whereas the CO_2 surface areas are down to a factor of 20 lower than a BTESE xerogel. We relate this phenomenon to a lower availability of adsorption sites due to the extensive presence of alkyl groups. As additional evidence for the effect of the R-groups, a substantial increase of the water contact angle was observed compared to the BTESE-based xerogel. Interestingly, the length of the R-group has a more pronounced effect on the water contact angle than the RTES content.

The fact that the polarity and the microstructure of organic-inorganic hybrid silica materials can be tuned by the introduction of a terminal alkyl fragment is highly relevant for future applications. It is shown that transparent xerogels can be obtained for the complete range of precursors from C_1 up to C_6 with a RTES/BTESE ratio of 0.25. In addition, it is clear that low concentrations of the R-group have a pronounced influence on the material properties. We foresee excellent applicability of this class of materials in cases where affinity for or rejection of specific components is required. Specifically, we are aiming at membranes that allow separation based on polarity, whilst retaining the excellent stability and mechanical properties of the hybrid silica structure.

References

[1] C. Sanchez, L. Rozes, F. Ribot, C. Laberty-Robert, D. Grosso, C. Sassoye, C. Boissière, and L. Nicole, ''Chimie douce'': A land of opportunities for the designed construction of functional inorganic and hybrid organic-inorganic nanomaterials, *C.R.Chimie*, 13, 3-39, 2010

[2] J. Livage and J. Lemerle, Transition Metal Oxide Gels and Colloids, *Annual Review of Materials Science*, 12, 103-122, 1982

[3] C.J. Brinker and G.W. Scherer, Sol-Gel Science-The Physics and Chemistry of Sol-Gel Processing, Academic Press, New York, 1990

[4] G. Cerveau, R.J.P. Corriu, and E. Framery, Nanostructured organic-inorganic hybrid materials: kinetic control of the texture, *Chemistry of Materials*, 13, 3373-3388, 2001

[5] J.S. Beck, J.C. Vartuli, W.J. Roth, M.E. Leonowicz, C.T. Kresge, K.D. Schmitt, C.T.W. Chu, D.H. Olson, E.W. Schepard, S.B. McCullen, J.B. Higgins, and K.D. Schmitt, A New Family of Mesoporous Molecular Sieves Prepared with Liquid Crystal Templates, *Journal of the American Chemical Society*, 114, 10834-10842, 1992

[6] F. Hoffmann and M. Froba, Vitalising porous inorganic silica networls with organic functions - PMOs and related hybrid materials, *Chemical Society Reviews*, 40, 608-620, 2011

[7] K. Kanamori and K. Nakanishi, Controlled pore formation in organotrialkoxysilane-derivated hybrids: from aerogels to hierarchically porous monoliths, *Chemical Society Reviews*, 40, 2,754-770, 2011

[8] A. Mehdi, C. Reye, and R.J.P. Corriu, From molecular chemistry to hybrid nanomaterials. Design and functionalization, *Chemical Society Reviews*, 40, 2,563-574, 2011

[9] B. Boury and R.J.P. Corriu, Auto-Organization in Sol-Gel Type Polycondensation: A Door to the Nanosciences, *The Chemical Record*, 3, 120-132, 2003

[10] K.J. Shea and D.A. Loy, Bridged polysilsesquioxanes. Molecular-engineered hybrid organic-inorganic materials, *Chemistry of Materials*, 13, 3306-3319, 2001

[11] A. Shimojima and K. Kuroda, Designed Synthesis of Nanostructured Siloxane–Organic Hybrids from Amphiphilic Silicon-Based Precursors, *The Chemical Record*, 6, 53-63, 2006

[12] H. L. Castricum, A. Sah, R. Kreiter, D.H.A. Blank, J.F. Vente, J.E. and ten Elshof, Hydrothermally stable molecular separation membranes from organically linked silica, *Journal of Materials Chemistry*, 18, 2150-2158, 2008

[13] M. Kanezashi, K. Yada, T. Yoshioka, and T. Tsuru, Organic–inorganic hybrid silica membranes with controlled silica network size: Preparation and gas permeation characteristics, *Journal of Membrane Science*, 348, 310-318, 2010

[14] R. Kreiter, M.D.A. Rietkerk, H.L. Castricum, H.M. van Veen, J.E. ten Elshof, and J.F. Vente, Stable hybrid silica nanosieve membranes for the dehydration of lower alcohols, *ChemSusChem*, 2, 2, 158-160, 2009

[15] H.M. van Veen, M. D.A. Rietkerk, D.P. Shanahan, M.M.A. van Tuel, R. Kreiter, H.L. Castricum, J.E. ten Elshof, and J.F. Vente, Pushing membrane stability boundaries with HybSi® pervaporation membranes, *Journal of Membrane Science*, 380, 124-131, 2011

[16] G. Dubois, W. Volksen, T. Magbitang, M.H. Sherwood, R.D. Miller, D.M. Gage, and R.H. Dauskardt, Superior mechanical properties of dense and porous organic/inorganic hybrid thin films, *Journal of Sol-Gel Science and Technology*, 48, 1,187-193, 2008

[17] H.L. Castricum, G.G. Paradis, M.C. Mittelmeijer-Hazeleger, R. Kreiter, J.F. Vente, and J.E. ten Elshof, Tailoring the Separation Behavior of Hybrid Organosilica Membranes by Adjusting the Structure of the Organic Bridging Group, *Adv.Func.Mater*, 21, 9, 2319-2329, 2011

[18] R.M. de Vos, W.F. Maier, and H. Verweij, Hydrophobic silica membranes for gas separation, *Journal of Membrane Science*, 158, 1-2, 277-288, 1999

[19] W. Bras, SAXS/WAXS experiments using extreme sample environments, Nuclear Instruments and Methods in Physics Research Section B: Beam Interactions with Materials and Atoms, 199, 90-97, 2003

[20] T.M. Stawski, S.A. Veldhuis, H.L. Castricum, E.G. Keim, G. Eeckhaut, W. Bras, D.H.A. Blank, and J.E. ten Elshof, Development of nanoscale inhomogeneities during drying of sol-gel derived amorphous lead zirconate titanate precursor thin films, *Langmuir*, 27, 17, 11081–11089, 2011

[21] M.M. Dubinin, Progress in Surface and Membrane Science, New York, 1975

[22] © Micromeritics Instrument Corporation 2009-10, Gemini VII 2390 operator's manual V1.03, 2010

[23] D.A. Loy, C.R. Baugher, B.M. Baugher, D.A. Schneider, and K. Ramihian, Substituent Effects on the Sol-Gel Chemistry of organotrialkoxysilanes, *Chemistry of Materials*, 12, 3624-3632, 2000

[24] M.D. Porter, T.B. Bright, D.L. Allara, and C.E.D. Chidsey, Spontaneously Organized Molecular Assemblies. 4.Structural Characterization of n-Alkyl Thiol Monolayers on Gold by Optical Ellipsometry, Infrared Spectroscopy, and Electrochemistry, J*ournal of the American Chemical Society*, 109, 3559-3568, 1987

[25] A. Shimojima, N. Umeda, and K. Kuroda, Synthesis of Layered Inorganic-Organic Nanocomposite Films from Mono-, Di-, and Trimethoxy(alkyl)silane-Tetramethoxysilane Systems, *Chemistry of Materials*, 13, 10, 3610-3616, 2001

[26] A. Shimojima, Y. Sugahara, and K. Kuroda, Inorganic-organic layered materials Derived via hydrolysis and polycondensation of trialkoxy(alkyl)silanes, *Bulletin of the Chemical Society of Japan*, 70, 2847-2853, 1997

[27] A. Shimojima, Z. Liu, T. Ohsuna, O. Terasaki, and K. Kuroda, Self-Assembly of Designed Oligomeric Siloxanes with Alkyl Chains into Silica-Based Hybrid Mesostructures, *Journal of the American Chemical Society*, 127, 14108-14116, 2005

[28] B. Boury and R. J. P. Corriu, Auto-organisation of hybrid organic-inorganic materials prepared by sol-gel process, *Chemical Communications*, 795-802, 2002

[29] B. Boury, F. Ben, R.J.P. Corriu, P. Delord, and M. Nobili, Control of the anisotropic organization of nanostructured silica-based hybrid materials, *Chemistry of Materials*, 14, 730-738, 2002

[30] H.L. Castricum, A. Sah, J. Geenevasen, R. Kreiter, D.H.A. Blank, J.F. Vente, and J.E. ten Elshof, Structure of hybrid organic-inorganic sols for the preparation of hydrothermally stable membranes, *Journal of Sol-Gel Science and Technology*, 48, 11-17, 2008

Chapter 4

From hydrophilic to hydrophobic HybSi® membranes: a change of affinity and applicability

This chapter is submitted for publication. The published version might differ from this chapter. The paper will be published with the co-authors:

Goulven G. Paradis, Donough P. Shanahan, Robert Kreiter, Henk M. van Veen, Hessel L. Castricum, Arian Nijmeijer, and Jaap F. Vente

Abstract

The present study describes the effect of the presence of terminating alkyl groups on the performance of organic-inorganic hybrid silica membranes. By incorporation of different R-triethoxysilanes (R = C_1 to C_{10} alkyl) into 1,2-bis(triethoxysilyl)ethane (BTESE) based materials the affinity could be tailored from hydrophilic to hydrophobic. The separation properties of the membrane based on these materials was found to be strongly dependent on the length of the R-group. Gas permeance measurements indicated reduced molecular sieving properties and an enhanced affinity for CO_2 for longer R-groups. Longer R-groups also resulted in lower permeate water purity, falling from >99% to ~40 for C_{10} in the dehydration of *n*-butanol/water (95/5 wt%) by pervaporation. Concomitantly, the permeate n-butanol purity in the pervaporation of *n*-butanol/water mixtures (0.5 to 6.8 wt% of n-butanol) increased to a value of >40% for R = C_{10}. This membrane exhibited constant separation factors over a large range of temperatures (30 to 90 °C) and *n*-butanol feed concentrations (0.5 to 6.8 wt%). By increasing the temperature from 30 to 90 °C, the *n*-butanol flux reached a value as high as 3 kg/m^2.h for a feed mixture containing 4.5 wt% of *n*-butanol.

4.1. Introduction

The separation or purification of alcohol/water mixtures is performed using capital- and energy-intensive distillation. To replace distillation, less energy demanding separation processes as gas stripping, stream stripping, liquid-liquid extraction can be used [1, 2]. Among them, also organophilic pervaporation is considered to be a viable alternative for alcohols separation from aqueous solutions [1-3]. The membrane development has been focused on hydrophobic, polymeric materials [1, 3-6]. Recently, we developed hybrid organic-inorganic HybSi® membranes to overcome the stability boundaries of inorganic silica [7]. The introduction of an organic fragment in a silica network by using ethylene-bridged bis-silane precursors lead to membranes having a life time of over 1000 days in alcohol dehydration at high temperatures (150 °C) without a decrease in the selectivity [8]. The intrinsic hydrophilicity of this bridged organic silica limits the applicability of these membranes to the separation of polar from less polar molecules. However, by changing the nature/structure of the precursors and the content of organic fragments in the hybrid silica network, the membrane behavior can be controlled [9-11]. For example, the introduction of functional amine groups in the network resulted in highly water-permeable hydrophilic membranes [11]. This implies that the incorporation of well-defined organic groups can be used to tailor the membrane affinity to specific applications. In the current study, we aim to develop intrinsically hydrophobic membranes by the introduction of precursors with large organic fragments in the hybrid silica network. Combined with the proven solvent and water stability of the hybrid membrane material, this approach was designed to result in stable hydrophobic hybrid silica membranes that would be suitable for a range of solvent separation processes. Such processes include upgrading of bioalcohol/water mixtures to fuel grade and harvesting of valuable alcohols from aqueous process streams [12, 13].

Here, we present the development and characterization of such hydrophobic membranes. The membranes were developed starting from the precursor 1,2-bis(triethoxysilyl)ethane (BTESE). This precursor with a bridging organic group is commonly used for the preparation of hydrophilic hybrid silica HybSi® membranes. To introduce a hydrophobic character in

these membranes, terminating alkyl-groups, R-triethoxysilanes (RTES, R = C_1 to C_{10} alkyl), were added during the preparation (Figure 4.1). The relations between the alkyl chain length, the pore size and the affinity of the membranes were studied. The performances of all membranes in pervaporation were measured in the dehydration of *n*-butanol for butanol-rich mixtures, and in the recovery of n-butanol for water-rich mixtures. The influence of the operating conditions on the performance of the most promising membrane was subsequently determined. Finally, the applicability of these membranes in bio-butanol recovery from fermentation broths is compared to other organophilic membranes.

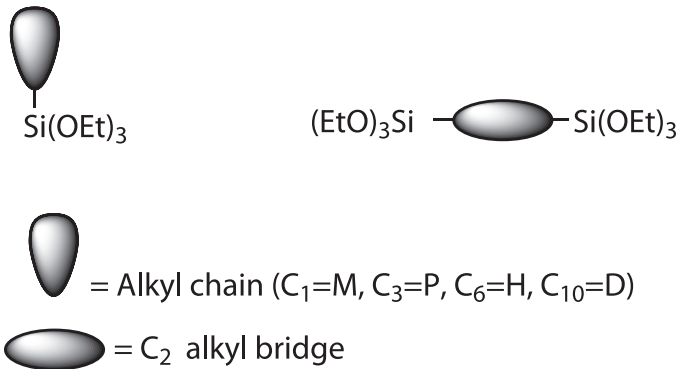

Figure 4.1. Precursors used in this study

4.2. Experimental

Materials

1,2-Bis(triethoxysilyl)ethane (E, ABCR, 97%), methyltriethoxysilane (M, ABCR, 98%), *n*-propyltriethoxysilane (P, ABCR, 97%), *n*-hexyltriethoxysilane (H, ABCR, 95%), *n*-decyltriethoxysilane (D, ABCR, 97%), nitric acid (69 wt%, Aldrich), and EtOH (p.a., Aldrich) were used as received. Water was deionized at 18 MΩ/cm using a Millipore purification system. Pervaporation measurements were performed with distilled water and *n*-butanol (P.A. grade) from Aldrich. The membranes are further named according to the precursors used: the letter E refers to pure BTESE membranes and for the other membranes the letters M, P, H, D refer to the alkyltriethoxysilanes introduced in the BTESE-based hybrid silica network. The precursors were present in equimolar ratios.

Membrane development

The BTESE/RTES mixed sols were synthesized according to a two-step synthesis procedure. In all cases, the preparations were started by mixing the required amounts of nitric acid and water, and by diluting, the 1:1 ratio of BTESE and RTES precursors with ethanol. Half of the acid/water mixture was then added dropwise under stirring to the precursor/EtOH mixture, and kept at 333 K under continuous stirring for 1.5 hours. Subsequently, the second half of the acid/water mixture was added dropwise, while keeping the mixture at 333 K, after which this mixture was stirred during another 1.5 hours at 333 K. All the sols were synthesized with overall compositional ratios of $Si/EtOH/H^+/H_2O = 1/6.36/0.08/3$.

After adjustment of the silica sol concentration, sols were filtered over 0.8 µm cellulose acetate filters (Whatman®). Membrane coatings were applied in a class-1000 cleanroom on 30 cm long tubular supports composed of α-Al_2O_3 layers and a final smooth mesoporous γ-Al_2O_3 layer [14]. After overnight drying in the clean room, the membranes were heat treated at 523 K under N_2 for two hours with heating and cooling rates of 0.5 °C/min. Four cycles of vacuum/N_2 purge of one hour each were performed before the start of the heat treatment. All membranes were sealed using stainless steel caps and graphite as packing material [15].

Supported film characterization

Layer thickness determinations and surface observations were carried out on samples taken from the middle of the heat treated membranes by means of a high resolution JEOL JSM-6330F Field Emission scanning Electron Microscope (SEM). Single gas permeance measurements were performed at 523, 423 and 323 K with feed pressures from 3 to 9 bara. Pressure differences of 2 bar were applied except for the point at 2 bar feed pressure for which a pressure difference of 1.5 bar was used. A bleed of 50 ml/min was applied for all measurements. Measurements were performed using He, H_2, N_2, CH_4, and CO_2 (99.999% pure). Before starting the measurement, each membrane was dried in the setup for two hours at 523 K under N_2. H_2 permeance measurements were performed both as first and last measurement. The gas permeabilities were calculated based on the permeances and the layer thicknesses measured by SEM. The pictures of water drops were taken at a fixed distance with drops of 10 µl deposed manually on the surface of the tubular membranes using a Mettler Toledo micro-pipette.

Membrane performance

The pervaporation measurements were performed on a standard glass pervaporation setup, as described in detail by Van Veen [8]. The *n*-butanol dehydration measurements were carried out with an *n*-butanol/water (95/5 wt%) feed mixture at 368 K. The n-butanol enrichment pervaporation measurements were performed with *n*-butanol/water feed mixtures ranging from 0.5/99.5 wt% to 7/93 wt%. Measurement temperatures for these measurements were 303, 333 and, 363 K. In all cases, the permeate pressure was kept constant at 10 mbar and measurements were performed after stabilization. Feed and permeate compositions were determined using refractive index measurements on a Mettler Toledo RA510M device. The *n*-butanol/water permeate samples that exhibited two phases were homogenized by addition of a known amount of water before the refractive index determination.

Overall pervaporation process selectivities ($\alpha_{process}$) were analyzed as a combination of the evaporation selectivity (α_{evap}) and the intrinsic membrane selectivity (α_{mem}) [16,17]:

$$\alpha_{\text{process}} = \alpha_{\text{evap}} \times \alpha_{\text{mem}} \quad (4.1)$$

with:

$$\alpha_{\text{evap}} = \frac{P_{\text{b}}/P_{\text{w}}}{n_{\text{b}}/n_{\text{w}}} \quad (4.2)$$

and

$$\alpha_{\text{mem}} = \frac{P_{\text{bp}}/P_{\text{wp}}}{P_{\text{b}}/P_{\text{w}}} \quad (4.3)$$

with P_b and P_w the partial pressure in the vapor phase on the feed side of *n*-butanol (b) and water (w); n_b and n_w the molar fraction of *n*-butanol (b) and water (w) at the feed side liquid phase, and Pv_{bp} and P_{wp} the partial pressures of *n*-butanol (b) and water (w) in the permeate. The vapor liquid equilibrium (VLE) calculations necessary to determine the evaporation selectivity were performed with Aspen Plus v7.2. The vapor pressure was calculated with the extended Antoine vapor pressure equation, with the default parameters from the Aspen from DB-PURE20 database. Separation factors were experimentally determined using:

$$\alpha_{\text{process}} = \frac{m_{\text{bp}}/m_{\text{wp}}}{m_{\text{b}}/m_{\text{w}}} \quad (4.4)$$

With m_b and m_w the mass fractions of *n*-butanol (b) and water (w) in the feed and m_{bp} and m_{wp} the mass fraction of *n*-butanol (b) and water (w) in the permeate.

4.3. Results and Discussion

Membrane preparation & characterization

The M, P, H and D sols were coated using total silica concentrations of 1.5, 1.2, 1.0 and 1.0 mol/l respectively. After heat treatment, SEM micrographs showed thin and defect-free hybrid silica layers, with thicknesses ranging from 200 to 550 nm (for an example see Figure 4.2).

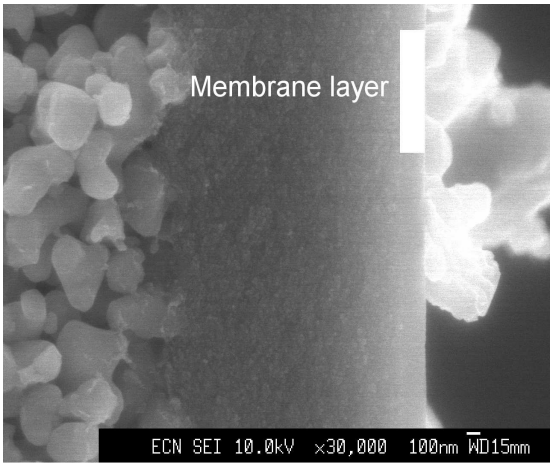

Figure 4.2. SEM cross section of the H membrane; layer thickness ~200 nm

The measured gas permeances were constant over the range of average pressures for all BTESE/RTES membranes. Consequently, no indications for viscous flow through defects were found and no large defects were present in the nanoporous membrane layers [18]. In all cases, only minor (<10%) differences were observed between the first and the second H_2 permeance measurement in the series, meaning that no major structural changes occurred during the measurement. The single gas permeance measurements also revealed the importance of the length of the R-group on the micropore structure and permeation properties of the BTESE/RTES membranes (Table 4.1). While the H_2 permeabilities for all membranes were similar, the H_2/N_2 permeability ratio was clearly affected by the length of the R-group. The M membrane showed a H_2/N_2 permeability ratio of 15.2, which is comparable to the reference BTESE (E) membrane. Membranes containing longer R-groups had a much lower H_2/N_2 ratio. Neither H_2 nor N_2 molecules have a particular affinity for the hybrid silica network. The E membrane therefore showed a clear size-based sieving, while the D membrane exhibited a H_2/N_2 ratio equivalent to the Knudsen diffusion value of 3.74 [4]. Consequently, the lower H_2/N_2 ratios for longer R-groups result from higher N_2 permeabilities. This suggests that the pores of the E membrane are small enough to retain the N_2 molecules, whereas the D membrane has large enough pores to permeate both H_2 and N_2 molecules. As a result the compositions with longer R-groups have a much lower (P

and H) or even absent (D) molecular sieving effect. The length of the pendant alkyl groups thus seems to lower the molecular sieving properties whilst retaining the H_2 permeabilities. As demonstrated by Li et al. for phenyltriethoxysilanes [10], the introduction of pendant groups possibly lead to a more open structure allowing the N_2 molecules to permeate while the pendant groups hinder the transport of all gas molecules. This leads to a decrease of the molecular sieving properties without an increase of the gas permeances.

Table 4.1. H_2/N_2, CO_2/H_2 permeability ratios and the hydrogen permeabilities of the BTESE (E) and BTESE/RTES membranes

	T (°C)	E[(1)]	M	P	H	D
H_2/N_2 ratio	250	16.2	15.2	10.3	4.5	3.8
CO_2/H_2 ratio	50	0.9	0.9	0.8	2.0	2.3
H_2 permeabilities (10^{-4} mol·nm /m^2.s.Pa)	50	2.3	2.2	3.4	2.9	2.4

(1) From [9]

At 50 °C, the length of the R-group also clearly affected the affinity of the membranes for CO_2. The E, M and P membranes, exhibited similar CO_2/H_2 permeability ratios of about unity, whereas ratios of 2 and 2.3 were measured for the H and D membranes. These results are consistent with the observation that the CO_2/H_2 permeability ratio is higher for membranes containing bulky bridging groups like C_8 alkyl, phenyl or biphenyl, compared to those containing ethyl bridges [9]. Ratios in the range of 1.5-1.7 had been found. Possibly, the increase of the organic content in the hybrid layer leads to solubility of CO_2 in the hybrid network, leading to higher CO_2/H_2 permeability ratios.

The membrane surface properties were also affected by the increase of the length of the R-group. The contact angles of water drops deposited on the surface of the series of membranes clearly increased with the length of the alkyl chain (Figure 4.3). The contact angle measurements performed on supported films coated on flat glass slides similarly showed an increase of the contact angle from 65° for E to 111° for D [19]. This indicates that the surface of membranes becomes increasingly hydrophobic with increasing length of the R-group.

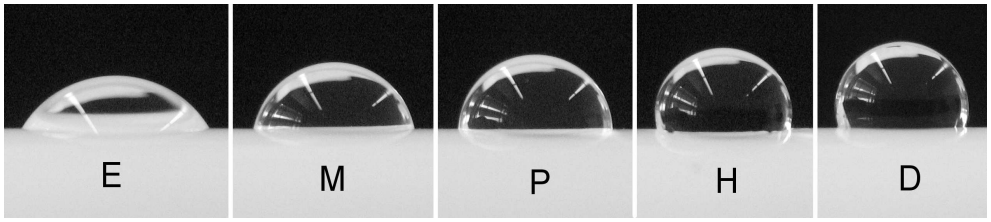

Figure 4.3. Pictures of water drops on the surface of the membrane series.

4.3.2 Pervaporation of water/*n*-butanol mixtures

Influence of the alkyl chain length on the membrane selectivities

As discussed above, the membrane performance in single gas permeance experiments depends on the length of the R-group. In addition, the contact angle measurements indicate a clear increase of the hydrophobicity with increasing length of the R-group. To determine the influence of these properties on the pervaporation performance, all membranes were tested in the separation of *n*-butanol/water mixtures with either 5% water or 5% *n*-butanol (Figure 4.4).

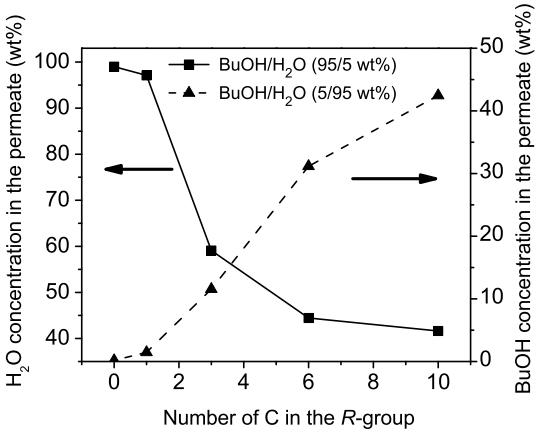

Figure 4.4. Permeate concentration as function of the number of C atoms in the R-group in pervaporation for *n*-butanol/water feed mixtures of 95/5 and 5/95 wt%. The feed concentrations were normalized to 5 wt% for direct comparison.

In pervaporation of the butanol rich mixture, a significantly lower water content in the permeate was measured for longer R-groups. The overall process selectivity ($\alpha_{process}$) decreased from ~1800 for the E (pure BTESE) membrane to ~ 13 for the D membrane having a C_{10} alkyl chain. The water concentration in the permeate for the D membrane was ~41 wt%, which is twice higher water vapor content of ~20% in a one single distillation step under similar conditions. So, the D membrane is still slightly selective for water.

Concomitantly, the *n*-butanol content in permeate increased with increased R-group length in the pervaporation of a water-rich feed mixture. For a feed mixture containing 5 wt% of *n*-butanol, the P, H and D membranes exhibited *n*-butanol permeate concentrations of 12, 31 and, 42 wt%, respectively. These concentrations correspond to process selectivities ($\alpha_{process}$) of ~2, ~9, and ~14, respectively. For this feed at a temperature of 90 °C, a single evaporation step would have a selectivity of ~12. The D membrane is under these conditions slightly selective towards *n*-butanol. This confirms that the selectivity of hybrid membranes can be tuned towards an organic species by hydrophobization of the organic/inorganic network, by e.g. changing the length of the alkyl R-group. For water-selective BTESE membranes, size exclusion is the dominant separation mechanism. With the introduction of R-groups this effect has much less influence, which is probably related to the lower molecular sieving properties, as observed in gas permeation measurements (Table 1). In the case of enrichment in *n*-butanol, size-based separation cannot be used and affinity should be the driving mechanism. In this case, process selectivities higher than the evaporation selectivity can only be obtained if the material has a higher affinity for *n*-butanol than for water. We propose that the currently observed selectivity for the D membrane is a result of the affinity for organic species over water and that this affinity is caused by the large organic fraction in the material.

Influence of operating conditions on selectivity and flux

The most hydrophobic membrane, D, was selected to further investigate the influence of the temperature and the feed composition on the membrane performance. A 500 nm thick membrane was selected from a set of four membranes with similar performances in a single pervaporation measurement.

Figures 4.5 and 4.6 show that the process selectivity varies between 14 and 16 for all measurement conditions; the feed temperature and the n-butanol feed concentration have only minor effects. The membrane performance is not strongly affected by the feed composition and temperature, in contrast to polymeric membranes in similar separation processes [6, 20, 21].

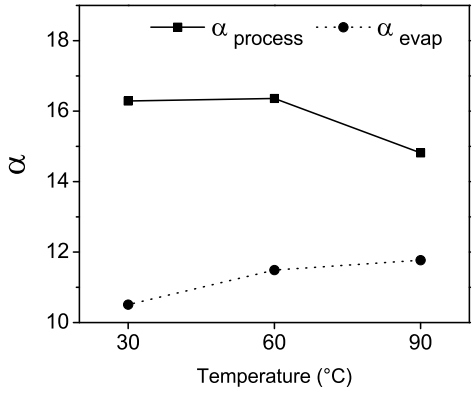

Figure 4.5. α_{evap} (dashed) and measured $\alpha_{process}$ (solid) of the D membrane against the feed temperature at 5 wt% *n*-butanol in water

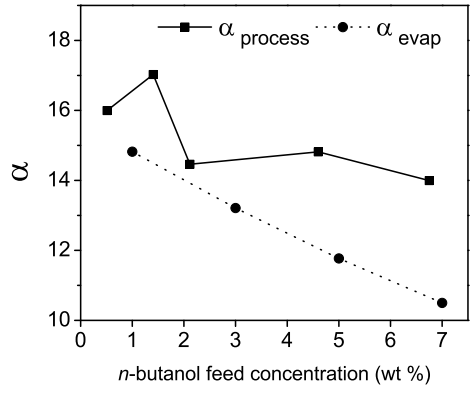

Figure 4.6. α_{evap} (dashed) and measured $\alpha_{process}$ (solid) of the D membrane against the concentration of *n*-butanol in the feed at 90 °C.

The evaporation selectivity (α_{evap}) shows a stronger dependence on the conditions, especially on the feed concentration. The evaporation selectivity (α_{evap}) of a feed mixture with 5 wt% of *n*-butanol increases from 10.5 at 30 °C to 11.7 at 90 °C (Figure 4.5). At 90 °C, the α_{evap} decreases from 14.8 to 10.5 when increasing the feed concentration of *n*-butanol from 1 to 7 wt%. As the decrease of the process selectivity is small compared with that of the evaporation selectivity, we conclude that the membrane operation becomes more effective at higher levels of *n*-butanol. We propose that the relatively rigid inorganic Si-O-Si backbone of the D membrane prevents significant swelling of the membrane material as this would lead to a substantial selectivity decrease at higher temperatures and higher *n*-butanol feed concentrations. The constant process selectivity at increasing *n*-butanol feed concentration, i.e. the constant relative fluxes of *n*-butanol and water, indicates that the pervaporation selectivity is likely governed by the membrane affinity.

A nearly linear dependence of the *n*-butanol flux on the *n*-butanol feed concentration was measured (Figure 4.7). The fluxes were in the range of 20 - 300 g/m^2.h at 30 °C, 0.45 - 1.400 kg/m^2.h at 60 °C, and up to 0.2 - 3 kg/m^2.h at 90 °C.

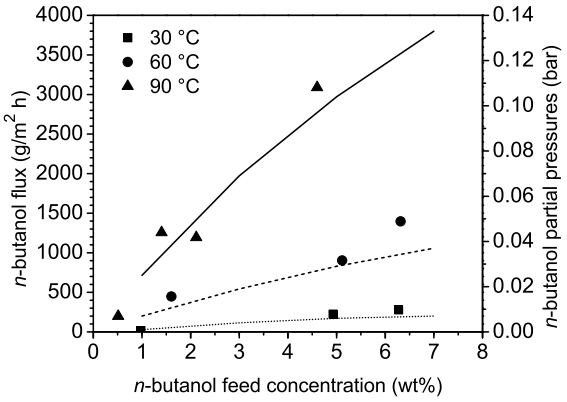

Figure 4.7. *n*-Butanol flux (points) and partial pressures of n-butanol on the feed side (lines) against the concentration of *n*-butanol in the feed for 3 measurement temperatures

The *n*-butanol flux can be understood using standard pervaporation theory. The driving force and the resulting flux in pervaporation are based on the chemical potential difference (gradient) between the feed and the permeate side of the membrane. The flux of a component i through the D membrane can be written as [17]:

$$J_i = \frac{D_i K_i^G (P_{io} - P_{il})}{l} \qquad (4.5)$$

with D_i the diffusion coefficient of the species i, K_i^G the solubility coefficient of the component i in the gas phase in the membrane, l the layer thickness of the membrane and P_{io} and P_{il} the partial pressures of the component i on either side of the membranes. This flux is related to the intrinsic properties of the membrane through the factor $K_i^G D_i$ /l , which can be considered to be constant for non-swelling membranes, [4] and to the experimental conditions through the difference of partial pressures between the feed and the permeate side of the permeating molecule. As the total permeate pressure was maintained below 4 mbar for all measurements, the permeate partial pressure can be neglected. Consequently, the *n*-butanol flux is directly related to the *n*-butanol partial pressure of the feed. The observed dependence of the flux on concentration and temperature is thus only related to the change of the driving force at the different process conditions.

4.4. Implications for bio-butanol enrichment

Bio-butanol is typically produced with the ABE fermentation process which consists of the transformation of sugars or starches into acetone, butanol and ethanol using solventogenic bacteria. The state of the art of the fermentation processes yields butanol concentrations of 1.5-2 wt% in the fermentation broth [23][22]. After fermentation, the bio-butanol needs to be separated and purified before further use.

In Table 4.2, some organophilic membranes for bio-butanol enrichment are shown. To the best of our knowledge, only few membranes exhibit butanol fluxes higher than 1 kg/m^2.h. Among non-commercial membranes, a promising example was developed by Claes and al.,

who reported, for a silica filled poly[1-(trimethyl-silyl)propyne] (PTMSP) membrane, an *n*-butanol selectivity of 104 and a flux of 8 kg/m^2 h at 50°C [23]. The authors note that long term stability still needs to be tested. Also a silicalite-1 filled PDMS membrane showed a viable flux for iso-butanol (~ 3 kg.m^{-2} h^{-1}) combined with process selectivities for butanol/water of 27.5 at 2 wt% of iso-butanol in the feed and at 80 °C [24]. However, iso-butanol has a much higher vapor pressure than *n*-butanol and lower *n*-butanol fluxes are expected. As an example of a commercially available membrane, the Pervap4060 from Sulzer exhibits a process selectivity of 39 and an *n*-butanol flux of 2.2 kg/m^2 h.

All of these membranes are polymer or polymer based composite membranes. The D membrane developed in this study is, to our knowledge the first membrane with a silica-based network that has an *n*-butanol flux higher than 1 kg/m^2 h combined with a respectable selectivity. The D membrane even reached *n*-butanol fluxes of 3 kg/m^2 h at 90 °C at an n-butanol feed concentration of about ~5 wt%.

Table 4.2. Representative examples of the PV performance of organophilic membranes in butanol/water mixtures. More examples can be found in the mentioned references and in [5, 25]

Type	T of the feed mixture (°C)	Feed butanol concentration (wt%)	Selectivity	Butanol flux (Kg/m^2 h)	Reference
Hydrophobic HybSi®	90	2	15	1.2-1.5	This work
	60	2	15	0.5-0.6	This work
Filled PTMSP (Vito 1)	50	5	104	8.0(1)	[23]
PDMS (Pervap 4060)	50	5	39	2.2(1)	[23]
Silicalite/silicon	70	1	93	0.3(1)	[26]
Zeolite GE-ZSM-5	30	5	19	0.009	[27]
PDMS filled silicalite	80	2	27.6	3 (2)	[24]

(1) Calculated from the total fluxes and selectivities of the references
(2) *iso*-Butanol flux

In addition to the respectable n-butanol fluxes measured for the D membrane, its main advantages for the bio-butanol production process arise from its intrinsic membrane material properties. The absence of swelling leads to nearly constant process selectivity over a large range of operating conditions.

As part of the development of a viable bio-butanol process, a strong effort is put on the improvement of the efficiency of the solventogenic bacteria leading to higher alcohol yields [28]. As the D membrane is not very sensitive for the alcohol concentration in the feed over the measured range of *n*-butanol concentrations, increased fermentation yields would also lead to a higher *n*-butanol concentration in the permeate for this membrane. In contrast, if polymeric membranes would be used at higher concentrations of alcohols, the membranes would become less selective due to their swelling [21,24]. As an example, for silicalite filled PDMS membranes, Fouad [21] and Lui [24] reported a decrease of the process selectivity from 40 to 25 and from 43 to 10 by increasing the butanol feed concentration from 0.25 to 3 wt% and from 0.05 to 0.3 wt% respectively. The observed constant *n*-butanol selectivity of the D membrane over the range of measurement temperatures is also clearly an advantage as it allows for temperature variations in the industrial process without strong influence on the permeate composition. Despite these promising properties, the selectivity of the D membrane is still too low to be economically viable. If only the evaporation energy is taken in account, Vane et al. estimated the minimum required process selectivity to be ~ 30 [2].

Nevertheless, the results presented here can be considered as a breakthrough in the development of an organophilic hybrid silica-based membrane. Given the fact that the required selectivities seem within reach, a bio-butanol production process without distillation can be envisaged. In such a process setup, organophilic HybSi® membranes could concentrate the butanol stream up to 60 to 80 wt% after which a hydrophilic HybSi® membrane could be used to dehydrate the product up to the desired specification.

4.5. Conclusions

We developed and characterized the first hydrophobic hybrid silica membranes based on a series of alkyltriethoxysilanes (RTES) precursors mixed with BTESE. After the optimization of the silica concentration of the sols, thin defect free-membranes were obtained. An increase of the length of the R groups resulted in both a gradual decrease of the molecular sieving properties of the membranes in gas permeation measurements and in an increase of their hydrophobicity. Dehydration of 5/95 wt% n-butanol/water mixtures by pervaporation clearly demonstrated that a higher membrane hydrophobicity for longer R-groups resulted in a much lower selectivity towards water. In parallel, the membranes showed a higher affinity for butanol in pervaporation of 5/95 wt% *n*-BuOH/water mixtures. The D membrane showed a higher selectivity towards *n*-butanol than a purely evaporation-based process, proving that its separation properties are based on affinity. As a result of its rigid network, neither the feed temperature nor the *n*-butanol concentration of the feed mixture affected the process selectivity of the D membrane which remained constant around 15. This constant selectivity combined with butanol fluxes of over 1 kg/m^2 h range are a major advantage for their further implementation in *n*-butanol enrichment of fermentation broth. This first hydrophobic hybrid silica membrane is a breakthrough opening new concept routes to the development of stable, non-swelling hydrophobic pervaporation membranes.

References

[1] A. Oudshoorn, L.A.M. van der Wielen, and A.J.J. Straathof, Assessment of options for selective 1-butanol recovery from aqueous solution, *Industrial & Engineering Chemistry Research*, 48, 7325-7336, 2009

[2] L.M. Vane, Separation technologies for the recovery and dehydration of alcohols from fermentation broths, *Biofuels, Bioprod.Bioref.*, 2, 553-588, 2008

[3] B. Smitha, D. Suhanya, S. Sridhar, and M. Ramakrishna, Separation of organic-organic mixtures by pervaporation - a review, *Journal of Membrane Science*, 241, 1-21, 2004

[4] R.W. Baker, Membrane Technology and Applications, 2007

[5] V. Garcia, J. Päkkilä, H. Ojamo, E, Muurinen, and R.L. Keiski, Challenges in biobutanol production: How to improve the efficiency?, *Renewable and Sustainable Energy Reviews*, 15, 964-980, 2011

[6] G.Liu, W. Wei, H. Wu, X. Dong, M. Jiang, and W. Jin, Pervaporation performance of PDMS/ceramic composite membrane in acetone butanol ethanol (ABE) fermentation-PV coupled process, *Journal of Membrane Science*, 373, 121-129, 2011

[7] H.L. Castricum, A. Sah, R. Kreiter, D.H.A. Blank, J.F. Vente, and J.E. ten Elshof, Hybrid ceramic nanosieves: stabilizing nanopores with organic links, *Chemical Communications*, 1103-1105, 2008

[8] H.M. van Veen, M.D. Rietkerk, D.P. Shanahan, M.M.A. van Tuel, R. Kreiter, H.L. Castricum, J.E. ten Elshof, and J.F. Vente, Pushing membrane stability boundaries with HybSi® pervaporation membranes, *Journal of Membrane Science*, 380, 124-131, 2011

[9] H.L. Castricum, G.G. Paradis, M.C. Mittelmeijer-Hazeleger, R. Kreiter, J.F.Vente, and J.E. ten Elshof, Tailoring the Separation Behavior of Hybrid Organosilica Membranes by Adjusting the Structure of the Organic Bridging Group, *Advanced Funcional Materials*, 21, 9, 2319-2329, 2011

[10] G. Li, M. Kanezashi, and T. Tsuru, Preparation of organic-inorganic hybrid silica membranes using organoalkoxysilanes: The effect of pendant groups, *Journal of Membrane Science*, 379, 287-295, 2011

[11] G.G. Paradis, R. Kreiter, M.M.A. van Tuel, A. Nijmeijer, and J.F. Vente, Amino-functionalized microporous hybrid silica membranes, *Journal of Materials Chemistry*, 22, 15, 7258 - 7264, 2012

[12] V.V. Teplyakova, V.S. Khotimskii, A.V. Yakovleva, M.G. Shalygina, G. Gasanovaa, V.B. Zen'kevichb, and A.I. Netrusovc, Membrane Systems for the Recovery of Energy Carriers from Products of Organic Waste Recycling, *Catalysis in Industry*, 3, 1,62-69, 2011

[13] L.M. Vane, A review of pervaporation for product recovery from biomass fermentation processes, *Journal of Chemical Technology and Biotechnology*, 80, 6,603-629, 2005

[14] B.C. Bonekamp, Preparation of Asymmetric Ceramic Membrane Supports by Dip-Coating, in: A.J. Burggraaf and L. Cot (Eds.), Fundamentals of Inorganic Membrane Science and Technology, Elsevier, Amsterdam, 1996

[15] F.T. Rusting, G. de Jong, P.P.A.C. Pex, and J.A.J. Peters, Sealing socket and method for arranging a sealing socket to a tube, EP 1128118, 2001

[16] S. Sommer and T. Melin, Performance evaluation of microporous inorganic membranes in the dehydration of industrial solvents, *Chemical Engineering and Processing*, 44, 1138-1156, 2005

[17] M.H.V. Mulder, Basic principles of membrane technology, Kluwer Academic Publishers, 2000

[18] R.S.A. de Lange, Microporous sol-gel derived ceramic membranes for gas separation, Thesis Dissertation, University of Twente,1993

[19] G.G. Paradis, H.L. Castricum, R. Kreiter, and J.F. Vente, Structural organization in hydrophobic hybrid silica xerogels, *In submission process*, 2012

[20] E.A. Fouad, and X. Feng, Use of pervaporation to separate butanol from dilute aqueous solutions: Effects of operating conditions and concentration polarization, *Journal of Membrane Science*, 323, 428-435, 2008

[21] E.A. Fouad and X.Feng, Pervaporative separation of n-butanol from dilute aqueous solutions using silicalite-filled poly(dimethyl siloxane) membranes, *Journal of Membrane Science*, 339, 1-2, 120-125, 2009

[22] E. M. Green, Fermentative production of butanol-the industrial perspective, *Current opinion in Biotechnology*, 22, 3,337-343, 2011

[23] S. Claes, P. Vandezande, S. Mullens, K. De Sitter, R. Peeters, and M.K. Van Bael, Preparation and benchmarking of thin film supported PTMSP-silica pervaporation membranes, *Journal of Membrane Science*, 389, 265-271, 2011

[24] X.Liu, Y. Li, Y. Liu, G. Zhu, J. Liu, and W. Yang, Capillary supported ultrathin homogeneous silicalite-poly(dimethylsiloxane) nanocomposite membrane for bio-butanol recovery, *Journal of Membrane Science*, 369, 228-232, 2011

[25] N. Qureshi, and H.P. Blaschek, Butanol recovery from model solution/fermentation broth by pervaporation: evaluation of membrane performance, *Biomass and bioenergy*, 17, 175-184, 1999

[26] J. Huang, and M.M. Meagher, Pervaporative recovery of n-butanol from aqueous solutions and ABE fermentation broth using thin-film silicalite-filled silicone composite membranes, *Journal of Membrane Science*, 192, 231-242, 2001

[27] S. Li, V.A. Tuan, J.L. Falconer, and R.D. Noble, Properties and separation performance of Ge-ZSM-5 membranes, *Microporous and Mesoporous Materials*, 58, 137,154, 2003

[28] T.C. Ezeji, C. Milne, N.D. Price, and H.P Blaschek, Achievements and perspectives to overcome the poor solvent resistance in acetone and butanol-producing microorganisms, *Applied Microbiology and Biotechnology*, 85, 1697-1712, 2010

Chapter 5

Initial solvent nanofiltration measurements of microporous organic-inorganic hybrid silica membranes

5.1. Introduction

Nanofiltration (NF) membranes are usually identified as being at the interface between Reverse Osmosis (RO) and UltraFiltration (UF) membranes [1]. Such membranes are able to reject multivalent negative ions, reject positively-charged or non-charged species based on size and typically have a rejection of sodium chloride from about 70 % down to 0 %. The first NF membranes, which appeared in the 1960s, were made of Cellulose Acetate (CA) and were applied in seawater desalination. The potential applicability of NF membranes in organic media in the food, chemical, pharmaceutical, and petrochemical industries was already identified in the 1970s. However, the first examples of solvent resistant nanofiltration (SRNF) polymeric membranes appeared only in the early 1990s as the MPT series from Kyriad-Weizmann [2]. Polymeric nanofiltration membranes are now widely applied in aqueous processes such as water treatment, removal of dyes, food processing in organic media, petrochemistry, catalysis, and recovery of pharmaceuticals [3], or for the removal of poly-aromatic and organometallic solutes from fuels [4]. One of the typical examples of a relatively robust class of polymeric nanofiltration membranes is that of PDMS-based membranes. At the same time, such membranes suffer from major swelling and compaction effects induced by the organic solvent and the applied pressure. These factors lead to strong variations of the flux and of the effective molecular weight cut-off (MWCO) of the membranes, depending on the specific solvent-membrane combination [5-7]. Consequently, their use is limited to a low number of possible applications per membrane, and successful examples cannot be extrapolated to other conditions.

Ceramic membranes have proven to be chemically and thermally stable and do not show the swelling and compaction effects of polymeric NF membranes. Ceramic NF membranes with MWCO values as low as few hundred Daltons were developed [8-12]. Also in the case of ceramic membranes solvent/membrane interactions affect the performance. The intrinsic hydrophilicity of microporous ceramic oxide membranes results in lower flux [13] and reduced retention [9] in apolar solvents. The lower retention can be ascribed to a lower adsorption of non-polar molecules in the pores as compared to polar molecules and thus

an increased effective pore size Attempts to hydrophobize these intrinsically hydrophilic materials by alkyl grafting were reported [11, 14-16]. However, none of the membranes reached the microporous range. Consequently, non-swelling hydrophobic SRNF membranes with a low MWCO (150-300 Da) are still lacking [13]. Rather than hydrophobizing an intrinsically hydrophilic material, we wanted to focus on materials that are hydrophobic by nature and at the same time have all the benefits of ceramics.

In Chapter 4 of this thesis, hydrophobic hybrid silica membranes were presented. Some of these membranes show an absence of molecular sieving properties in gas permeation and relatively high fluxes in pervaporation measurements, compared to the reference BTESE membrane (Table 2). Contact angle measurements on these membranes indicated that they are highly hydrophobic (Chapter 2). Based on this information, we set out to investigate their behavior in the permeation of a polar (acetone) and an apolar solvent (toluene) under nanofiltration conditions. The pure solvent fluxes of the hybrid silica membranes are first targeted and compared to those of the γ-Al_2O_3 support material. Retention measurements on the γ-Al_2O_3 support and the hybrid silica layers using dye molecules are also described.

5.2. Experimental

5.2.1 Materials

1,2-Bis(triethoxysilyl)ethane (E, ABCR, 97%), 1,2-bis(triethoxysilyl)octane (O, ABCR, 97%), methyltriethoxysilane (M, ABCR, 98%), *n*-propyltriethoxysilane (P, ABCR, 97%), *n*-hexyltriethoxysilane (H, ABCR, 95%), *n*-decyltriethoxysilane (D, ABCR, 97%), nitric acid (69 wt%, Aldrich), and EtOH (p.a., Aldrich) were used as received. Water was deionized at 18 MΩ/cm using a Millipore purification system. Pervaporation measurements were performed with distilled water and n-butanol (p.a. grade) from Aldrich. The membranes are further named according to the precursors used: the letter E refers to pure BTESE membranes. The letters M, P, H, D refer to the alkyltriethoxysilanes introduced in the BTESE-based hybrid silica network. The letters O and O+D refer to the pure BTESO and to the BTESO/DTES membranes.

5.2.2 Membrane preparation

The ratios of the RTES/BTESE sols and the two steps synthesis procedure are described in Chapter 4. The BTESO/DTES sol was synthesized using the same procedure with the ratios Si/EtOH/H^+/H_2O = 1/50/0.6/3 and a heating time of 90 min. The sol was coated without further dilution. The BTESO sol was synthesized in a one-step synthesis described elsewhere [17]. The heat treatment and the characterization procedures were also described in Chapter 4. All the membranes were sealed using stainless steel caps and graphite as packing material.

5.2.3 The nanofiltration setup

The nanofiltration measurements were performed using an in house developed cross flow nanofiltration setup. The set up allows NF measurements up to a feed pressure of 10 bars and is resistant to a number of common organic solvents, including acetone, toluene, methylethyl ketone, and hexane. The setup consists of a 12 L feed tank (D-01) feeding the shaft sealed solvent resistant feed pump (P-01) which is able to deliver a solvent flux of 2 m^3/h at a feed pressure of 10 bars (Figure 5.1). The feed mixture is sent to the membrane module (S-01) in which the feed pressure is regulated by applying a back pressure using valve V-11. The permeate is collected through V-23 while the retentate is sent back to the feed vessel. The set up can also be used in continuous mode by routing the permeate back into the feed vessel through valve V-22. The permeating volume is then measured by FR-01/FT-01 and the permeate samples collected through V-01.

In addition, a cooling system using a glycol/water mixture at 0.5 °C is used to regulate the feed mixture temperature. For safety purposes, different release valves and a bypass (V-04) have been installed. Several flexible exhaust pipes are available to have local vapor removal on open points like sampling points or vent maintaining the feed vessel at atmospheric pressure. A N_2 flushing system (not shown) has also been installed to allow a proper emptying and flushing of the module and/or the complete setup. Using a similar module concept, the same membrane sample can tested in nanofiltration, gas permeation, permporometry, and pervaporation, without changing the steel end caps.

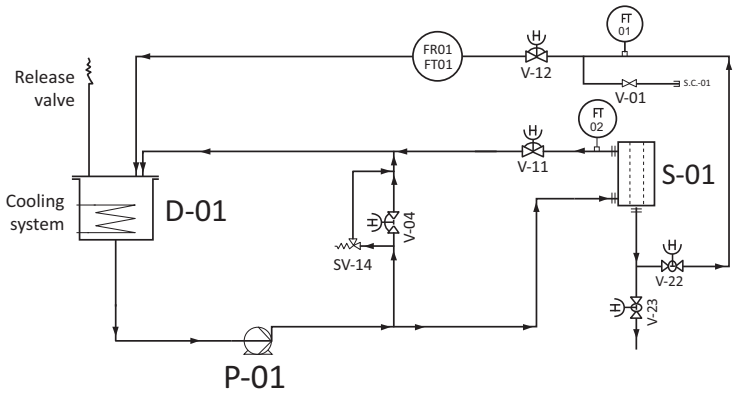

Figure 5.1. Simplified Piping and Instrumentation Diagram (P&ID) of the NF setup

5.3. Measurement procedure

5.3.1 General and pure solvents

A general measurement procedure was developed for hybrid silica membranes. A stabilization period of 30 min at 10 bars feed pressure was set to allow a stabilization of the feed temperature at 20 ºC (+/- 0.5 ºC) and of the feed flow between 1.8 and 2 m^3/h. After the stabilization period, the fluxes were determined by measuring the permeate volumes in measuring cylinders. Each measuring cylinder was regularly weighed to confirm the measured flux. The γ-alumina supports were tested under the same experimental conditions. However in the case of the support, fluxes were measured after only one minute of testing.

5.3.2 Membrane retention measurements

Retention measurements were performed in acetone using two different dyes: Bengal Rose (BR) and Sudan Blue (SD), having molecular weights of 1017 and 350 g/mol, respectively (Figure 5.2). The two dyes were first dissolved in acetone and then added to the feed mixture to reach a final concentration of 100 ppm for both dyes.

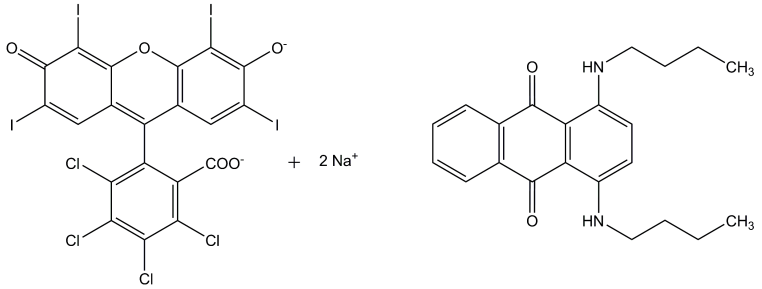

Figure 5.2. Structure of the Sudan Blue and Bengal Rose dyes used in the retention measurements

5.4. Results

5.4.1 Membrane characterization

SEM measurements were performed on all the membranes after the heat treatment and before the nanofiltration measurements. Due to the measurements in acetone/dye solution performed after the measurement in acetone, new E, M, P, H, and D membranes, with different thicknesses as the first series were used for the measurements in toluene. For the O and O+D membranes, the same membranes were measured in acetone after the toluene measurement. These measurements revealed that all the membranes were crack free and exhibited layers thicknesses ranging from 85 nm to 1.7 µm (Table 5.1).

Table 5.1. Layer thicknesses (nm) of the membranes tested in pure acetone and toluene

Solvent	E	M	P	H	D	O	O+D
Acetone	1000	1150	1660	940	85	255	75
Toluene	880	470	185	795	120		

The performances of the different types of membrane in single gas permeance and pervaporation were also evaluated in the previous chapter. The O+D membrane, which was developed for this chapter, was subjected to the same characterization techniques. The gas permeances and the total fluxes in pervaporation of an n-butanol/water mixture (5/95 wt%) were measured. The results were compared with these obtained for the other membranes in the previous chapters (Table 5.2).

Table 5.2. H_2/N_2 permeance ratio at 250 °C, and total fluxes in pervaporation of a H_2O/BuOH (95/5 wt%) mixture

	E	M	P	H	D	O	O+D
H_2/N_2 permeance ratio	16.2[(1)]	15.2	10.3	4.5	3.8	5.3[(1)]	4
Total Flux H_2O/*n*-BuOH (kg/m^2·h)	1.2	8	5.5	9.7	6.2	9.2	17

(1) From [17]

The H_2/N_2 permeance ratios and the total fluxes are useful to predict the behavior of the membranes in nanofiltration. First, the H_2/N_2 permeance ratio can be related to the molecular sieving properties of the membranes as the permeation of both H_2 and N_2 is based on the size of the molecules and not on the affinity of the network. A low H_2/N_2 ratio reveals the absence of molecular sieving properties of the membrane and indicates possible larger pore sizes than the parent E membrane. This could also translate into a high flux in nanofiltration. The total fluxes in pervaporation can also be taken as an indication of the openness of the glassy network. Obviously and independently of the selectivity, the more open the network is, the higher the total flux would be. A component flux would be more related to the selectivity (affinity) of the membrane. Consequently, membranes with a low H_2/N_2 ratio and a high total flux in pervaporation are likely to exhibit high fluxes in nanofiltration.

The H, D, O and O+D membranes exhibited both a H_2/N_2 ratio lower than 6 and total fluxes higher than 6 kg/m²·h. Therefore, these membranes are expected to have the highest fluxes in nanofiltration. The E and P membranes exhibited a H_2/N_2 permeance ratio above 10 and pervaporation fluxes below 6 kg/m²·h which could translate to low fluxes. The M membrane shows a H_2/N_2 equivalent to the E membrane but with a much higher flux in pervaporation making predictions more difficult.

5.4.2Solvent fluxes

γ-Al_2O_3 *support*

The resistance of the support can limit the gas or liquid fluxes of the separating layer of asymmetric supported membranes. To evaluate the resistance of the γ-Al_2O_3 support on the solvent permeation properties of the hybrid silica layers, its acetone and toluene fluxes were measured (Figure 5.3). The flux of both solvents declined strongly over time. The acetone flux decreased 45 % from 27.5 L/m²·h to 16 L/m²·h during the first hour of measurement. In the same period of time, the toluene flux decreased only 15 % from 19.7 to 16 L/m²·h.

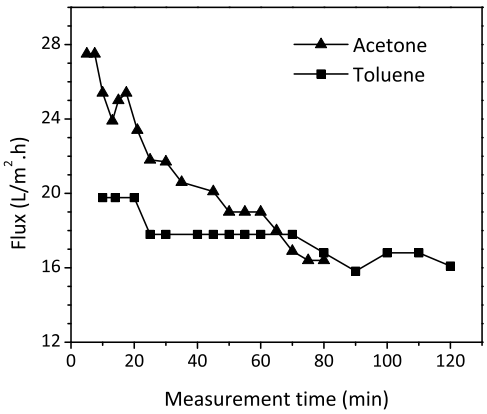

Figure 5.3. Acetone and toluene fluxes in time of a γ-Al_2O_3 support at a feed pressure of 9 barg

Hybrid silica membranes

For all hybrid silica membranes acetone fluxes could be determined at a feed pressure of 10 barg. No flux was observed during the 30 min of stabilization. After this stabilization period, the first acetone permeation was observed only after a certain onset time, ranging from 5 min for the O membrane to over 90 min for the M membrane. The acetone fluxes measured volumetrically ranged from 0.4 to 1.08 L/m^2·h. As a further check, the fluxes were also determined by regularly weighing the measuring cylinder. The flux determinations by mass were equal to the volumetric measurements.

Independent of the transport mechanism (pore flow, solution diffusion), the pure solvent flux through a membrane is directly proportional to the thickness of the separating layer [18]. The layer thicknesses of the current membrane series varied up to a factor 11 (Table 5.1). Therefore, the fluxes of the different membranes in acetone were normalized to a layer thickness of 100 nm, allowing for a more direct comparison of the material properties (Figure 5.4).

All the membranes exhibited nearly constant fluxes over the full measurement period. The E membranes exhibited the highest acetone flux with an average normalized flux of 3.2 L/m^2·h. For the BTESE/RTES membranes, the M, P, H, and D membranes showed average normalized acetone fluxes of 0.45, 2.35, 0.9, and 0.3 L/m^2·h, respectively. The O and O+D membranes showed normalized average fluxes of 2.85, 0.8 and L/m^2·h, respectively. No clear trend related to the length of the alkyl group could be derived from this first set of measurements in acetone. To confirm the exceptionally high flux for the E membrane, an additional acetone nanofiltration measurement was done on a fresh sample in a dead end setup at 30 barg. This membrane exhibited no acetone flux even after 3 hours of measurement.

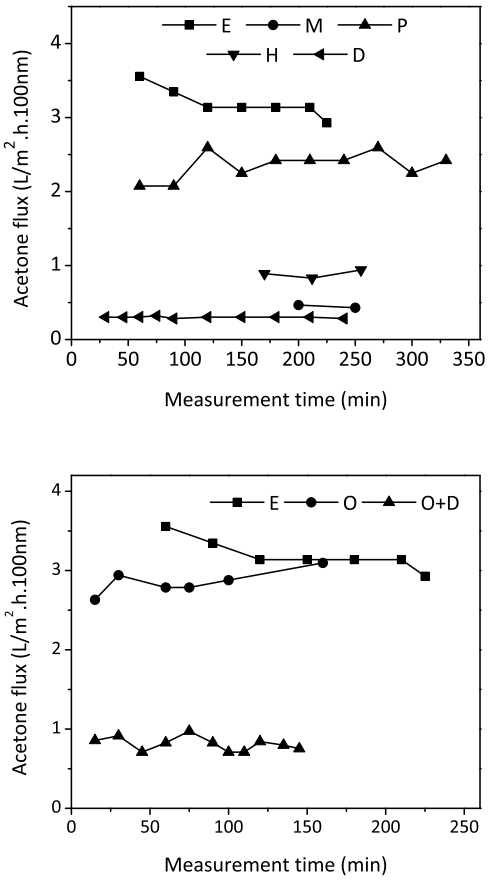

Figure 5.4. Normalized acetone fluxes in time at 10 barg

Toluene flux measurements were also performed. In this solvent only the H, O and O+D membranes were permeable, whereas the E, M, P, and D membranes showed no flux after several hours at 10 bars. The E, M, P, H, D membrane samples tested in toluene were different samples than those tested in acetone. Layer thicknesses of these membranes were very similar or in some cases lower (Table 5.1).

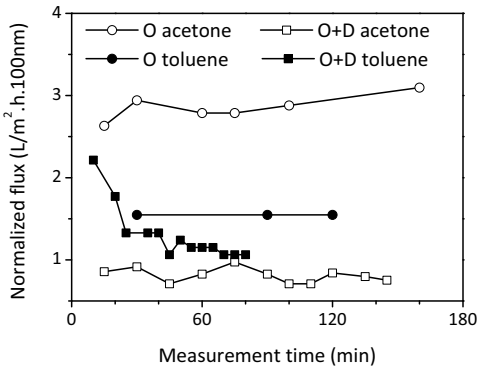

Figure 5.5. Normalized acetone and toluene fluxes of the O and O+D membranes at a feed pressure of 10 barg

Similar to the acetone results, the toluene fluxes were normalized for a layer thickness of 100 nm, assuming a linear relation between the solvent flux and the layer thickness. Comparing acetone and toluene fluxes for the O and O+D membranes (Figure 5.5), the O membrane exhibited a normalized flux of 1.5 L/m^2·h for toluene and 3.0 L/m^2.h for acetone. Surprisingly, the toluene flux of the O+D membrane strongly decreased from 2.4 L/m^2·h to 1.4 L/m^2·h during the first 80 min of measurement reaching a value similar to the flux of acetone. The H membrane exhibited similar fluxes of 0.8 L/m^2·h for both solvents.

5.4.3 Retention measurements

The γ-Al_2O_3 support

The behavior of the γ-Al_2O_3 support in the presence of dyes was assessed and compared to the pure acetone flux (Figure 7). The acetone flux of the γ-Al_2O_3 membrane was significantly lower in the presence of the dyes and did not exceed 12 L/m^2.h. Compared to the pure acetone flux, the flux in the presence of the dyes was much more constant and ranged from 12.2 L/m^2·h to 9.5 L/m^2·h in time.

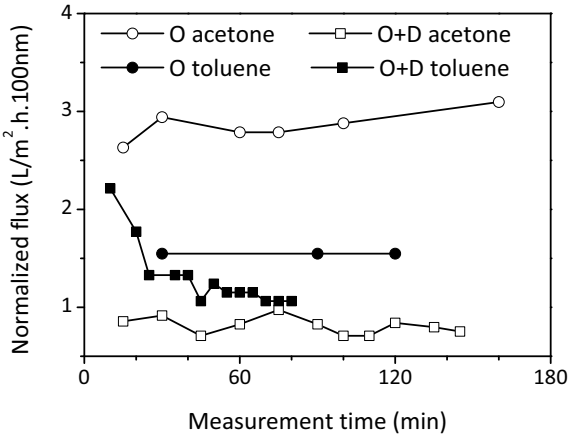

Figure 5.6. Fluxes of γ-Al_2O_3 support in pure acetone (acetone) and in the dyes solution (acetone+BR) in time at a feed pressure of 9 barg

After the measurement in the dye solution in acetone, the appearance of the γ-Al_2O_3 membrane was dark pink and blue (Figure 5.6). Cleaning of the membrane with fresh acetone revealed that the Sudan Blue dye could be removed, whereas the Bengal Rose remained on the membrane (Figure 5.7, right). In parallel, γ-Al_2O_3 powder was dipped in the same dye/acetone mixture and it appeared that the Bengal Rose also adsorbed strongly to this material.

Figure 5.7. Pictures of the γ-Al_2O_3 support after the measurement in the acetone/dye mixture before (left) and after the cleaning with acetone (right)

Despite of the strong adsorption of the Bengal Rose on the surface of the pores of the γ-Al_2O_3, retention coefficients were measured for both dyes. The γ-Al_2O_3 reached an almost total retention for the Bengal Rose (99 %), while only about 10 % of the Sudan blue was retained. Possibly, part of the Bengal Rose adsorbed on the pore surface of the γ-Al_2O_3 reducing the effective pore size which was then small enough to fully retain this dye. The alternative explanation of full adsorption of the dye on the alumina is unlikely, because of the large volume (10 L) and relatively small membrane sample.

Hybrid membranes

Retention measurements were performed for the full series of hybrid silica membranes. In pure acetone, the onset of the flux appeared between 30 min and 3 hours after the start of the measurement. In presence of dyes, no measurable acetone fluxes were observed, also for prolonged measurement times of four to six hours.

Figure 5.8. Overview of the hybrid silica membranes after the test in the dye solution

After the measurement, most of the membranes showed colored patterns on their surface (Figure 5.8). The M membrane exhibited small pink spots, while the E membrane exhibited a large pink area, possibly because of a larger defect. This membrane sample was the same one tested in pure acetone which exhibited the highest flux of all hybrid membranes. The

rest of its surface remained white similar to the P and H membranes. The O and O+N membranes showed a blue surface in addition to small pink spots. Interestingly, it appeared that the blue color had lengthwise pattern, consistent with the flow direction in the module, whereas the pink color was concentrated on small and defined spots. This suggests that the adsorption of the blue color is related to the intrinsic properties of the porous structure, whereas the adsorption of the pink color is related to the presence of point defects. For the pink spots, we assume that the Bengal Rose permeated through the hybrid silica top layer adsorbed on the γ-Al_2O_3 layer.

5.5. Discussion

The large flux decrease observed in pure solvent during the first 80 minutes of measurement and the strong adsorption of the Bengal Rose showed the important contribution of the hydrophilic nature of the γ-Al_2O_3 material. As the γ-Al_2O_3 is chemically stable in both solvents, the decrease of the flux observed in experiments with pure solvents can only arise from the adsorption of molecules in the γ-Al_2O_3 structure. The hydroxyl groups in the material favor the adsorption of polar molecules through hydrogen bonding. A decrease of flux in time as also been observed in toluene which cannot form hydrogen bonds. This suggests that the solvents themselves are not the cause of the decrease of flux in time. Possibly, the limited amount of water in the solvents accumulates in the porous structure of γ-Al_2O_3 that reduces the effective pore size and consequently decreases the solvent flux. Possibly, the water concentration in acetone is higher, which could explain the larger decrease of the acetone flux.

In the dye retention measurements, the fact that Bengal Rose is an ionic dye plays an important role. It can partially dissociate in a polar solvent such as acetone, leading to the formation of carboxylate groups that strongly interact with the hydrophilic surface groups of γ-Al_2O_3. The use of a strong acid solution enabled the cleaning of the γ-Al_2O_3 material and dissolution of the Bengal Rose, which supports this hypothesis. We propose that the adsorbed Bengal Rose decreased the effective pore size resulting in a lower acetone flux as compared

to pure acetone feed. The observation that the flux remains much more constant in the dye solution can also be ascribed to this effect. In pure acetone, water molecules can adsorb on the surface aluminol groups, leading to a higher resistance of the membrane and hence a drop in the flux. In the presence of adsorbed Bengal Rose molecules, the adsorption sites are already occupied or shielded by the large dye molecule, preventing further adsorption of water and/or acetone. This adsorption not only has an effect on the MWCO determination but also on the future applicability of hybrid silica NF membranes supported by a γ-Al_2O_3 layer. A number of separation processes for which nanofiltration might be suitable involves charged molecules. In such applications, the γ-Al_2O_3 support will potentially bind the charged molecules, which might result in an increased resistance of the support and possibly to a large decrease of the flux.

After a stabilization time of about 80 min, the γ-Al_2O_3 support exhibited a pure solvent flux of about 16 L/m^2·h. The fluxes are at least an order of magnitude higher than those of the hybrid silica membranes. Consequently, we can safely consider that the resistance of the γ-Al_2O_3 support does not affect the fluxes of the hybrid silica membranes.

Over the BTESE/RTES series both the H_2/N_2 permeance ratios and fluxes in pervaporation show consistent trends towards larger pore sizes and increased hydrophobicity for longer R-groups. At the same time, in nanofiltration the BTESE/RTES membranes exhibited extremely low fluxes of 0.05 to 1.12 L/m^2·h in acetone and toluene permeance only for the H membrane. Normalized for layer thicknesses of 100 nm, the acetone fluxes never exceeded 3 L/m^2·h at 10 barg of feed pressure and the parent BTESE membranes exhibited the highest flux. However, the retention measurement using the dye revealed the presence of a large defect in the E membrane, which is possibly responsible for this flux. The additional experiment performed at 30 barg on a fresh sample confirmed this. No clear trend related to the length of the R-group was found in the acetone fluxes of the RTES/BTESE series. Interestingly, the only membranes that showed a measurable flux in both acetone and toluene are the H, O and O+D membranes which exhibited the lowest H_2/N_2 ratios and the highest fluxes in pervaporation. The O and O+D membranes showed additional features. In

addition to the high pervaporation fluxes and the very low H_2/N_2 ratios, both membranes showed a lengthwise blue color pattern after the dye measurement. This effect probably results from the infiltration of the Sudan Blue, and can be ascribed to a more open structure because of the octane bridge. Interestingly, the O membrane showed higher fluxes than the O+D membrane. This suggests that the introduction of a C_{10} R-group hinders the permeation of both solvents. In pervaporation, no effect of the presence of the R-group was found. Possibly, the higher temperature of the pervaporation experiment makes the alkyl chains of the terminal side group mobile, allowing for smooth transport of the permeant molecules. This could be an indication that long bridging groups should be favored over large organic side groups in the development of hybrid silica nanofiltration membranes.

Surprisingly, none of the hybrid silica membranes permeated in the presence of acetone/dyes mixtures. This possibly arises from the osmotic pressure generated by the Bengal Rose and Sudan Blue. Alternatively, the smaller dye (Sudan Blue) might have blocked the pores of certain membranes by a fouling process. This is supported by the blue color observed on the O and O+D membranes. Flushing the outside of the membrane does not remove the color, which indicates that the Sudan Blue infiltrated in the pores. In the absence of further evidence, both of these explanations are equally likely.

5.6. Conclusion

This chapter aimed to assess the applicability of a series of hybrid silica membranes in solvent nanofiltration. Pure acetone and toluene fluxes were measured and retention measurements performed. Our current setup allows safe measurements at a regulated temperature for several hours. The γ-Al_2O_3 support showed fluxes of at least one order of magnitude higher than that of the hybrid silica membranes, also after initial decline of the flux. This proves that the resistance of the support is negligible compared to that of the hybrid silica layer. The acetone fluxes measured for the hybrid silica membranes were very low and did not exceed 3 L/m^2.h at 10 bars. Only three of these membranes showed a toluene flux at the same pressure. No clear trend corresponding to the length of the R-group could be found

in the acetone fluxes of the BTESE/RTES series. For the O and O+D membranes, the octane bridge has a positive influence on the apparent pore size of the material. At the same time, the presence of the C_{10} R-group causes a much lower flux. We conclude that the presence of large organic side groups leads to blocking of the porous structure under these nanofiltration conditions. Our experiments also show that charged dyes should not be used for ceramic membranes, because of the presence of surface hydroxyl groups. This effect of charged molecules could also limit the applicability of ceramic nanofiltration membranes. Alternative supports materials which do not have strong interactions with charged species should be found to overcome this issue.

References

[1] A.I. Schäfer, A.G. Fane, and T.D. Waite, Nanofiltration Principles and Applications, Elsevier, 2005

[2] M. Perry, J. Yacubowicz, C. Linder, and R. Shavit, Novel Chemically stable SelROTM nanofiltration membranes and modules for application in chemical processes and treatment of waste streams, *Aachener Membran Kolloquim preprints*, 213-229, 1993

[3] P. Vandezande, L.E.M. Gevers, and I.F.J. Vankelecom, Solvent resistant nanofiltration: separating on a molecular level, *Chemical Society Reviews*, 37, 365-405, 2008

[4] E.S. Tarleton, J.P. Robinson, and J.S. Low, Nanofiltration: A technology for selective solute removal from fuels and solvents, *Chemical Engineering Research and Design*, 87, 3, 271-279, 2009

[5] D.R. Machado, D. Hasson, and R. Semiat, Effect of solvent properties on permeate flow through nanofiltration membranes. Part I: Investigation of parameters affecting solvent flux, *Journal of Membrane Science*, 163, 93-102, 1999

[6] D.F. Stamatialis, N. Stafie, K. Buadu, M. Hempenuis, and M. Wessling, Observations on the permeation performance of solvent resistant nanofiltration membranes, *Journal of Membrane Science*, 279, 424-433, 2006

[7] E.S. Tarleton, J.P. Robinson, S.J. Smith, and J.J.W. Na, New experimental measurements of solvent induced swelling in nanofiltration membranes, *Journal of Membrane Science*, 261, 129-135, 2005

[8] T. van Gestel, C. Vandecasteele, A. Buekenhoudt, C. Dotremont, J. Luyten, R. Leysen, B. van de Bruggen, and G. Maes, Alumina and titania multilayer membranes for nanofiltration: preparation, characterization and chemical stability, *Journal of Membrane Science*, 207, 73-89, 2002

[9] J. Geens, B. van der Bruggen, B. Verrecht, A. Buekenhoudt, C. Dotremont, and C. Vandecasteele, Nanofiltration in organic solvents: comparison between polymeric and ceramic membranes, *Conference proceeding, International Conference on Porous Ceramic Material*, 2005

[10] J. Sekulic, J.E. ten Elshof, and D.H.A. Blank, A microporous titania membrane for nanofiltration and pervaporation, *Advanced Materials*, 16, 17, 1546-1550, 2004

[11] T. Tsuru, H. Kondo, T. Yoshioka, and M. Asaeda, Permeation of nonaqueous solution through organic/inorganic hybrid nanoporous membranes, *AIChE Journal*, 50, 5, 1080-1087, 2004

[12] I. Voigt, G. Mitreuter, and M. Fütrag, The Pore Structure of Meso- and Microporous TiO_2-Membranes, *Journal of the German Ceramic Society (J. Der. DKG.)*, 79, 8, E39-E44, 2002

[13] C. Guizard, A. Ayral, and A. Julbe, Potentiality of organic solvents filtration with ceramic membranes. A comparison with polymer membranes, *Desalination*, 147, 1-3, 275-280, 2002

[14] S.R. Krajewski, W. Kujawski, F. Dijoux, C. Picard, and A. Larbot, Grafting of ZrO_2 powder and ZrO_2 membrane by fluoroalkylsilanes, *Colloids and Surfaces A: Physicochemical and Engineering Aspects*, 243, 1-3, 43-47, 2004

[15] C. Leger, H.D. Lira, and R. Paterson, Preparation and properties of surface modified ceramic membranes. Part III. Gas permeation of 5 nm alumina membranes modified by trichloro-octadecylsilane, *Journal of Membrane Science*, 120, 2, 187-195, 1996

[16] C. Picard, A. Larbot, E. Tronel-Peyroz, and R. Berjoan, Characterisation of hydrophilic ceramic membranes modified by fluoroalkylsilanes into hydrophobic membranes, *Solid State Sciences*, 6, 605-612, 2004

[17] H.L. Castricum, G.G. Paradis, M.C. Mittelmeijer-Hazeleger, R. Kreiter, J.F. Vente, and ten J.E. Elshof, Tailoring the Separation Behavior of Hybrid Organosilica Membranes by Adjusting the Structure of the Organic Bridging Group, *Advanced Functional Materials*, 21, 9, 2319-2329, 2011

[18] R.W. Baker, Membrane Technology and Applications, 2007

Chapter 6

Tuning of pore sizes in hybrid silica using a thermo reversible addition reaction

6.1. Introduction and concept

Since the 1990s surfactant templated sol gel processes have been widely utilized to develop membranes and materials with well-defined porosities and various functionalities [1-8]. Typically, the use of such micellar surfactants results in mesoporous materials with pore sizes that range from 3 to 50 nm. Only scarce examples of non-templated inorganic membranes with pore sizes in the super-microporous range (1-2 nm) are reported [9-12]. In addition, these examples are based on inorganic silica, which is highly reactive towards water and acids. Therefore, our aim is to use bridged organic-inorganic hybrid silica precursors as starting point for the development of templated membranes with pore sizes in this range. The ultra-microporous hybrid silica membranes developed recently are hydrothermally stable [13], resistant to acidic media [14], and are essentially non-swelling in organic media under drastic separation conditions. In addition, their affinity can be tuned from highly hydrophilic to hydrophobic by the introduction of a small amount of targeted functional precursors (Chapter 2 and 4). Their performance in hydrophilic and organophilic pervaporation is described in this thesis (Chapter 2 and 4). If alternative suitable templating method is developed, super-microporous hybrid silica membranes with tunable affinity can be envisaged. Such membranes would be of great interest for application in solvent media, such as solvent nanofiltration.

A number of templating methods that might be suitable have been published. The group of Brinker used tetraethylammonium bromide (TEAB) to template TEOS-based silica membranes [15] or co-polymerized tetraethoxysilane (TEOS) with 3-methacryloxypropylsilane (MPS) [16]. In both cases the removal of the templates was performed using heat treatment at temperatures of 350 °C or higher. This temperature range cannot be applied when the organic part of the hybrid backbone needs to be conserved. For the same reason, the use of plasma oxidation of hydrocarbon templates in a silica matrix proposed by Loy cannot be used [17]. Katz [18], Defreese [19] and Zhu [20] showed interesting and highly successful examples of molecular imprinting of microporous/mesoporous silica materials. These methods consist of lengthy and complex procedures to release the capping agent that can hardly be translated to membrane preparation. Alternatively, Shaltout and McClain reported a simple templating

method of hybrid silica powders through the use of the Diels-Alder (DA) and retro-DA reactions [21, 22]. This reaction is a concerted cycloaddition reaction between a diene (e.g. 1,3-butadiene) and a dienophile (e.g. ethylene) (Figure 6.1). The retro reaction can be performed by heat treatment.

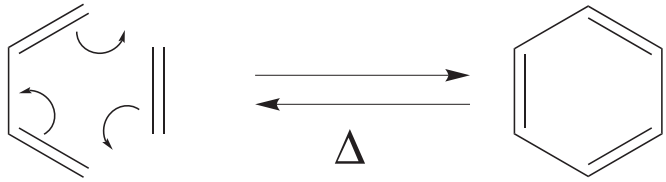

Figure 6.1. Schematic representation of the Diels-Alder and retro-Diels-Alder reactions

This templated approach offers many advantages. First, the size of the adduct can be varied to target specific pore sizes. In addition, an appropriate choice of the adduct allows the retro-DA reaction to be performed at lower temperatures than the decomposition temperatures of the organic group in the hybrid silica network. In this way, the hybrid network remains untouched. Importantly, the use of DA adducts incorporated in the hybrid silica precursors allows for facile introduction into hybrid silica membranes without lengthy and costly additional procedures. The heat treatment, which is standard for consolidation of hybrid silica membranes, promotes the release of thermo labile adducts. This should create a templated porous network whilst the organic component of the hybrid network remains intact. This concept is schematically represented in the Figure 6.2.

It was demonstrated by others that the pore size of the network after removal of the template is similar to the size of the templating organic group [16, 17, 23]. In this study, we aimed at a final pore size of about 1 nm. To this end, cyclopentadiene, with a molecular size of about 0.25 nm was chosen as diene. The expected pore size compared to the parent hybrid silica pore size of 0.5-0.6 nm is about 0.8-0.9 nm. In addition, the relative small size of the cyclopentadiene moiety should allow an easy removal of the adduct. Two templating approaches were investigated. A first one in which the DA adduct is situated on the bridging organic group of the ethylene-bridged 1,2-bis(triethoxysilyl)ethylene (BTESEt) precursor, and a second approach in which the adduct is placed on a terminal organic fragment vinyltriethoxysilane (VTES) (Figure 6.3).

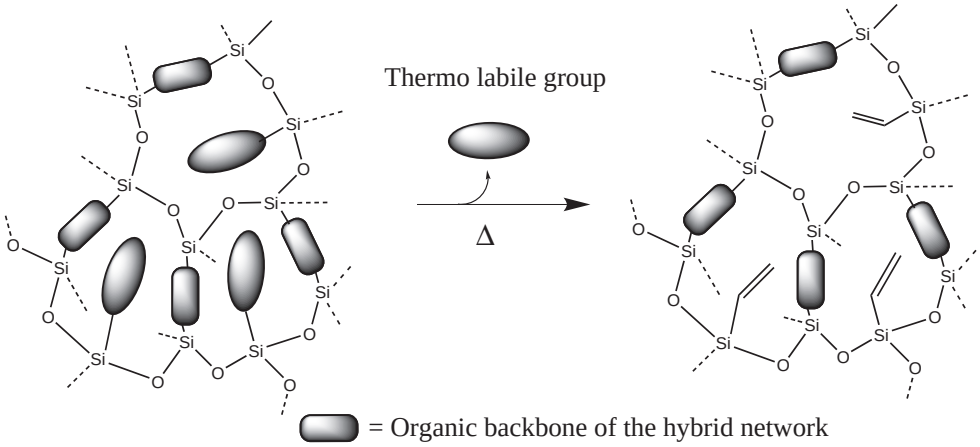

Figure 6.2. Conceptual representation of the use of the retro-DA reaction as alternative pore templating approach. In the figure the thermo labile groups are placed on the terminal organic group of a triethoxysilane precursor.

6.2. Experimental

6.2.1 Materials

1,2-Bis(triethoxysilyl)ethane (BTESE, ABCR, 97%), 1,2-bis(triethoxysilyl)octane (BTESO, ABCR, 97%), 1,2-bis(triethoxysilyl)ethylene (BTESEt, ABCR, 95%), vinyltriethoxysilane (VTES, ABCR, 98%), 5-(bicycloheptenyl)triethoxysilane (BHTES, ABCR, 97%), nitric acid (69 wt%, Aldrich), and EtOH (p.a., Aldrich) were used as received. Water was deionized at 18 MΩ/cm using a Millipore purification system.

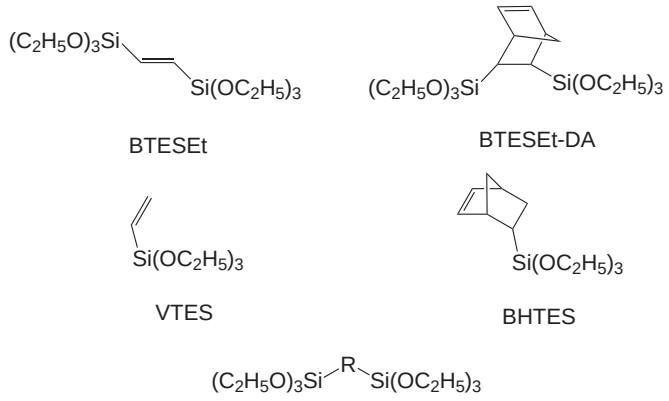

Figure 6.3. Overview of the precursors used in this chapter

6.2.2 Synthesis of the BTESEt-DA adduct

As the BTESEt-DA adduct 1,2-Bis(triethoxysilyl)norbornene was not commercially available, a synthesis procedure was developed. This procedure involved four steps: The cracking of the di-cyclopentadiene, the DA reaction, the purification of the DA adduct and the characterization of the final product.

The pure cyclopentadiene slowly dimerizes at room temperature and needs to be freshly distilled from the commercial dimer. The distillation was performed at a temperature below the boiling point (b.p. 170 °C) of the dimer and the lower boiling monomer (b.p. 42 °C)

was collected. To obtain a sufficient yield, the DA reaction was performed in an autoclave (Parr) under autogenous pressure. The BTESEt was introduced in a PTFE cup and degassed by bubbling nitrogen trough a Pasteur pipette. Eight molar equivalents of freshly distilled cyclopentadiene were then added. After 40 hours at 110 °C thin layer chromatography (TLC) analysis showed a significant conversion of the BTESEt into BTESEt-DA adduct. The product mixture was recovered from the autoclave using acetone and concentrated using a rotary evaporator. The product was then purified by distillation under reduced pressure, using a fractioned distillation apparatus at a pressures lower than 1 mBar. The TLC analysis of the distillate showed a majority of the DA adduct, a trace amount of BTESEt, and no dicyclopentadiene. The final product was finally quantitatively characterized by proton NMR (and compared with the starting materials dicyclopentadiene and BTESEt) using a Bruker 400 MHz and chloroform as solvent.

Dicyclopentadiene ^{1}H: δ (ppm) = 5.95 (m, 2H), 5,49 (m, 2H), 3.21 (m, 1H), 2.28 (m, 1H), 2.78 (m, 1H), 2.71 (m, 1H), 2.18 (m,1H), 1.62 (m, 1H), 1.48 (m,1H), 1.30 (m, 1H).

BTESEt ^{1}H (trans and cis isomer): δ (ppm) = 6.72 (s, 0.27H), 6.62 (s, 2H), 3.8 (m, 16H), 1.2 (m, 24H).

BTESEt-DA adduct ^{1}H: δ (ppm): 6.74 (s, 0.16H), 6.64 (s, 0.32H), 6.07 (m, 1H), 5.97 (m, 1H), 3.8 (m, 20H), 3.05 (m, 1H), 2.94 (m, 1H), 1.40 (m, 1H), 1.20 (m, 27H), 0.7 (m, 1H).

The product molar composition was calculated according to the peak integration values as: 68 % of DA-adduct, 11 % of cis-BTESEt and 21 % of trans-BTESEt. No cyclopentadiene was found.

6.2.3 Membrane synthesis and characterization

All the sols were synthesized using a single-step procedure. For the BTESEt and BTESEt-DA sols, the required amounts of nitric acid and water were mixed beforehand. The precursors were separately mixed with ethanol and the acid water mixture was added in one shot to this

precursor mixture. The final mixture was heated to 60 °C for three hours. For the BTESO/VTES, BTESO/BHTES and BTESE/BHTES sols, the desired amounts of nitric acid, distilled water, and EtOH were premixed. The precursors were mixed and subsequently added in one shot to the mixture of EtOH, nitric acid, and water. The reaction mixture was subsequently heated to 60 °C for three hours . The ratios of all the sols are presented in Table 6.1.

Table 6.1 Overview of the ratios of the sols developed in this chapter

Sol	Molar Ratios ($Si/EtOH/H^+/H_2O$)
Pure BTESEt	1/7.36/0.04/1.2
Pure BTESEt-DA	1/5.3/0.03/1
Equimolar BTESO/VTES and BTESO/BHTES	1/23.6/0.15/3
BTESO/BHTES (75 mol% of BHTES)	1/16.0/0.11/3
BTESE/BHTES (equimolar and 75 mol% of BHTES)	1/3.9/0.05/3

The membrane layers were coated, heat treated, and characterized by SEM according to the procedures described in the chapters 2 and 4. Single gas permeance measurements were performed at 250, 150 and 50 °C at decreasing feed pressures from 9 to 3 bara, unless stated otherwise. Pressure differences of 2 bara were applied except for the point at 3 bara feed pressure for which a pressure difference of 1.5 bara was used. A retentate flow of 50 mL/min was applied for all measurements. Measurements were performed using He, H_2, N_2, CH_4, and CO_2 in a 5.0 purity. Before measurement, each membrane was dried for two hours at 523 K under N_2. H_2 permeance measurements were performed as first and last measurement.

The TGA measurements were performed on the xerogels with a MT TGA/SDTA851 in pure nitrogen with a heating ramp of 1°C/min. The xerogels were prepared by drying 10 ml of the sols in Petri dishes under a fume hood. After complete drying, the materials were ground before further characterization.

6.3. Results

6.3.1 Self-supported materials characterization

To assess the effectiveness of the retro-DA reaction, TGA measurements under N_2 were performed on self-supported xerogels. The weight loss of the two reference xerogels (BTESEt and BTESO/VTES) are compared with their corresponding DA-adducts (Figure 6.4). The weight loss differences between the parent compounds and their DA-adducts were significant.

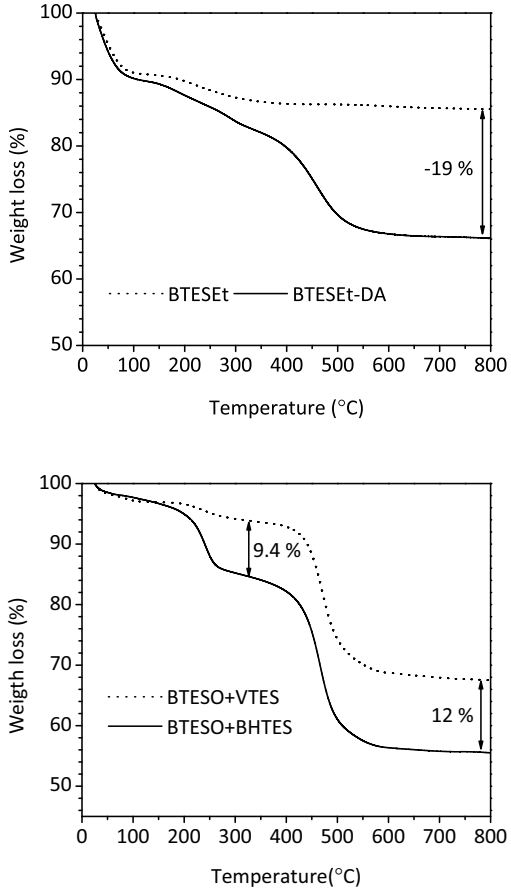

Figure 6.4. TGA of the DA-adducts as compared to the starting precursors (blank)

From RT to 120 °C, the BTESEt and the BTESEt-DA xerogels exhibited similar weight losses of about 10 wt%. A clear difference in weight loss was observed for both BTESEt-based xerogels between 100 °C and 700 °C. The pyrolysis of the BTESEt xerogels led to a weight loss of 5 wt% while the BTESEt-DA xerogel showed a weight loss of 24 wt% over this temperature range. The final difference in weight loss for both components was 19 wt%.

The BTESO/VTES and the BTESO/BHTES xerogels exhibited a similar weight loss of only 2 to 3 % from RT to 100 °C. Two consecutives weight loss steps were observed at 250 °C and 475 °C for both xerogels. For the BTESO/VTES xerogels the first weight loss was only 2 wt% while for the BTESO/BHTES this weight loss represented 11 wt%. The BTESO/VTES and BTESO/BTES xerogels exhibited similar weight loss at 475 °C with 26.5 and 29 % respectively.

6.3.2 Membrane Characterization

Bridging dienophile

The BTESEt and BTESEt-DA sols were coated on γ-Al_2O_3 supports. Interestingly, the BTESEt layers were particularly sensitive to the thickness of the layers and cracked during the heat treatment for thicknesses higher than 600 nm (Figure 6.5a). The first coating of the BTESEt-DA sol resulted in infiltrated layers with relatively rough surfaces (for an example see the figures 5b and 5c).

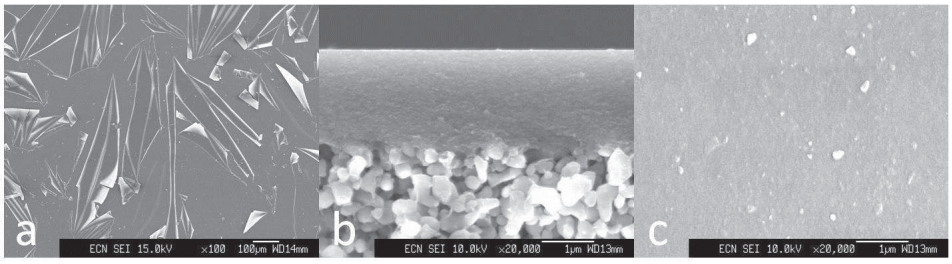

Figure 6.5. SEM pictures of a cracked BTESEt layer (a) and of an infiltrated BTESEt-DA layer (b, c)

Thicker BTESEt-DA membrane layers were coated after optimization of the ratios of the sol to Si/EtOH/H^+/H_2O = 1/3.8/0.08/2.55. Similarly to the BTESEt layers, the BTESEt-DA layers were particularly sensitive to layer thickness variations and cracked during the heat treatment despite been crack free after the overnight drying in the clean room and having layer thicknesses lower than 600 nm. Possibly, in both cases the presence of an ethylene bridge leads to a relatively stiff network. For layers above a certain critical thickness, the network then cannot properly accommodate the stress related to the drying and heat-treatment shrinkage. These processes probably lead to the macroscopic cracks and breakup of the top layer of the membranes (Figure 6.6). Further analysis was not performed because of these macroscopic cracks.

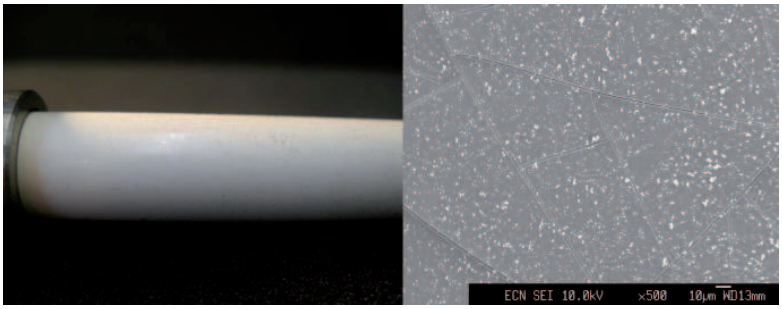

Figure 6.6. SEM and optical microscopy pictures of a BTESEt-DA membrane after heat treatment

Terminal dienophile

For BTESO/VTES and equimolar BTESO/BHTES membranes, the SEM images for these membranes after heat treatment showed that thin defect free hybrid layers with thicknesses ranging from 100 to 200 nm were obtained. Gas permeation measurements were performed on both types of membranes and the N_2, H_2, and CO_2 permeances were plotted against the average pressure (Figure 6.7).

Both membranes showed no significant dependence on the average pressure in gas permeance measurements. As explained in chapter 2, this is an indication of the absence of viscous flow and consequently of the membrane quality and absence of large defects [24]. In both cases

minor (<10%) differences between the first and the second H_2 permeance measurement were observed, so no major structural changes have occurred over the measurement series. A significant increase of the permeance of the BTESO/BHTES membrane was expected if the retro DA-reaction occurred. But despite of its small layer thickness, which should favor the occurrence of the retro-DA reaction, the BTESO/BHTES membrane showed similar permeances as the BTESO/VTES membrane. In addition H_2/N_2 ratios of both membranes were also similar with values of 5.5 and 6.7 respectively.

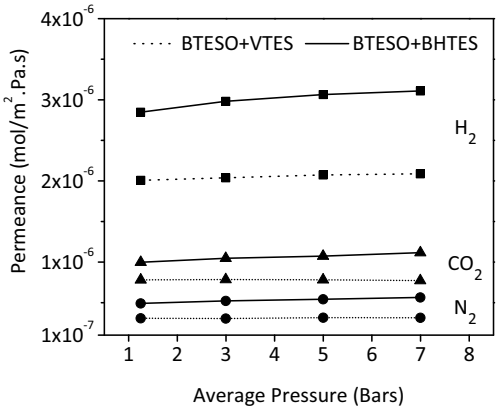

Figure 6.7. H_2, N_2, and CO_2 permeances of the BTESO/VTES and equimolar BTESO/BHTES membranes at 250 °C

Influence of the length of the bridge and of the BHTES molar ratio

The influence of the length of the bridge and the molar ratio of BHTES on the retro-DA reaction were investigated. The use of a C_2 bridged precursor (BTESE) was first studied. When taking into account the layer thicknesses of both membrane types, BTESE/BHTES and the BTESO/BHTES membranes have similar gas permeances (Table 6.2). Sols with 75 % of BHTES were also developed for both BTESO and BTESE. After heat treatment, the SEM measurements revealed smooth defect free hybrid layers of 60 and 100 nm. The gas permeation measurements also showed no viscous flow, thus confirming the absence of defects. The H_2 permeances and the H_2/N_2 ratios were equivalent to the equimolar membranes.

Table 6.2. H_2/N_2 ratios at 250 °C of the BTESE/BHTES and the BTESO/BHTES membranes with 50 and 75 mol% of BHTES

	BHTES concentration (mol%)	H_2/N_2	H_2 permeance (10^{-6} mol/m^2.Pa.s)
BTESE+BHTES	50	5.5	2.4
	75	5.2	6
BTESO+BHTES	50	6.4	3
	75	5.5	4

Alternative heat treatments

Three different alternative heat treatments were performed on BTESO/BHTES membranes to study the influence of the heat treatment conditions on the retro-DA reaction. The first heat treatment procedure was based on the standard 250 °C heat treatment with the additional condition of vacuum (< 100 mBar). For the second alternative heat treatment, a green membrane was installed in the gas permeation setup. This membrane was exposed to temperatures of 100 °C, 200 °C and 300 °C for 10 hours each, with a N_2 pressure difference (ΔP) of 2 bars. The N_2 permeance was measured every hour. Finally a last treatment was performed in the gas permeation setup. At 300 °C, two different ΔP (2 and 5 bars) were applied across the membrane and the N_2 permeance was measured every hour during 10 hours. In all cases, characterization was carried out by standard gas permeance after the heat treatment. The heat treatment under vacuum resulted in no differences compared to membranes treated under standard conditions, and similar H_2 permeances and H_2/N_2 ratio were measured. Also no significant permeance changes were observed for the second and third heat treatment performed in the gas permeation setup.

As a last measurement, four membrane types were subjected to a heat treatment procedure of stepwise increasing temperatures in the gas permeation setup (Figure 6.8). The temperature was gradually increased from 250 to 450 °C and the N_2 permeance was measured after 2 hours of residence time at each temperature.

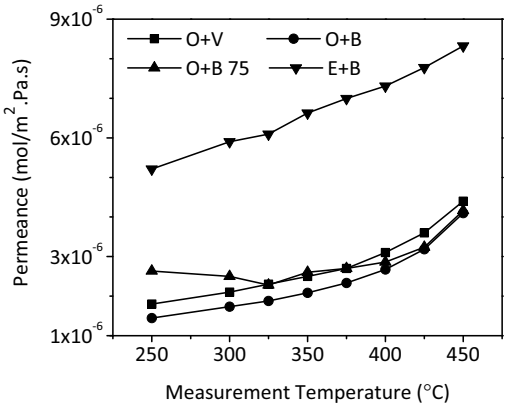

Figure 6.8. Gas permeances of BHTES-based membrane against the measurement temperature. The letter O stands for BTESO, E for BTESE, B for BHTES, V for VTES and 75 for 75 mol% of BHTES in the sol

For all membranes, we expected a stepwise increase of the permeance at a certain temperature if the retro-DA reaction would have occurred. Clearly, such stepwise increase of the permeance was not observed for any of the membranes. In addition, the H_2/N_2 ratio of the membranes stayed relatively constant over the temperature range with values between 4.5 and 7.

6.4. Discussion

The aim of this chapter was to investigate the pore size templating of hybrid silica membranes using thermo labile DA adducts. The success of such templating first requires the release of the template at temperatures below the decomposition temperature of the organic part of the hybrid network (≈ 300-350 °C). Secondly, the template removal has to result in a percolation path without creating defects. If both requirements are fulfilled, defect free templated hybrid membranes with a pore size of about 0.8-0.9 nm are expected.

The TGA was a powerful tool to assess the temperature of the retro-DA reaction in the BTESEt and the equimolar BTESO/BHTES xerogels. Interestingly, all the xerogels exhibited lower total weight losses than expected from the weight of the organic part of

the xerogel network, whereas the final weight losses differences were close to the calculated values based on the weight of the DA adduct. The total weight losses measured for the BTESEt, BTESEt-DA, BTESO/VTEs and BTESO/BHTES were 15, 34, 33, and 45 wt% respectively, whereas the expected values were of 20, 40, 48, and 57 wt% respectively. Final weight loss differences of 9 and 12 wt% were measured for the BTESEt : BTESEt-DA and the BTESO/VTES : BTESO/BHTES xerogels respectively. The expected values were 10 and 9 wt% respectively. This observation and the black appearance of the xerogels after the TGA measurements indicate that under inert conditions the DA adduct decomposed and probably evaporated as gaseous component while a part of the bridges, which varies between the xerogels, probably remained in the xerogel as carbon.

The decomposition patterns of the BTESEt and BTESEt-DA xerogels show a weight loss trajectory between 100 and 700 °C. This suggests that the retro-DA reaction did not occur at a sufficiently low temperature and that the organic part of the network comprising the ethene bridge and the DA adduct degraded simultaneously in the BTESEt-DA xerogel. For the BTESEt-DA based xerogels the first requirement of template removal at suitable temperatures is not reached. All the BTESEt-DA based membranes cracked during the heat treatment. The same behavior was observed for the BTESEt membranes suggesting that the rigid ethylene bridge is not suitable for such a templating method. More reactive adducts, such as suggested by Shaltout [21], would be released at lower temperatures but would also induce the same stress as the cyclopentadiene to the rigid BTESEt-DA network. Consequently, the use of more reactive adducts would also result in cracked membranes.

For the equimolar BTESO/BHTES and BTESO/VTES xerogels in which the cyclopentadiene is placed on a terminal group, two clear consecutive weight loss steps were observed at 250 °C and 475 °C. At 250 °C the weight loss difference was equivalent to the theoretical 9 wt% while both xerogels exhibited similar weight losses at 475 °C. This suggests that the majority of the cyclopentadiene was released at 250 °C for BTESO/BHTES and that the remaining organic part of the network degraded at 475 °C for both xerogels. Clearly, the retro-DA reaction occurred quantitatively below the decomposition temperature of the bridging

organic fragment for the BTESO/BHTES xerogels, thereby fulfilling the first requirement for successful templating.

We anticipated that template removal in the layers would lead to a pore size of around 1 nm and would therefore result in clear changes of the gas permeance and H_2/N_2 ratios of the membranes. Unfortunately, the characterization of the BTESO/BHTES and BTESO/VTES membranes showed that both membranes exhibited similar gas permeance properties. Alternative heat treatments, the use of an ethane bridge or the increase of the amount of BHTES in the sol up to 75 mol% did not result in clear changes of the H_2/N_2 ratios and H_2 permeances of the membranes. Clearly, this approach of pore size templating using thermo-labile groups situated on a pendant group also failed. This failure can be ascribed to failure of the approach in general or to more specific intrinsic properties of the hybrid silica network.

In chapter 2, we showed that for sols based on a mixture of bridging and terminal alkoxysilanes, the ratios of precursors present in the sol and in the resulting layer are not automatically equal. For amino-functionalized precursors, the XPS measurements showed that the amount of functionalized precursors can be up to a factor 10 lower in the hybrid layers compared to in the sols. Similar differences between the BHTES concentration in the sols and in the layers are possible. Brinker's group showed that in the case of a pure silica network templated with 3-methacryloxypropylsilane (MPS) an amount of 10 vol% of MPS is sufficient to create a percolation path when the template is quantitatively removed [16]. In our case, the effective amount of template (BHTES) present in the hybrid layer might even be lower. Unfortunately, no quantitative analysis of the amount of BHTES in the layers and of the yield of the retro-DA reaction could be performed due to the compositional similarity between the VTES and the BHTES. Alternatively, the intrinsic properties of the hybrid silica network might also explain the failure of this templating method. For hybrid silica networks involving long bridged precursors [25] a collapse of the porosity of the hybrid xerogel was reported. For templated (hybrid) silica materials or membranes in which micellar templates are used, microporous walls are created around the mesoporous structure. These stay intact after the thermal or chemical removal of the template. Here, we have used small templates

that are covalently bonded to a precursor which is part of the relatively flexible hybrid silica network. Castricum et al. discuss this flexibility for BTESO membranes [26]. A collapse of the porosity might occur during the retro-DA reaction, which would only allow the release of the cyclopentadiene moieties that are present at the surface. Currently, we regard this potential collapse of porosity as the most important issue. Additional and alternative experiments are suggested in the next chapter.

6.5. Conclusion & recommendations

In this chapter, an alternative pore size templating method of hybrid silica membranes using the retro-DA reaction was explored. The DA adduct was placed either on the bridge of the ethylene bridged 2,3-Bis(triethoxysilyl)ethene (BTESEt) precursor or on the terminal silane vinyltriethoxysilane (VTES). For the first option, the TGA measurements showed that the BTESE-DA xerogel did not meet the most important requirement for successful templating: the DA adduct could not be removed at a suitable temperature. The organic part of the hybrid network and the DA-adduct pyrolyzed simultaneously. In addition, the ethylene bridge of the BTESEt and BTESEt-DA layers imposed too much rigidity in the hybrid structure. Therefore, we favor the use of terminal groups for templating. Using this approach, the retro-DA reaction occurs quantitatively in the xerogels and at sufficiently low temperatures to preserve the organic part of the hybrid network. Despite this apparent removal of the template, no influence on the membrane performance was observed. We presume that collapse of the porous structure is responsible for the lack of successfully templated supermicropores.

For further development, we propose that the DA-adduct should be carefully chosen such that a quantitative analysis of the amount of DA-adduct in final the layer and the yield of the retro-DA reaction is possible. The use of electron acceptor functional groups with hetero-atoms that are not present in the hybrid backbone would facilitate the analysis and could improve reactivity at the same time. Further studies should focus first on xerogels, before membranes are prepared. Only when the adduct is removed and remaining porosity is proven, membranes should be coated and characterized.

References

[1] T. Asefa, M.J. MacLachlan, and N. Coombs, Periodic mesoporous organosilicas with organic groups inside the channel walls, *Nature*, 402, 867, 1999

[2] J.S. Beck, J.C.Vartuli, W.J. Roth, M.E. Leonowicz, C.T. Kresge, K.D. Schmitt, C.T.W. Chu, D.H. Olson, E.W. Schepard, S.B. McCullen, J.B. Higgins, and K.D. Schmitt, A New Family of Mesoporous Molecular Sieves Prepared with Liquid Crystal Templates, *Journal of the American Chemical Society*, 114, 10834-10842, 1992

[3] S.L. Burckett, S.D. Sims, and S. Mann, Synthesis of hybrid inorganic-organic mesoporous silica bu co-condensation of siloxane and organosiloxane precursors, *Chemical Communications*, 1367-1368, 1996

[4] M.C. Burleigh, M.A. Markowitz, M.S. Spector, and B.P. Gaber, Direct synthesis of Periodic Mesoporous Organosilicas: Functional Incorporation by Co-condensation with Organosilanes, *J.Phys Chem.B*, 105, 9935-9942, 2001

[5] M. Calvo, P.C. Angelome, V.M. Sanchez, D.A. Scherlis, F.J. Williams, and G.J.A.A. Soler-Illia, Mesoporous aminopropyl-functionalized hybrid thin films with modulable Surface and environment-responsive behavior, *Chemistry of Materials*, 20, 4661-4668, 2008

[6] G.E. Fryxell, The synthesis of functional mesoporous materials, *Inorganic Chemistry Communications*, 9, 11, 1141-1150, 2006

[7] R. Mouawia, M. Ahmad, C. Reye, and R.J.P. Corriu, Direct synthesis of ordered and highly functionalized organosilicas containing carboxylic acid groups, *Journal of Materials Chemistry*, 17, 616-618, 2007

[8] G.J.A.A. Soler-Illia, P.C. Angelome, and P. Bozzano, Highly ordered hybrid mesoporous bifunctional thin film, *Chemical Communications*, 2854-2855, 2004

[9] T. Tsuru, T.Sudoh, T. Yoshioka, and M. Asaeda, Nanofiltration in non-aqueous solutions by porous silica-zirconia membranes, *Journal of Membrane Science*, 185, 253-261, 2001

[10] T. Tsuru, Nanoporous titania membranes for permeation and filtration of organic solutions, *Desalination*, 233 (1-3), 1-9, 2008

[11] T. van Gestel, H. Kruidhof, D.H.A. Blank, and H.J.M. Bouwmeester, ZrO_2 and TiO_2 membranes for nanofiltration and pervaporation: Part 1. Preparation and characterisation of a corrosion-resistant ZrO_2 nanofilytration membrane with a MWCO<300, *Journal of Membrane Science*, 284, 128-136, 2006

[12] T. van Gestel, D. Sebold, H. Kruidhof, and H.J.M. Bouwmeester, ZrO_2 and TiO_2 membranes for nanofiltration and pervaporation: Part 2. Development of ZrO_2 and TiO_2 toplayers for pervaporation., *Journal of Membrane Science*, 318, 413-421, 2008

[13] H.L. Castricum, R. Kreiter, H.M. van Veen, D.H.A. Blank, J.F. Vente, and J.E. ten Elshof, High-Performance Hybrid Pervaporation Membranes with Superior Hydrothermal and Acid-Stability., *Journal of Membrane Science*, 324, 1-2,111-118, 2008

[14] H.M. van Veen, M.D. Rietkerk, D.P. Shanahan, M.M.A. van Tuel, R. Kreiter, H.L. Castricum, J.E. ten Elshof, and J.F. Vente, Pushing membrane stability boundaries with HybSi® pervaporation membranes, *Journal of Membrane Science*, 380, 124-131, 2011

[15] G. Xomeritakis, S. Naik, C.M. Braunbarth, C.J. Cornelius, R. Pardey, and C.J. Brinker, Organic-Templated silica membranes I. Gas and vapor transport properties, *Journal of Membrane Science*, 215, 225-233, 2003

[16] Y. Lu, G. Cao, R.P. Kale, S. Prabakar, G.P. Lopez, C.J. and Brinker, Microporous Silica Prepared by Organic Templating: Relationship between the Molecular Template and Pore Structure, *Chemistry of Materials*, 11, 1223-1229, 1999

[17] D.A. Loy, R.J. Buss, R.A. Assink, G. Beaucage, K.J. Shea, and H. Oviatt, Porous materials by design. Plasma oxidation of hydrocarbon templates in polysilsesquoxanes, *Polym. Prepr. Am. Chem. Sot. Div. Polym. Chem.*, 34, 244-245, 1993

[18] A. Katz and M.E. Davis, Molecular inprinting of bulk, microporous silica, *Nature*, 403, 286-289, 2000

[19] J.L. Defreese and A. Katz, Shape-selective covalent binding in bulk, microporous imprinted silica, *Microporous and Mesoporous Materials*, 89, 25-32, 2006

[20] W. Zhu, T. Shengyang, C. Tao, W. Li, C. Lin, M. Li, Y. Wen, and G. Li, Hierarchically Imprinted Porous Films for Rapid and Selective Detection of Explosives, *Langmuir*, 27, 8451-8457, 2011

[21] R.M. Shaltout, D.A. Loy, M.D. McClain, S. Prabakar, J. Greaves, and K.J. Shea, Structural modification of sol gel materials through retro Diels-Alder reaction, *Polymer Preprints*, 41, 1,508-509, 2000

[22] M.D. McClain, D.A. Loy, and S. Prabakar, Controlling porosity in bridged polysilsesquioxanes through elimination reactions, 1996

[23] C.J. Brinker, R. Sehgal, S.L. Hietala, R. Deshpande, D.M. Smith, D.A. Loy, and C.S. Ashley, Sol-gel strategies for controlled porosity inorganic materials, *Journal of Membrane Science*, 94, 85-102, 1994

[24] R.S.A. de Lange, Microporous sol-gel derived ceramic membranes for gas separation, Thesis Dissertation, University of Twente, 1993

[25] D.A. Loy, G.M Jamison, B.M. Baugher, E.M. Russick, R.A. Assink, S. Prabaker, and K.J. Shea, Alkylene-bridged polysilsesquioxane aerogels: highly porous hybrid organic-inorganic materials, *Journal of Non-Crystalline Solids*, 186, 44-53, 1995

[26] H.L. Castricum, G.G. Paradis, M.C. Mittelmeijer-Hazeleger, R. Kreiter, J.F. Vente, and ten J.E. Elshof, Tailoring the Separation Behavior of Hybrid Organosilica Membranes by Adjusting the Structure of the Organic Bridging Group, *Advanced Functional Materials*, 21, 9, 2319-2329, 2011

Chapter 7

Conclusion and recommendations

7.1. Functionalization of microporous hybrid silica membranes

7.1.1 Evaluation

A major part of this thesis describes the functionalization of organic-inorganic hybrid silica membranes based on bridged α,ω-bis(triethoxysilyl)alkanes. Triethoxysilanes containing alkane or amino-functional groups were used as functionalized precursors. Thin defect free membranes with properties clearly related to the nature of the triethoxysilane introduced in the hybrid network were obtained. Hydrophilic amino functionalized triethoxysilanes and hydrophobic alkyltriethoxysilanes resulted in hydrophilic and hydrophobic membranes, respectively. In addition, the hydrophobic membranes exhibited constant selectivity in pervaporation as a result of the three dimensional hybrid silica network. Clearly, this shows that functionalized triethoxysilanes precursors can be used to modify the affinity of hybrid silica membranes towards targeted applications. In short we have demonstrated that:

- Functionalized triethoxysilanes of completely different nature can be easily accommodated in a hybrid silica microporous network
- The affinity of the functional groups governs the properties of the resulting membranes
- The hybrid silica network retains its non-swelling properties

In addition to their nature, the amount of functionalized triethoxysilane precursor in the hybrid layer is essential. We clearly showed in Chapter 2 that a minimum loading of amino-functionalized precursors is required to benefit from their hydrophilicity. Above this threshold value, all the membranes exhibited high water selectivity in pervaporation of low water content water/alcohol mixtures. Importantly, these threshold concentrations were low for all amino-functionalized precursors. A low concentration of terminally functionalized triethoxysilane means that the network is mainly composed of BTESE moieties that have a twice-higher connectivity than triethoxysilanes. This connectivity has been proposed as

one of the main factors in the stability of the hybrid silica network [1]. We thus expect that this has positive effects on the hydrothermal stability of the membranes and that the hybrid functionalized membranes have comparable stability as their parent BTESE membranes.

Possible applications of both the amino-functionalized and the hydrophobic RTES/BTESE membranes are water removal and concentration of organics by pervaporation, respectively. The amino-functionalized membranes have shown equivalent selectivities and fluxes as the BTESE membranes in the dehydration of low water content water/alcohol mixtures by pervaporation. Importantly, the most hydrophobic membrane (D membrane of chapter 4) proved to be the first butanol selective hybrid silica membrane example in organophilic pervaporation. Despite its reasonable n-butanol flux, the selectivity of this membrane type needs to be doubled to envisage implementation.

We have demonstrated that the separation mechanism of both functional hybrid silica membrane types is based on affinity rather than on molecular sieving, as usually observed for non-functionalized hybrid silica membranes [2]. For the amino-functionalized membranes, the adsorption of multi layers of water in the pores of the membranes increased their selectivity in the process. For the hydrophobic hybrid silica membrane, the selectivity was independent of the evaporation selectivity. In addition the most hydrophobic membrane was n-butanol selective in the pervaporation of water/n-butanol mixtures with low n-butanol concentration. Because the n-butanol molecule is obviously larger than water, the separation can only be based on the affinity of n-butanol towards the membrane network.

7.1.2 Recommendations & outlook

As mentioned above, a functionalized hybrid network with a low concentration of functionalized triethoxysilane precursors is expected to conserve the hydrothermal stability of the BTESE-based hybrid network. None of the amino- and the alkyl-functionalized membranes showed a deterioration of their performances during the pervaporation tests that lasted up to 10 days. Nevertheless, it is advisable to test these membranes in long term pervaporation experiments using real industrial mixtures. In this way, the high potential of these membranes can be confirmed.

The amino-functionalized membranes have large potential for improvement of the performance. In general, the decrease of the layer thickness of a membrane results in a direct flux increase. In return, thin layers in ceramic membranes increase the probability of defects. This generally results in a decreased selectivity when the separation mechanism is based on molecular sieving. In the case of the amino-functionalized membranes, water molecules strongly adsorb on the amino groups that are present in the micropores. The same phenomenon would also occur in larger pores or small defects and decrease their effective size. Consequently, the selectivity of the membranes should not be affected by the presence of such larger pores, or at least not as severely as the parent BTESE membranes. Thus, we foresee that the fluxes can be largely increased by optimizing the layer thickness, without a significant decrease of the selectivity.

Turning to hydrophobic membranes, the pervaporation measurements clearly showed that the selectivity of the membranes is directly related to the intrinsic hydrophobicity of their network. As mentioned above, the future applicability of these membranes requires an increase of their selectivity. To this end, a number of options can be suggested.

As a first step, the amount of hydrophobic alkyl fragments introduced in the layers can be increased. For this purpose, alkyltriethoxysilanes with longer chains than C_{10} could be envisaged. However, we have shown in Chapter 3 that the introduction of C_{18} alkyltriethoxysilanes in a BTESE sol leads to precipitation of the sol. Possibly, the solvent and/or the nature of the acid have to be adapted: less polar solvents and/or weaker acids might be required. To counter these issues resulting from the use of long linear alkyl chains, but at the same time increase the content of alkyl fragments in the hybrid layer, branched alkyltriethoxysilanes could be a suitable alternative. The increased organic content likely results in a higher hydrophobicity. And, more importantly, branched chains will decrease the probability of sol precipitation, as hydrolyzed branched alkyltriethoxysilane moieties would be less amphiphilic than their linear counterparts.

Secondly, the nature of the hydrophobic fragment could be changed. Commercially available fluorinated precursors are commonly and successfully used for the hydrophobization of

mesoporous membranes [3,4]. A similar effect can be expected if such hydrophobic groups are introduced in a microporous hybrid silica network.

Finally, examples of polymeric membranes based on PDMS and PTMSP with high organic selectivities were given in Chapter 4 (Table 4.2 and references therein). As for the hydrophobic membranes developed in this thesis, their selectivity for organics can be ascribed to the intrinsic hydrophobicity of the material. Such polymers could be used to further hydrophobize the already hydrophobic hybrid silica network, by suitable blending methods. A possible approach is to dissolve the polymer directly in the hybrid silica sol at the end of the sol synthesis. In this way, the hybrid silica sol blended with the hydrophobic polymers could be coated similarly as a standard sol. After a careful thermal treatment allowing for both the consolidation of the layer and survival of the polymer functionality, membranes which potentially combine the affinity of the hydrophobic polymers with the non-swelling behavior of the hybrid network are expected.

7.2. Pore size tuning of hybrid silica membranes using thermo-labile groups

7.2.1 Evaluation

Chapter 6 was dedicated to the exploration of the use of thermo-labile templating groups to tune the pore size of the hybrid silica membranes. In this pore size templating method the templates are covalently bonded to the hybrid silica network and should be removed by use of a thermal treatment. Apart from the importance of the reactivity of the adduct, this study highlighted that the rigidity of the host network plays a major role. The experiments performed on the BHTES/BTESR membranes revealed the possible collapse of the porosity of the network after the removal of the Diels Alder adduct. At the same time, it was observed that the ethylene bridge of the BTESEt precursor is too rigid and imposes stress during the heat treatment, eventually leading to cracks. Clearly, the applicability of such templating methods depends on the ability to find the right bridged precursor that is flexible enough to allow the removal of the template without defect formation, but also rigid enough to prevent the collapse of the porosity.

7.2.2 Recommendations & outlook

The use of the retro Diels-Alder reaction can be further explored mainly to find a bridged precursor exhibiting the proper rigidity. With this idea in mind, the benzene and biphenyl bridged precursors mixed with BHTES could be a suitable candidate. We showed that the BHTES was quantitatively removed at a relatively low temperature and that defect free membranes can be obtained with both bridged precursors [5]. The properties were clearly related to the higher rigidity compared to the alkane bridged precursor. Such groups can be seen as intermediates between the flexible alkane bridge and the rigid ethylene bridge. Clearly, these functional groups have one degree of freedom less than ethane bridges but also one more compared to ethylene groups. This could offer the perfect intermediate flexibility to allow the removal of the Diels Alder adduct from the BHTES moieties while retaining the porosity created by the removal of the adduct.

The use of a thermal treatment can also be seen from a different perspective. A controlled thermal decomposition of the hybrid network could be used to tune the pore size of hybrid silica membranes. The main application of a microporous membrane with a pore size ranging from 1 to 2 nm would be organic nanofiltration. For such specific application, the organic backbone of the hybrid network is not as important as for pervaporation. Li demonstrated that in pure triethoxysilane xerogels the phenyl pendant group starts to degrade at about 400 °C while the methyl groups are stable up to 500 °C [6]. The development of hybrid silica membranes with organic groups decomposing at different temperatures could be envisaged. A controlled thermal degradation of the less thermally stable groups of the organic fragments will possibly create large pores while a sufficient amount of organic fragments remains in the network to maintain the hydrophobicity of the membranes. A complete thermal decomposition of the hybrid silica network also creates silica membranes with increased pore sizes [7]. However, the result would possibly be a structure in which the remaining carbon fraction is not connected to the silica backbone, which might remove all the hydrothermal stability benefits of the organic-inorganic hybrid silica network.

Finally, we already suggested to blend hybrid silica sols with hydrophobic polymers to further hydrophobize hybrid silica membranes. Such concept can also be used with the polymers as templates rather than as hydrophobizing agent. This concept is similar to the concept of interpenetrating networks that used for polymeric membranes to tune their pore size [8]. In our case, the approach would be to combine a polymer network and a hybrid silica network. This interpenetrated composite material can be used for the formation of a continuous porous structure of well-defined size. The polymers would be introduced in hybrid silica sols, similar to the approach in which they are used as hydrophobizing agent, and the resulting sol coated. But in this case, the polymers will be removed from the membrane layer using either a washing step or a thermal treatment creating new porous network. Ideally, this results in hybrid silica membranes with pore of the diameter of the polymers. The main issue with such a method would probably be the optimization of the polymer loading. The density of the polymer should allow the formation of a strong enough hybrid matrix after removal of the polymer. But at the same time a sufficient loading of polymer should be present to ensure the formation of a percolation path after the washing procedure. If such concept proved to be successful, all kind of functionalized membranes with various pore sizes and functionalities can be developed.

7.3. Conclusion

Functionalized microporous hybrid silica membranes as described in thesis are the next step in the hybrid silica membrane concept as compared to BTESE-based membranes. The separation mechanism of such membranes is based on affinity, adding an extra dimension to the tuneability of porous hybrid silica materials towards specific separation processes. Moreover, the introduction of large organic fragments in the hybrid structure implies that these membranes shift further from inorganic and organically modified silica towards (dense) polymeric membranes. Ultimately, as proposed in this chapter, the current concept of hybrid membranes can be extended to hybrid-composite materials by physically mixing hybrid silica sols and polymers, leading to yet unprecedented membrane properties.

References

[1] H. L. Castricum, A. Sah, R. Kreiter, D.H.A. Blank, J.F. Vente, and J.E. ten Elshof, Hybrid ceramic nanosieves: stabilizing nanopores with organic links, *Chemical Communications*, 1103-1105, 2008

[2] R. Kreiter, M.D.A. Rietkerk, H.L. Castricum, H.M. van Veen, J.E. ten Elshof, and J.F. Vente, Stable hybrid silica nanosieve membranes for the dehydration of lower alcohols, *ChemSusChem*, 2, 2, 158-160, 2009

[3] W. Kujawski, S. Krajewska, M. Kujawski, L. Gazagnes, A. Larbot, and M. Persin, Pervaporation properties of fluoroalkylsilane (FAS) grafted ceramic membranes, *Desalination*, 205, 1-3, 75-86, 2007

[4] C. Picard, A. Larbot, E. Tronel-Peyroz, and R. Berjoan, Characterisation of hydrophilic ceramic membranes modified by fluoroalkylsilanes into hydrophobic membranes, *Solid State Sciences*, 6, 605-612, 2004

[5] H.L. Castricum, G.G. Paradis, M.C. Mittelmeijer-Hazeleger, R. Kreiter, J.F. Vente, and J.E. ten Elshof, Tailoring the Separation Behavior of Hybrid Organosilica Membranes by Adjusting the Structure of the Organic Bridging Group, Advanced Functional Materials, 21, 9, 2319-2329, 2011

[6] G. Li, M. Kanezashi, and T. Tsuru, Preparation of organic-inorganic hybrid silica membranes using organoalkoxysilanes: The effect of pendant groups, *Journal of Membrane Science*, 379, 287-295, 2011

[7] C.J. Brinker, R. Sehgal, S.L Hietala, R. Deshpande, D.M. Smith, D.A. Loy, and C.S. Ashley, Sol-gel strategies for controlled porosity inorganic materials, *Journal of Membrane Science*, 94, 85-102, 1994

[8] M. Ulbricht, Advanced functional polymer membranes, *Polymer*, 47, 7, 2217-2262, 2006

Summary

The research presented in this thesis focuses on the functionalization and pore size tuning of microporous hybrid silica membranes for liquid separation. The research described covers hybrid silica materials properties, ranging from extremely hydrophilic up to hydrophobic porous materials. Alternative routes for directing the pore size in sol-gel membranes are covered. In addition, the application of these materials as membranes in aqueous and organophilic pervaporation, and solvent nanofiltration is described.

Chapter 1 gives a general introduction on porous membranes to then focus on asymmetric supported microporous hybrid silica membranes. This introductory chapter highlights the unprecedented hydrothermal stability of 1,2-bis(triethoxysilyl)ethane (BTESE) based hybrid silica membranes, and emphasizes the benefits of functionalization and tuning of the pore size of such microporous hybrid silica membranes. Both approaches potentially allow for a much broader field of application of this class of sol-gel membranes.

Chapter 2 presents the first example of functionalization of hybrid silica membranes for molecular separations. The effect of the incorporation of amino-functionalized terminating groups on the behavior and performance of hybrid silica membranes is presented. The characterization of the membranes clearly shows the ability to modify the affinity of BTESE-based membranes by introducing a suitable precursor: hydrophilic precursors lead to hydrophilic membranes. In addition, this study highlights that for each precursor a minimum concentration level is present above which the hydrophilic properties of the amino-functionalized precursors are fully present. At amine concentrations higher than this threshold value, the membranes exhibited high water selectivities in dehydration of water/alcohol feed mixtures. This presence of a minimum concentration of functionalized precursors is intrinsic to terminal functional groups and can probably be extended to all functionalization types.

Chapter 3 focuses on the synthesis and characterization of BTESE/R-triethoxysilane (RTES, R = C_1-C_{18} alkyl) xerogels. Small Angle X-ray Scattering (SAXS), CO_2 and N_2 adsorption, as well as contact angle measurements were performed to assess the properties of these materials. This chapter highlights the structural organization, the changing adsorption properties and hydrophobicity of the xerogels depending on the length of the R-group. In addition, the RTES/BTESE molar ratio and the synthesis conditions influence these properties. It was found that longer R groups, more reactive sol synthesis conditions and pre-hydrolysis of the RTES precursor all lead to more organized nano–domains in the final material. In contrast, the hydrophobicity and adsorption properties were more dependent on the length of the R-group in the RTES precursor than on the synthesis conditions.

The equimolar BTESE/RTES (R = C_1-C_{10} alkyl) compositions were selected for coating and characterization as hybrid silica membranes in **Chapter 4**. The incorporation of R-triethoxysilanes (R = C_1 to C_{10}) resulted in a change of the membrane affinity from hydrophilic (for R = C_1) to hydrophobic (for R = C_6 and longer). A strong relation between the separation properties of the membrane and the length of the R-group was found, in pervaporation of water/n-butanol mixtures. Longer R-groups resulted in lower water separation factors, whereas the separation factor towards n-butanol increased. The most hydrophobic membrane showed a stable selectivity over a large range of operating conditions as well as total fluxes in the range of several $kg.m^{-2}.h^{-1}$. This is the first example of a hybrid silica membrane exhibiting a selectivity towards n-butanol. Based on these results, the potential use in biobutanol production was discussed and compared to the state of art of organophilic polymeric membranes.

These BTESE/RTES (R = C_1-C_{10} alkyl), a BTESO (C_8 ethane bridge) and a BTESO/C_{10}TES membrane were tested and compared to the γ-Al_2O_3 support under nanofiltration conditions in **Chapter 5**. Despite their high pervaporation fluxes, low acetone and toluene fluxes were measured for all membranes. Nevertheless, this study revealed the possible adsorption of water on the γ-Al_2O_3 support and provided leads for future research directions.

The membrane tests described in chapter 5 indicate that the pore size of these hydrophobic hybrid silica membranes are possibly too small for nanofiltration applications. Therefore, **Chapter 6** is dedicated to the exploration of an alternative pore templating method for hybrid silica membranes using thermo-labile adducts. The Diels-Alder adduct was selected for this approach, because it allows for selective thermal removal of the template, whilst leaving intact the hybrid silica backbone. The measurements performed on xerogels and membranes highlight the essential role of flexibility in the hybrid silica network for this approach. The concept and the approach used in thus study are discussed and new research directions are proposed.

Finally, the conclusive **Chapter 7** is dedicated to a broader evaluation of the functionalization and pore size tuning of hybrid silica membranes. The work described in this thesis shows that a wide range of (functional) precursors can be incorporated in a hybrid silica matrix. The functionality of the precursors is transferred to the functionality of the material and also of membranes derived from these materials. This means that an extensive toolbox of options is available for dedicated and tailor made membrane development.

Samenvatting

Het onderzoek beschreven in dit proefschrift richt zich op de functionalisering en het sturen van de poriegrootte van microporeuze hybride silica membranen voor vloeistof scheidingen. Het beschreven onderzoek heeft betrekking op de eigenschappen van de hybride silica materialen, die variëren van zeer hydrofiel tot hydrofoob. Daarnaast worden alternatieve routes voor het sturen van de poriëngrootte in sol-gel membranen worden behandeld. De toepassing van deze materialen als membraan in waterige en organofiele pervaporatie en organische nanofiltratie wordt ook beschreven.

Hoofdstuk 1 geeft een algemene inleiding over poreuze membranen en richt zich vervolgens op asymmetrische microporeuze hybride silica membranen. Dit inleidende hoofdstuk belicht de ongekende hydrothermale stabiliteit van hybride silica membranen op basis van 1,2-bis(triethoxysilyl)ethaan (BTESE), en benadrukt de voordelen van functionalisering en het sturen van de poriegrootte van deze microporeuze silica hybride membranen. Beide benaderingen bieden mogelijkheden voor een veel breder toepassingsgebied van deze klasse van sol-gel-membranen.

In **hoofdstuk 2** wordt het eerste voorbeeld van functionalisering van hybride silica membranen voor moleculaire scheidingen beschreven. Het effect van de toevoeging van amino-gefunctionaliseerde eindstandige groepen op het gedrag van de hybride silica membranen wordt weergegeven. De karakterisering van de membranen toont duidelijk aan dat de affiniteit van membranen gebaseerd op BTESE gestuurd kan worden door een geschikte precursor in te bouwen: hydrofiele precursors leiden hier tot hydrofiele membranen. Bovendien blijkt uit deze studie dat voor elke precursor een minimum concentratie bestaat waarboven de hydrofiele eigenschappen van de amino-gefunctionaliseerde precursors volledig worden benut. Bij amine concentraties boven deze drempelwaarde, hebben de membranen een hoge selectiviteit voor water in het ontwateren van water/alcohol mengsels. Deze sterke invloed van een relatief lage concentratie van gefunctionaliseerde precursors is inherent aan de gebruikte eindstandige functionele groepen en kan waarschijnlijk worden vertaald naar alle types van functionalisering.

Hoofdstuk 3 richt zich op de synthese en karakterisering van BTESE / R-triethoxysilaan (RTES, R = C_1-C_{18} alkyl) xerogels. Small Angle X-ray Scattering (SAXS), CO_2 en N_2 adsorptie en contacthoekmetingen zijn uitgevoerd om de eigenschappen van deze materialen te bepalen. In dit hoofdstuk worden de structurele eigenschappen, de adsorptie-eigenschappen en hydrofobiciteit van de xerogelen gerelateerd aan de lengte van de R-groep. Daarnaast zijn de invloed van de RTES/BTESE molaire verhouding en de syntheseomstandigheden op de structurele eigenschappen onderzocht. Gebleken is dat langere R-groepen, meer reactieve sol syntheseomstandigheden en pre-hydrolyse van de RTES precursor alledrie leiden tot georganiseerde nano-domeinen in het uiteindelijke materiaal. De hydrofobiciteit en adsorptie-eigenschappen zijn vooral afhankelijk van de lengte van de R-groep in de RTES precursor en veel minder sterk afhankelijk van de syntheseomstandigheden.

De equimolaire BTESE / RTES (R = C_1-C_{10} alkyl) samenstellingen werden geselecteerd voor het coaten en karakterisering van hybride silica membranen in **Hoofdstuk 4**. Het gebruik van de R-triethoxysilaan precursors (R = C_1 tot C_{10}) leidde tot een verandering van de membraan affiniteit van hydrofiele eigenschappen (voor R = C_1) tot hydrofobe eigenschappen (voor R = C_6 en langer). Een sterke samenhang tussen de scheidingseigenschappen van het membraan en de lengte van de R-groep werd gevonden in pervaporatie van water/n-butanol mengsels. Langere R-groepen resulteren in lagere scheidingsfactoren voor water, terwijl de scheidingsfactor voor n-butanol hoger wordt. Het meest hydrofobe membraan bleek een stabiele selectiviteit te laten zien over een breed scala van testomstandigheden en het heeft een totale flux van enkele $kg.m^{-2}.h^{-1}$. Dit is het eerste voorbeeld van een hybride silica membraan dat een selectiviteit voor n-butanol vertoont. Op basis van deze resultaten zijn de mogelijkheden voor dergelijke membranen in biobutanol productie onderzocht en vergeleken met die van bestaande organofiele polymere membranen.

De BTESE/RTES(R = C_1-C_{10} alkyl) membranen, een BTESO (C_8 ethaan brug) en een BTESO/C_{10}TES membraan werden getest in organische nanofiltratie en vergeleken met de γ-Al_2O_3 drager in **hoofdstuk 5.** Ondanks hun hoge fluxen in pervaporatie werden lage aceton en tolueen fluxen gemeten voor alle membranen in nanofiltratie. Uit dit onderzoek kwam naar voren dat adsorptie van water op de γ-Al_2O_3 drager mogelijk van grote invloed is. Daarnaast werden diverse leads voor toekomstig onderzoek gevonden.

Uit de experimenten beschreven in hoofdstuk 5 blijkt dat de poriegrootte van de hydrofobe hybride silica membranen mogelijk te klein is voor nanofiltratie toepassingen. Daarom is **hoofdstuk 6** gewijd aan de verkenning van een alternatieve templating methode voor hybride silica membranen met behulp van thermo-labiele adducten. Het Diels-Alder adduct werd geselecteerd voor deze aanpak, omdat daarbij selectieve thermische verwijdering van de template mogelijk is met behoud van het hybride silica-netwerk. De metingen aan xerogels en membranen laten zien dat flexibiliteit in het hybride silica-netwerk essentieel is voor deze aanpak.

Tenslotte beschrijft **hoofdstuk 7** een bredere evaluatie van de functionalisering en het sturen van de poriegrootte van hybride silica membranen. Uit het onderzoek beschreven in dit proefschrift blijkt dat een groot aantal (functionele) precursors kan worden opgenomen in een hybride silica matrix. De functionaliteit van de precursors wordt overgedragen op het materiaal en de membranen die uit deze materialen worden gemaakt. Dit betekent dat een breed scala aan opties beschikbaar is voor membranen die specifiek zijn ontwikkeld voor bepaalde toepassingen.

Acknowledgment

During the last few busy months spent behind my desk finalizing my thesis, and even now, I couldn't have realized that I had already been working in ECN for four years and moreover living in the Netherlands…. the time indeed flies very fast!!! So, now that I have this opportunity, I would like to thank everybody who made a wonderful experience of this stay and who was there to support me during the difficult times! Please remember that I am really grateful to all of you! Hartelijk Bedankt!!!

Peter and Martin, I would like to thank you for giving me the opportunity to do my PhD in ECN. This was a perfect environment for me to discover both the "fundamental" part of membrane development and the interesting aspects of the commercialization of our HybSi® membranes. I would not be able to obtain such a broad vision in an university and this experience will definitely turn into an advantage to tackle my future professional challenges.

Rob, you are the person with whom I worked the closest all along these four years. I want to sincerely thank you for trusting me and making everything possible to offer me the chance of doing my PhD on HybSi®! A unique subject! I am also very grateful for all the efforts you put into helping me become an independent researcher and for all the freedom you gave me to conduct my research. I think I could not have successfully completed my thesis without your help and advice! Helping me to write this thesis was a long process requiring a lot of effort from your side but you remained patient reviewing draft after draft. Even if I was sometimes disconcerted by your comments like "It is a mess, clarify all this"; I now realize how much I learnt from it and how much it helped me to structure my writing!!! Merci pout tout!!!

Jaap, you were quite busy all this time as our group leader but you always found time to follow my research and showed a lot of interest in my work. You also constantly encouraged me to pursue my efforts and finish my PhD not only in words but also in acts! Your corrections of the articles with your global vision of my work were of great help!! Thank you for your efforts and availability!

Rob and Jaap, even if you were my bosses, I really appreciate the “human side” of our cooperation. Both of you were there for me during the difficult times of my personal life and you made everything to make me feel better! Thanks a lot, I will never forget it!

During the three first years at ECN I spent most of my time in the lab(s) and I would like to particularly thank everybody who made this time one of the best periods of my PhD!!! This thesis would not have been possible without the “lab team” members with whom we worked as a real team always ready to help each other! Henk M. and Johan, please know that without both of you the labs would never be as safe, clean, and enjoyable to work in as they are now! Also, I want to thank both of you for all your help! Rudy, I also would like to thank you for all the supports you are delivering to the entire group! I am also grateful to the “measurement team” composed of Donough, Mariëlle, and Marc for all the measurements they have performed for me! Mariëlle, thank you for all the permpometry measurements and for your patience to sometimes do multiple measurements to get (or not) a proper one! Marc, thank you for the pervaporation measurements and also for the nice time outside work. I will not forget the jump in the canal! Donough, you have become more than a colleague for me, I consider you my friend! I really enjoyed the nice time we had in the lab and the good discussions around (few) beers on various subjects and in various bars! Keep your positive attitude!!

Apart from the people of our group, I also would like to thank all the people from E&S who helped me to perform diverse tasks.

My research has also given me an opportunity to work with different people outside ECN. Among these I would like to particularly thank Hessel. Thank you for taking me to Grenoble to conduct SAXS experiments. This was a tiring but wonderful experience. I really enjoyed working on this impressive “scientific toy” and all the time we spent outside with the other people from Twente. I would also like to thank you for all the fruitful and interesting discussions we shared on my thesis subject and for your patience with the article which we wrote together (we only had 16 versions and it is not finished yet). You are a real scientist who loves science!! Please keep it this way!

I am also thankful for the warm welcome received from all the people from the IM group in Twente where I spent a few weeks. Arian, I would like to thank you for having been my promotor, for the interest you showed in my work and for motivating me during every meeting we had. I really appreciated your fast reaction to correct my thesis chapters during the "rush time" despite of the fact that you have a more than busy life!

As I already said, I really enjoyed working in ECN in a group full of enthusiastic people! Thus, I want to thank all of these people. Henk V.V thank you for nice discussions on PV or NF and for availability and enthusiasm to answer to my numerous questions! Marcel, thank you for all the conversations we had around the "few" cigarettes we smoked together! Please stay positive, luck will come!! Also I got very close with people from the former PI group. Marija and Dick, it was a real pleasure to share with you my successive offices! Lucie and Arend, it was a pleasure to spend with you the long evenings at work! Raghu, I am glad to have met you, enjoy your stay in NL! Yvonne, even if you have been my group leader for only few weeks, thanks for your attention and for giving me the opportunity to present my results this summer in ICIM. Dolf and Annatolie it was nice to have you in our open office. But this small world wouldn't turn smoothly without our secretaries. Thanks a lot to all of you (Trudy, Arline, Annoesjka) for your help, availability and your good mood!

Finally, I would like to thank all the 'slaves' (synonym of trainee) I had during my PhD. Thanks for all your work Thomas, Lucie and Nicolas! I learned a lot coaching you and I hope this was reciprocal!

But life is not only about work and the free time has to be enjoyed as well. Among all people I met during these last years; I would like to thank the ones I spent most of my time with. I really enjoyed the time we had together sharing diverse activities, going out, playing poker or having football matches as an excuse to drink some beers together in Merv's! Alain and Virginie, I am really glad we have met and became good friends! Thanks you for all the good moments we spent together and for being there to support me!

Finally, almost a year and a half, I also found love in Netherlands. Maria a special thanks to you with whom I spent unforgettable moments. I hope this will continue! Thanks for all your encouragements and support, the nice diners you cooked for me when back late from work. Finally please accept my apologize to have sometimes been a “grumpy grandpa” when back home after heavy days! hehe

Il est temps de remercier tous les amis français qui sont passés me voir une ou plusieurs fois: Florent, Neven, Gildas, Mathilde, Antoine, Eloi, Benoit B., Benoit R., Batiste, Yann, Sam, Brice et Laetitia. Aussi je voudrais particulièrement remercier Stephanie&Yann et en particulier Yann pour être venu me soutenir dans un moment difficile !! Enfin un grand merci à Florent sans qui cette thèse n’aurait pas de couverture ainsi que pour son aide pour le reste!!

Je voudrais particulièrement remercier mes parents sans qui je ne serais jamais arrivé jusque-là!! Bien qu’il n’y ai point de mots pour qualifier tout ce qu’ils m’ont apporté, je tiens à leurs dédicacer cette thèse! Une pensée particulière pour mon père qui nous a quitté il y a quelques semaines….